Scale analysis of the diurnal cycle of precipitation over Continental United States

Paloma Celina Borque

Department of Atmospheric and Oceanic Sciences

McGill University, Montreal

August 2010

A thesis submitted to McGill University in partial fulfilment of the requirements for the degree of Master of Science

Abstract

This work studies the geographical and the scale variability of the summer diurnal cycle of precipitation over Continental United States through the analysis of 12 years of radar mosaics during the period 1996-2007. Wavelet analysis was performed to understand the importance of different spatial scales ranging from 8 km to 512 km. The objective of this thesis is to study the dependence of the variability of the rainfall field on location and time of day and how spatial scale explains this variability.

The results of this analysis show that the maximum activity for the different spatial scales occurs at different times of day: the larger the scale, the later their maximum influence occurs. The initiation of precipitation is scale-dependent: the onset is associated with the small scales, which later on they grow to form larger rainfall patterns. Over the Great Plains the average precipitation field presents two temporal maxima: one occurring during the afternoon and related to small scales (associated with the radiative forcing) and another one occurring during night hours related to larger scales (organized rainfall systems propagating from the west). In the eastern U.S., the precipitation pattern is also scale-dependent, it presents a similar behavior to that over the eastern lee of the Rocky Mountains. In particular, the maximum rainfall rates occur in the afternoon in association with small-scale processes. Monthly precipitation, and its scale decomposition, is also analyzed to present the differences in the diurnal cycle of precipitation for each summer month.

Résumé

Cette étude porte sur la variabilité géographique et d'échelle du cycle diurne des précipitations estivales, au-dessus des États-Unis continentaux, par l'analyse de mosaïques radars de 12 ans pour la période de 1996-2007. Les transformées en ondelettes sont utilisées pour saisir l'importance des différentes échelles spatiales de 8 à 512 km dans le cycle diurne. L'objectif de cette mémoire est d'étudier la dépendance de la variabilité du champ de précipitation sur l'endroit géographique et la période du jour, et comment cette variabilité est expliquée par les différentes échelles.

Les résultats de cette analyse montre que l'activité maximale de précipitation survient à un temps différent pour différentes échelles spatiales : plus large est l'échelle, plus tard se produit l'importance maximal de l'échelle. L'initiation de précipitation dépend de l'échelle : le début est associé aux petites échelles, qui s'organisent plus tard pour former des chutes de pluie à plus grande échelle. Sur les Grandes Prairies, la moyenne du champ de précipitation montre deux maximums : un en après-midi et relié aux petites échelles (associé au forçage radiative); un second durant la nuit, relié aux grandes échelles (systèmes de chute de pluie se propageant de l'ouest). Au dessus de la région Est, la distribution de précipitation est également dépendante de l'échelle; elle montre un comportement similaire au-dessus du côté Est des Rocheuses. En particulier, un taux maximal de chute de pluie advient en après-midi en association avec des processus de petites échelles. La précipitation mensuelle, et sa décomposition par échelles, est aussi analysée afin d'identifier les différences dans le cycle diurne de précipitation de chaque mois estival.

Acknowledgements

I would like to thank my supervisor, Professor Isztar Zawadzki, for the opportunity to work with him and also for his trust and guidance during the entire process of this research. I would also like to thank Marc Berenguer for his valuable assistance, especially at the beginning of this research. Without them this thesis would have been very hard if not impossible to complete. I would also like to extend my appreciation to all the members of the Radar Group for whom I only have words of appreciation. I would like to thank Xue Meng Chen for the translation of the abstract and Christopher Simmons for proofreading this thesis.

I am also grateful to many people in the academic and administrative staff at the Department of Atmospheric and Oceanic Sciences for their kindness though these years, making this an enjoyable experience by allowing me to mainly concentrate in research.

To my friends who I was bless to share this moment with, either here or kilometers away, they helped in more ways than they can imagine.

Finally, I would like to thank my family for their unconditional support and encouragement throughout these years, without them this thesis, too, would not have been possible.

Table of Contents

List of Figures

Figure 3.6: The first moment of summer precipitation averaged over the 9 the sub-domains depicted on figure 4 for each year in the 1996-2007 period (thin color lines) and the 12-year average (thick black line). Note that these curves represent space averages over 256 km^2.

Figure 3.7: Idem Fig. 3.6 but for the second moment of summer precipitation.

Figure 3.8: *Idem Fig. 3.6 but for summer precipitation coverage. Coverage units are number of grid points with precipitation larger than 0.22 mm* h^{-1}.

Figure 3.9: Idem figure 3.7 but for the month of June.

Figure 3.10: Idem fig. 3.7 but for the month of July.

Figure 3.11: Idem fig. 3.7 but for the month of August.

Figure 3.12: Diurnal cycle of summer variance of PP for the 9 sub-domains depicted on fig. 3.1.

Figure 3.13: Summer average PP for the year 2002 (red line), 2005 (green line), 2006 (blue line) and 2007 (black line) average over the CC (left panel) and NC (right panel) sectors.

Figure 3.14: Idem Figure 3.12 but for the month of June (blue line), July (green line) and August (red line).

Figure 3.15: Regions where the average for the longitudinal (shaded blue areas in the upper panel) and latitudinal (shaded green areas in the lower panel) Hovmöller diagrams were performed.

List of Tables

Chapter 1

Introduction

1.1 Motivation

The diurnal cycle of precipitation is a fundamental component of the variability of the global climate system and has important implications for both weather and climate; however, current models show clear deficiencies in their simulation of precipitation regimens. The diurnal cycle of rainfall activity at different temporal and spatial scales has not yet been fully-studied over the Continental United States. Furthermore, scale decomposition of rainfall fields illustrates precipitation evolution at the most significant spatial scales, and can potentially provide solutions for the deficiencies of numerical models.

1.2 Bibliographical review

The diurnal cycle of precipitation has been a topic of active research for several decades. In the early Twentieth Century, Kincer (1916) focused his analysis on the economic impact that timing of precipitation has on North American society. The earning capacity of the population dedicated to outdoor work is linked to the temporal and special distribution of precipitation (Kincer 1916), and thus the knowledge of the diurnal distribution of precipitation is an important factor to take into account when planning open-air activities.

Originally, studies on the behavior of precipitation fields have been centered on individual stations over North America or for the entire United States (U.S.) but with limited datasets. Examples of the former type of analysis

can be found in Alexander (1938), where the author focused on Oklahoma City, or in Cook (1939), where the analysis concentrated on Denver, Colorado. Both studies analyzed the warm season. An example of a continental-scale analysis can be found in Kincer (1916), who looked at the entire U.S. using statistical methods that did not required large computational resources. As time evolved, advances in computing area allowed for the analysis of bigger datasets and the application of more complex techniques. In one example, Wallace (1975) analyzed the entire United States with approximately 200 stations for all four seasons and was the first to use Fourier spectra to calculate the geographical variability of precipitation initialization in the Continental U.S. Later, as both radar and satellite data became available, combined datasets were used to describe in more detail the diurnal cycle of precipitation (Carbone et al. 2002, Tian 2005, Lee et al. 2007, Parker and Ahijevych 2007, among others) over the U.S.

Rainfall initiation is related to diurnal and semidiurnal forcing (Wallace 1975, Carbone et al. 2002, among others). Much of the observed warm season rainfall results from strong static instability combined with dynamics (Carbone et al. 2002) and synoptic processes (Riley et al. 1987). Consistent with the strong diurnal cycle of land surface temperature, over some continental regions deep convection tends to peak around the local afternoon and early evening hours. However, there is regional uniqueness in the precipitation pattern, implying a connection between regional characteristics, such as geographical or climatological factors, and the behavior of the precipitation field. Different elements, such as topography, land-sea contrast, coastline curvature and the location of the upper-level trough or low-level jet (among others), play an important role in the modulation of the diurnal cycle of precipitation (Wallace 1975, Riley et al. 1987, Tian et al. 2005, Lee et al. 2007 among others).

Three large and distinctive regions possessing substantial differences in the precipitation field can be identified over central and eastern United States

for the summer season: the Rocky Mountains, the Great Plains and the southeastern US (Wallace 1975, Lee et al. 2007 among others).

Over the western United States, the diurnal pattern is well organized, with a late afternoon maximum predominant along the eastern slopes of the Rocky Mountains and a mid-afternoon maximum evident west of the Continental Divide (Winkler et al. 1988). Several authors (e.g. Carbone et al. 2002, Tian 2005) described the eastern slope of the Continental Divide (105 °W) as a common longitude for the origin of precipitation systems in North America. Regions favored by continual thermal forcing, hydrodynamic instability, and other processes that can regularly initiate, maintain and regenerate organized convection (Carbone et al. 2002). The daily boundary-layer heating cycle plays a significant role in initiating and intensifying convection. In addition, synoptic configuration plays an important role in triggering summer precipitation over North America, as warm season lee troughs that form east of the mountains can act to organize and focus convective weather systems in mountainous regions (Riley et al. (1987). Ahijevych et al. (2004) further found that the lee of the Rocky Mountains is the source area for the majority of long-lived precipitation episodes.

In the summer season, there is a switch from the local afternoon maximum along the Continental Divide progressing to a near-midnight maximum over the Great Plains for the diurnal precipitation frequency (Riley et al. 1987). The boundary separating the eastern late afternoon precipitation maxima over the western United States and the nocturnal maxima over central United States is defined as the transitional zone (Tian 2005). Satellite data also show that the smooth transitions in the diurnal phase from late afternoon to early morning are in agreement with a decrease of the terrain elevation from the Rocky Mountains to the Great Plains (Tian 2005). The 200-meter elevation limit generally presents small diurnal amplitudes and a good agreement with the transitional zone (Tian 2005). During the warm season, the occurrence of

light and heavy hourly precipitation is strongly modulated by the diurnal heating cycle, as the transition zone becomes narrower as precipitation intensity increases (Winkler et al. 1988).

This switch from a near local afternoon maximum progressing to a midnight maximum toward the east suggest that mountain-initiated convection over the Rocky Mountains tends to propagate away, leading to the local evening and nighttime maximum over the adjacent plains (Lee et al. 2007). Carbone et al. (2002) found that propagation speed of precipitation systems was greater than can be attributed to large-scale forcing. These authors speculated that wavelike mechanisms, such as trapped gravity waves in the planetary boundary layer or gravity–inertia waves in the free troposphere, might contribute to the propagation of these systems. Their statistical approach also suggests that there are dynamical links between successive convective systems that are forced diurnally and in phase with each other. Spatial and temporal continuities of the phase and amplitudes of the diurnal cycle also support the idea that convective systems forming over the mountain region during the late afternoon would propagate eastward, affecting the Great Plains after sunset (Tian 2005 and Riley et al. 1987).

The daily occurrence of propagating episodes has a high impact on the continental diurnal cycle of precipitation. Furthermore, they account for a significant amount of the total summer precipitation that occurs in central United States (Parker and Ahijevych 2007 and Carbone and Tuttle 2008). Parker and Ahijevych (2007) analyzed 9-years of radar composites and found that approximately 90% of the episodes identified in the east-central United States were caused by systems propagating from the west. However, this percentage varies when considering different time durations for the rainfall activity, diminishing as the lifespan of the system increases. When considering a 24-hour duration, only 30% of the events are linked to systems initiated over the west (Carbone and Tuttle 2008). This propagating precipitation also

contributes to a delay in the daily maximum of thunderstorms frequency east of the mountains (Parker and Ahijevych 2007). The eastward propagating convective systems often arrive at the Appalachians during the late afternoon, time of the next day's diurnal maximum, which may provide a favorable situation for the re-intensification of convective storms or for the redevelopment of new storms over the high terrain (Carbone et al. 2002 and Parker and Ahijevych 2007).

The eastern portions of the Central Rockies and adjacent Great Plains are not only influenced by convective weather systems (which form over the mountains during the previous afternoon and propagate eastward) but are also affected by local convective systems that principally form at night (Riley et al. 1987). For example, upstream transient weather disturbances enhance and influence the longevity of some midsummer precipitation episodes. However, they are not essential to the diurnal cycle of precipitation systems (Trier et al. 2010). Furthermore, the presence of mesoscale disturbances, which help organize convection and large-scale environmental conditions, could favor locally-initiated nocturnal convection over long-lived progressive convection (Trier et al. 2010).

Tian et al. (2005) also related the nocturnal maximum in the central United States to not only the nighttime arrival of the eastward propagating convective systems from the Rocky Mountains but also to the suppression of afternoon convection. During the afternoon, subsidence induced by the downward velocity branch of the mountain-valley circulation between the Great Plains and Rockies is localized in the region and could partially explain why convection is suppressed over the Great Plains in the afternoon, even though the local diurnal forcing acts in its favor (Trier et al. 2010 and Tian et al. 2005). Furthermore, the nighttime upward motion associated with the reversal of this circulation acts to enhance the local convection at night and occurs approximately in phase with the arrival of the eastward-propating systems in the region (Carbone and Tuttle 2008).

The Great Plains Low-Level Jet (GPLLJ) is another factor that generates and/or intensifies convection over the Great Plains at night. The strong temperature and moisture advection and mass convergence associated with the deceleration region of the GPLLJ is located over this region, favoring instability and convection in the area (Bonner 1968). The nocturnal GPLLJ also enhances lower tropospheric vertical shear, which favors the upscale growth of convection (Trier et al. 2010). The westerly shear produced by the GPLLJ also favor continuous redevelopment on the forward (eastern) flank of the Mesoscale Convective Systems, and therefore promote eastward propagation (Trier et al. 2010).

There is a good agreement between the frequency of total precipitation and thunderstorm occurrence in the Central Plains (Wallace 1975, Riley et al. 1987 and Balling et al. 1985). Balling et al. (1985) showed that over 60% of the warm season rainfall occurs at night from southern Nebraska to western Oklahoma and portions of northern Texas. Harmonic analysis reveals a sharp uniform west-to-east gradient of approximately 1 hour for every 100 kilometers in the timing of maximum rainfall frequencies across much of the Great Plains (Balling et al. 1985). Heavy summer precipitation events show a stronger modulation in the diurnal cycle than total precipitation, with a maximum frequency occurring one to four hours earlier than the maximum frequency of all precipitation events (Balling et al. 1985), suggesting also that heavy summer nocturnal precipitation systems over the eastern Plains cannot be explained solely by the eastward propagation of mountain-generated systems from the previous afternoon (Riley et al. 1987).

A predominant feature of the diurnal cycle over North America is the land-sea contrast in coastal regions adjacent to the Pacific Ocean, the Gulf of Mexico and Atlantic Ocean. Over these areas, rainfall patterns provide a maximum of activity around local noon but with weaker intensity than over the

continent (Tian 2005). Several authors (Wallace 1975, Winkler et al. 1988, Tian 2005, Carbone and Tuttle 2008 among others) studied the impact of sea breeze circulations in the maximum frequency of occurrence of warm-season rainfall along the Gulf Coast. There is a general consensus that the land-sea breeze represents one of the most important physical mechanisms for the strong diurnal maximum in rainfall activity over the region.

Other factors were also analyzed for their role in the diurnal cycle of precipitation near the coasts; among them are local convective instability (Lee et al. 2007), coastline curvature and low-level convergence enhance by surface roughness Pielke (1974).

Over the southeastern region along the Gulf Coast, the diurnal cycle of precipitation is characterized by a standing oscillation with a strong late afternoon maximum and a suppression of convection at night (Wallace 1975, Winkler et al. 1988, Lee et al. 2007). Over the Florida Peninsula, there is a shift in the timing of the initialization of precipitation; it begins earlier over South Florida and at a later time to the north (Tian 2005). The location and timing of summer convection over this region depends on the strength and direction of the prevailing synoptic-scale flow (Pielke 1974). The interaction between the prevailing easterly flow along the southeast coast and westerly flow in the northeast coast with the summer sea breeze circulation over the state of Florida favors an afternoon convective precipitation maximum along the northeast coast, which tends to suppress the afternoon maximum along the immediate southeast coast (Schwartz and Bosart 1979).

1.3 Objectives and outline of the thesis

The main objective of this thesis is to provide a comprehensive description of the roles played by diurnal rainfall activity at different spatial

scales over the continental United States. To further illustrate this, an overview of the diurnal cycle of precipitation over the selected analysis regions is also presented, with particular attention to the dependence of rainfall activity on geographical position and time of day. In addition, monthly precipitation, and its scale decomposition, is analyzed in order to characterize the differences of the diurnal cycle of precipitation during each summer month.

This thesis has been organized into 5 chapters. Chapter 1 deals with the motivation, literature review, and objectives of this work. Chapter 2 describes the dataset and methodology used in this study, while chapter 3 discusses the diurnal cycle of precipitation over the Continental United States for the entire summer season as well as for each summer month. Chapter 4 provides a description of the influence of summer and monthly precipitation at spatial scales ranging from 8 to 512 km in the diurnal cycle of precipitation over central U.S. Finally, chapter 5 summarizes the major conclusions of this work.

Chapter 2

Data description and methodology

2.1 Radar data

For the analysis presented in Chapter 3, time series were analyzed from the NOWrad mosaic, produced by the WSI Corporation. WSI (Weather Services International) integrates Extended-Range Base Reflectivity data from the National Weather Service's NEXRAD radar sites located across the United States to produce the NOWrad product. This set of data provides an extensive coverage of the United States with a high temporal and spatial resolution. NOWrad uses overlapping radar sites to improve reliability and includes quality control that filters out false echoes. The set of data used in this work affords a three-step quality control with a 5 dBZ intensity resolution, a 15-minute temporal resolution and a 2 km spatial resolution. As common in the construction of radar composites, these mosaics show the highest reflectivity measured by any radar at each grid point for any of the 16 vertical levels. In the presence of melting particles the choice of the maximum may lead to overestimation of precipitation intensity.

The period analyzed in this work corresponds to 12 years of radar mosaics covering the years 1996 – 2007. The analysis focused on the diurnal cycle of rainfall activity during the summer period and on the difference between each summer month. The summer season was defined as the June through August average.

In order to analyze hourly precipitation fields, each reflectivity map, Z, was converted to rainfall rate, R, by the relation, $Z = 300\ R^{1.5}$. The 15 minutes resolution data was accumulated to obtain hourly rainfall data assuming rain intensity as constant over the 15 min period.

The diurnal cycle of precipitation was computed by averaging the precipitation field at each hour for every day in the 12-year period.

2.2 Precipitation field spatial decomposition.

Wavelets are suitable for scale decomposition of spatially discontinuous fields, and many different types of wavelets have been developed in previous studies. [For more detail in wavelet analysis and its mathematical derivation, see Kumar and Foufoula-Georgiou 1997 and Turner et al. 2004]. Each wavelet type is defined by a wavelet and a scaling function characterized by different shapes and mathematical properties. In this study Haar wavelets were used because they are simple to compute and because of their square shape, which best addresses sharp discontinuities.

The 1-D Haar wavelet transform of a function f, is defined as:

$$W_\lambda(t) = \int_{-\infty}^{+\infty} f(t)\psi_{\lambda,t}(x'-t)dx' \qquad (2.1)$$

where λ is a scale parameter, t is the variable and ψ are the wavelet functions, which depend on λ and t,

$$\psi_{\lambda,t}(x'-t) = 2^{-\lambda/2}\psi_0\left(\frac{x'-t}{2^\lambda}\right) \qquad (2.2)$$

with,

$$\psi_0(t) = \begin{cases} 1 & 0 \le t < 1/2, \\ -1 & 1/2 \le t < 1 \\ 0 & otherwise. \end{cases} \tag{2.3}$$

Therefore, a wavelet transform is characterized by a location and a scale, Haar wavelet uses the following translation and dilation functions. Figure 2.1 shows schematically the dilation and translation of the 1-D Haar wavelet function.

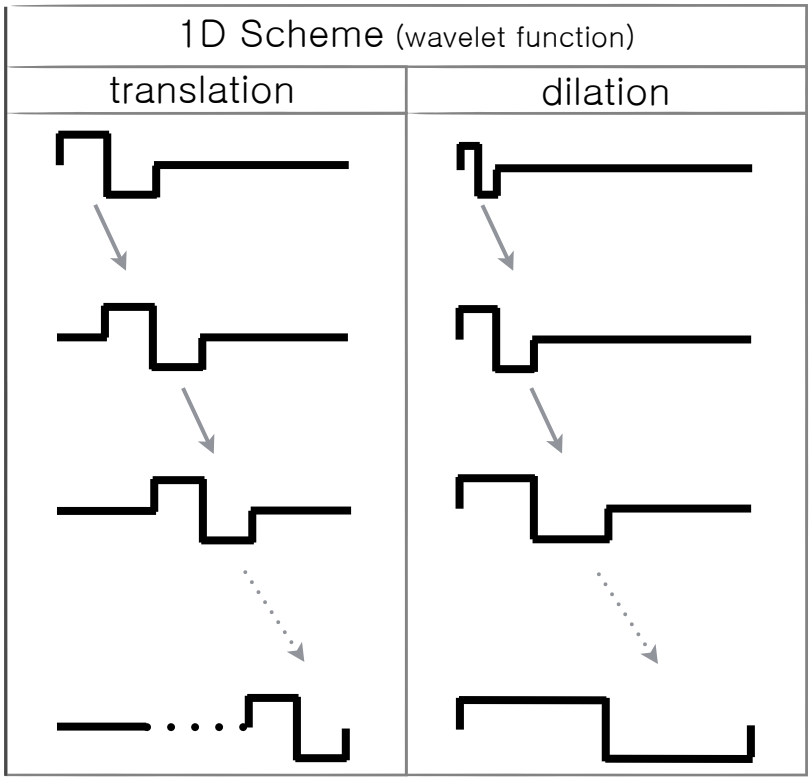

Figure 2.1: Scheme of dilation and translation of the 1-D Haar wavelet function.

For a 2-D field, the base for the wavelet function extends to three different functions in order to account for the variability in longitude (Fig. 2.2c), latitude (Fig. 2.2d), and in both directions at the same time (Fig. 2.2e).

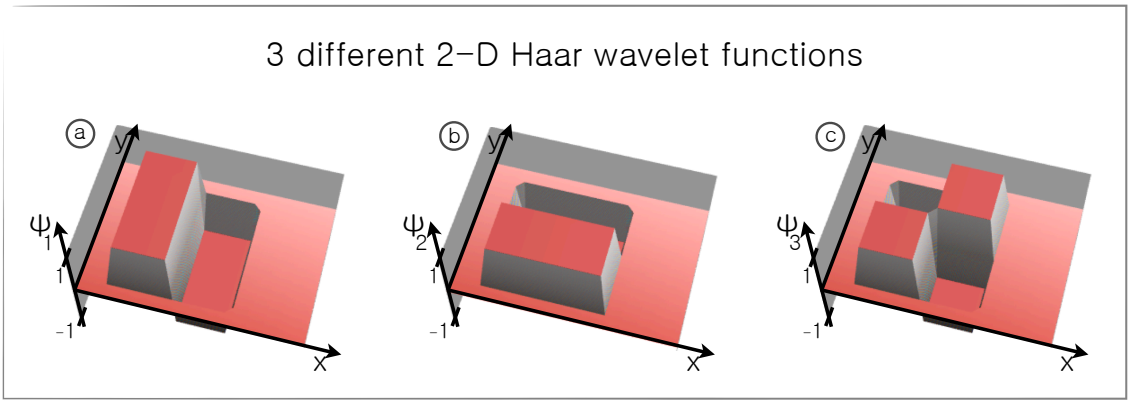

Figure 2.2: Scheme of the three 2-D Haar wavelet functions, considering the variability in x (a), in y (b) and in both directions at the same time (d).

The first moment of precipitation (P) is defined as the average of the values of the precipitation field over the largest domain analyzed:

$$PP(x,y,t) = \overline{P(x,y,t)} \tag{2.4}$$

where P is the precipitation field, x is longitude, y is latitude and t is time.

Similarly, the second moment of precipitation (PP) is defined as the average of the squared values of the precipitation field over the largest domain analyzed:

$$PP(x,y,t) = \overline{P(x,y,t)^2} \tag{2.5}$$

Since the different scale components are orthogonal, it follows that the second moment of precipitation is equal to the sum of the squared fields of its wavelets components:

$$PP(x,y,t) = \sum_{j=1}^{\infty} W_j{}^2(x,y,t) \tag{2.6}$$

Finally, the relative contribution of each scale to PP was defined as the ratio between the wavelet power spectrum and the second moment of precipitation. It thus follows that

$$RPP_\lambda(x,y,t) = \frac{S_\lambda(x,y,t)}{PP(x,y,t)} \tag{2.7}$$

The importance of rainfall activity at 7 spatial scales was analyzed in this work. The resolution of the wavelet components for λ=1, … , N=7 is equal to 2^λ grid points, corresponding to precipitation at 8, 16, 32, 64, 128, 256 and 512 km respectively.

The domain where the precipitation field was analyzed cover the region from 110°W to 78 °W and from 32°N to 45°N (Fig. 2.3). Wavelet decomposition was performed over the original domain enlarged by 2^{j-1} grid points on each side. Therefore, the computation of each wavelet function over the original domain does not have any border effect (Fig. 2.3).

Finally, when performing the wavelet decomposition, the missing values within the domain were excluded from the computations.

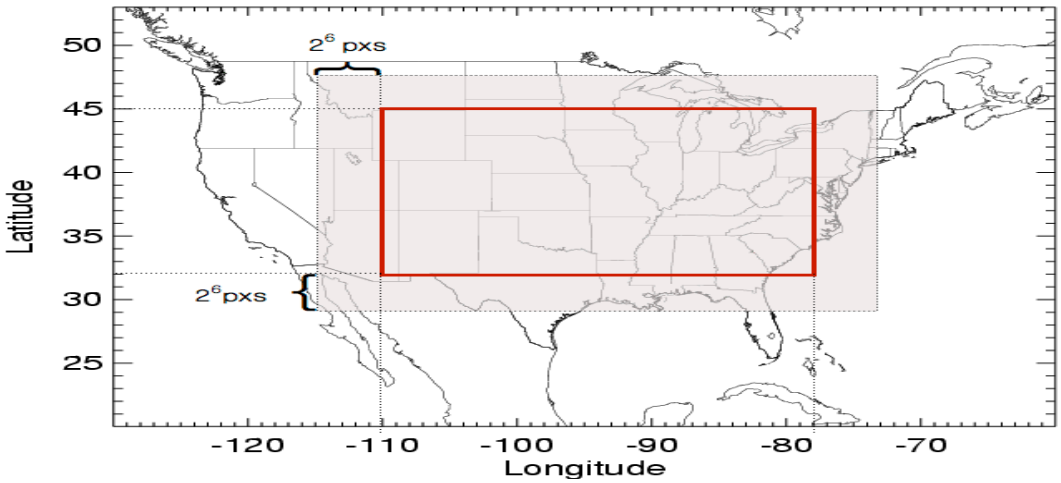

Figure 2.3: Domain where the wavelet components were computed (shaded rectangle) and subdomain where the analysis of rainfall activity and relative precipitation power was analyzed (red rectangle). Size in pixels of the extension made to the original domain for the wavelet calculations is also indicated.

Chapter 3

Characteristics of the diurnal cycle of precipitation over Continental United States

The goal of this chapter is to present a comprehensive overview of the diurnal cycle of precipitation over central United States [110W to 78W and 32N to 45N, Fig. 3.1]. The main features of the rainfall field over different sub-sectors within this region are further analyzed here.

3.1 Evolution of the precipitation field over Continental United States

3.1.1 Summer season analysis

Figure 3.2 shows the average precipitation rate over twelve summer seasons (June, July and August) for the years 1996 to 2007 during the 24-hour period.

The eastern lee of the Rocky Mountains, centered on 105W and ranging from 34N to 42N, is clearly shown to be an important region for the initiation of precipitation during the late morning and afternoon hours (Figs. 3.2i to 3.2j). This 12-year climatology of summer precipitation shows that three very localized precipitation areas are likely to occur south of 41N around 105W at 18Z (Fig. 3.2j). Precipitation over this area develops in intensity and extent, and by 00Z these three isolated features become two well-defined maxima, one centered on 39N and the second one around 35N (Fig. 3.2a). The northern

pattern (centered around 105W – 39N) reaches the maximum intensity, higher than 1.2 mm h^{-1}, between 00Z and 02Z (Fig. 3.2a and 3.2b).

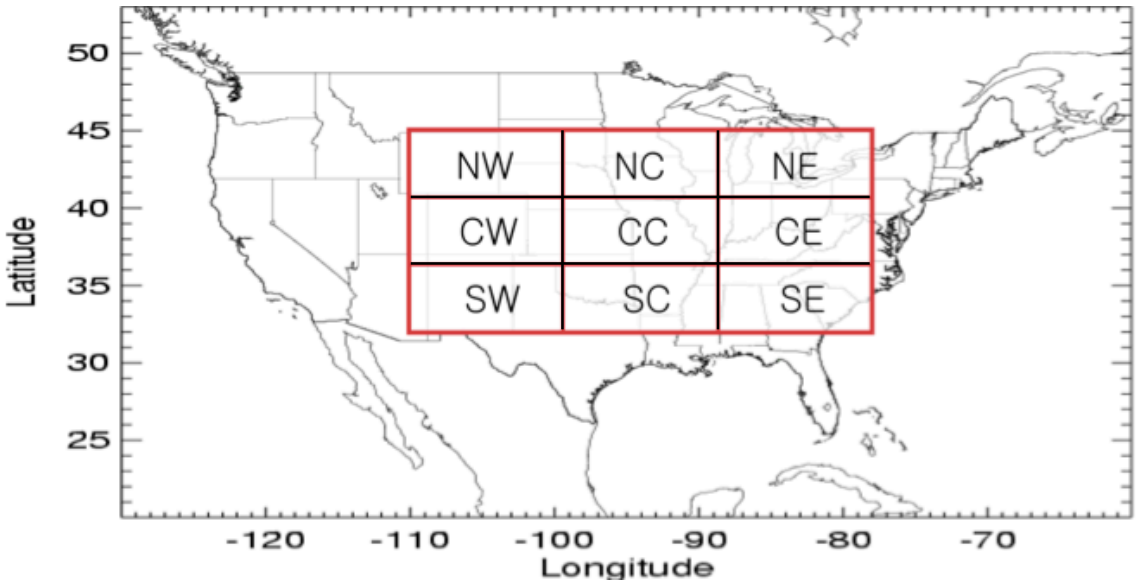

Figure 3.1: Region where the precipitation patterns are analyzed (red rectangle) and sub-domains where the diurnal cycle is averaged (black rectangles) in this work. The NW, CW and SW sectors will be referred as the western longitudes, the NC, CC, and SC as the central longitudes and the NE, CE and SE as the eastern longitudes.

After 04Z the area with average precipitation rates below 0.1 mm h^{-1} increases in coverage east of the Rocky Mountains until 16Z, when this region of precipitation expands as far east as 101W (Fig. 3.2c to 3.2i). In connection with this feature, and for the same time period, the average rainfall rate (higher than 0.5 mm h^{-1}) is expected to move further east with time (Fig. 3.2c to 3.2i).

The rainfall pattern over the northeastern region of the domain [north of 37N and east of 95W] is not as clearly organized as over the western longitudes. Precipitation is recurrent over this region, either as scattered cells during night hours or as organized convection during the morning and early afternoon hours

(Fig. 3.2). A minimum of rainfall activity with values smaller than 0.2 mm h^{-1} is likely to be present around 16Z (Fig. 3.2i). However, due to the scattered nature of the precipitation pattern there is no clear timing for a well-defined maximum.

An interesting feature can be seen over the area south of the Great Lakes. This region seems to favor rainfall activity during afternoon hours with maximum intensity just south of Lake Michigan from 20Z to 02Z (Figs. 3.2k to 3.2b). Lake Erie presents similar characteristics with precipitation likely to be present just south of it from 22Z to 00Z, although with weaker intensity than the pattern associated with Lake Michigan (Figs. 3.2l, 3.2a). Also, around 18Z rainfall activity is not present over the Great Lakes, but instead average precipitation rate higher than 0.3 mm h^{-1} tends to occur over the areas surrounding them (Fig. 3.2j). This behavior is probably in association with the different timing of the thermal forcing that favors the initiation of convection over land and water surfaces.

Over the southeastern U.S., rainfall activity tends to be very localized. As a likely response to land-sea breeze circulation, the precipitation pattern closely follows the coast. During the morning (the time of maximum cooling) convection is likely to occur over the ocean, whereas in the afternoon (the time of maximum heating) convection is mainly present over the continent (Fig. 3.2).

North of this region, precipitation is likely to occur around the southern edge of the Appalachian Mountains. At 00Z a thin line of average precipitation rates below 0.1 mm h^{-1} covers the region from 37N – 81W to 39N over the eastern boundary of the domain (Fig. 3.2a). At 10Z this region reaches its maximum extension covering an area of almost 5-degrees width, aligned southwest to northeast in agreement with the orientation of the Appalachian Mountains (Fig. 3.2f). Afterwards, precipitation tends to occur over the edges of this strip, and by 20Z the entire region is covered by average precipitation

rates higher than 1 mm h^{-1} (Fig. 3.2k). This rainfall pattern is probably related to the thermal circulation induced by the high topography in the area.

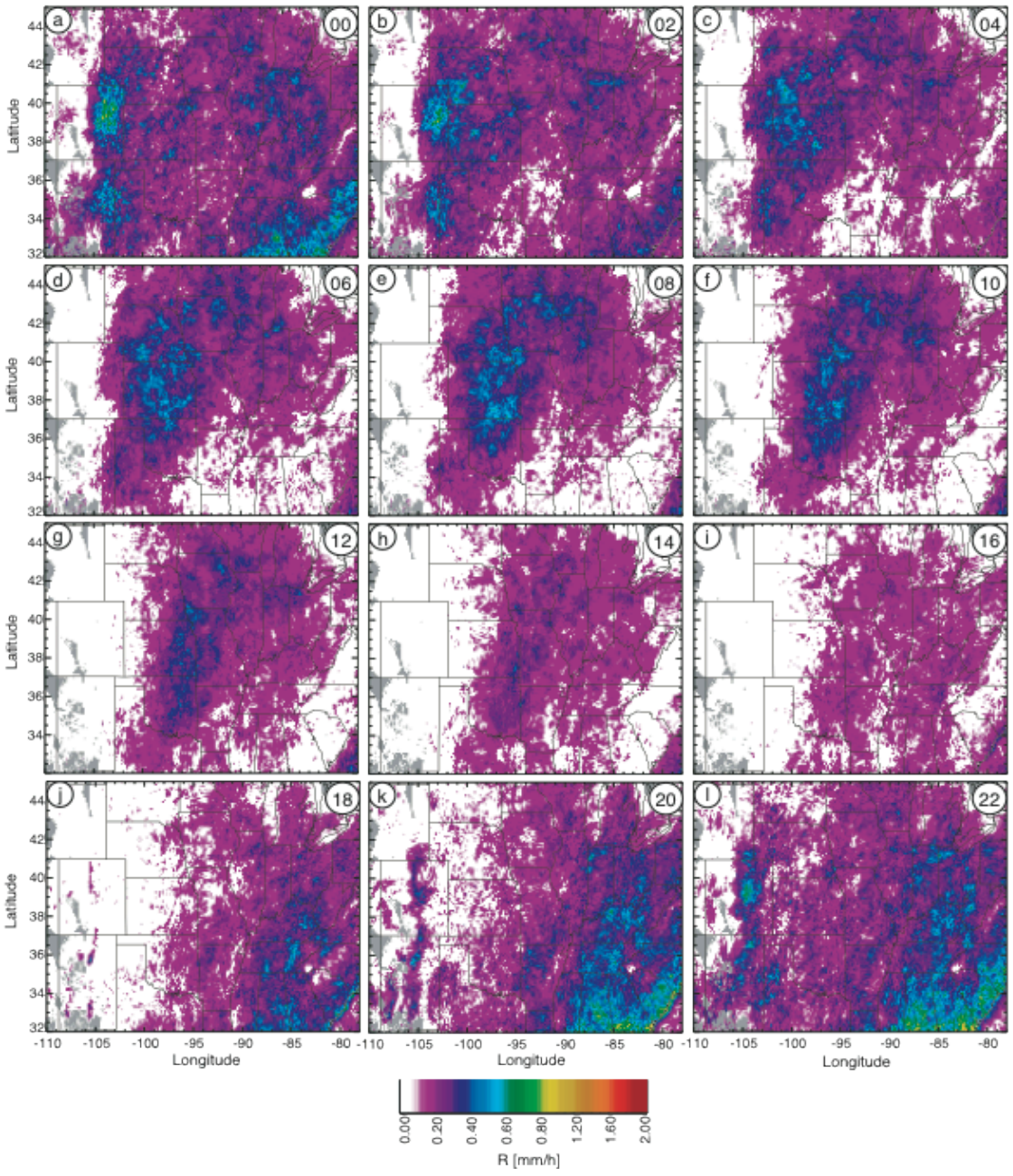

Figure 3.2: Average summer rainfall field in the period 1996-2007 derived from radar observations every 2 hours from 00Z on the upper left panel to 22Z on the lower right panel for the region depicted on figure 3.1. UTC time is written in the upper right corner of each panel.

3.1.2 Analysis for the summer months

The 12-year average of the rainfall field for each summer month is shown in figures 3.3 to 3.5. Monthly precipitation rate fields have similar characteristic to the ones described for the summer season; however, there are some noticeable differences.

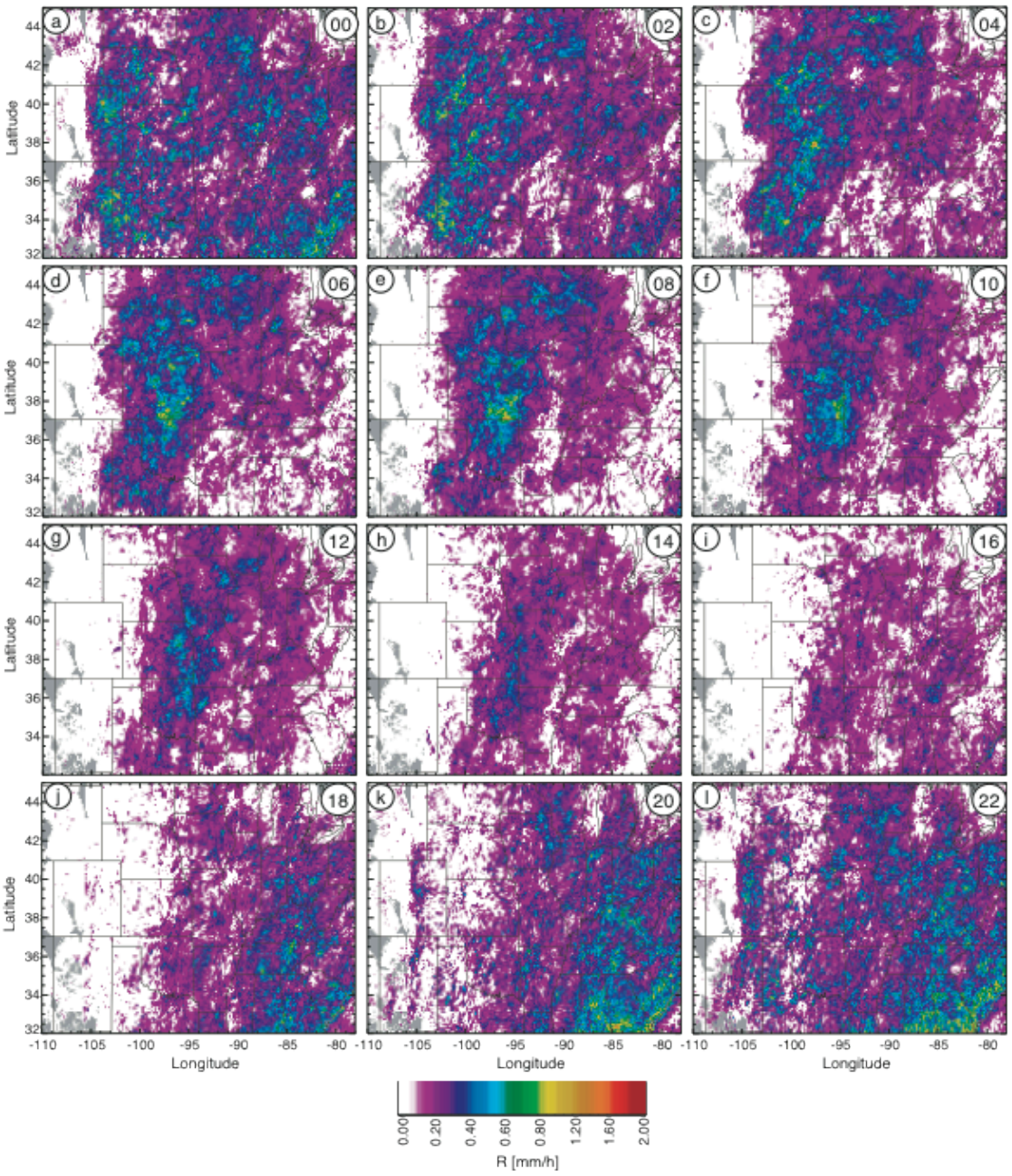

Figure 3.3: Idem figure 3.2 but for the month of June.

The average June precipitation rate, shown in Fig. 3.3, is generally more intense than the summer average. At night (from 04Z to 10Z) rainfall activity located from 94W to 97W and southern of 38N is also likely to be heavier (by at least 0.3 mm h^{-1}) in June than during the summer season (Figs. 3.3c to 3.3f). Precipitation occurring over the Great Plains also tends to be more intense during this month.

There is no preferred latitude for the initiation of June precipitation over the eastern lee of the Rocky Mountains (Fig. 3.3). However, after 04Z the average maximum rainfall intensity (higher than 1.2 mm h^{-1}) is likely to occur around 38N and 97W, maintaining its intensity for 6 hours and shifting slightly eastward with time (Figs. 3.3c to 3.3f).

An interesting feature in the July precipitation patterns is the shape change of the rainfall coverage during the 24-hour period. In the afternoon (from 20Z to 00Z), the precipitation field tends to be elongated longitudinally from 106W to 102W, in agreement with the position of the highest terrain (Figs. 3.4k, 3.4l and 3.4a). After 02Z the northern and southern edges of this band vanish while the central part grows longitudinally, leading to a more isotropic shape of the precipitation field at night (Figs. 3.4b to 3.4e). Furthermore, July precipitation is more intense over the southeastern U.S. However, over the rest of the domain, especially over the Central Plains, rainfall activity is weaker than during the summer season (Figs. 3.2 and 3.4).

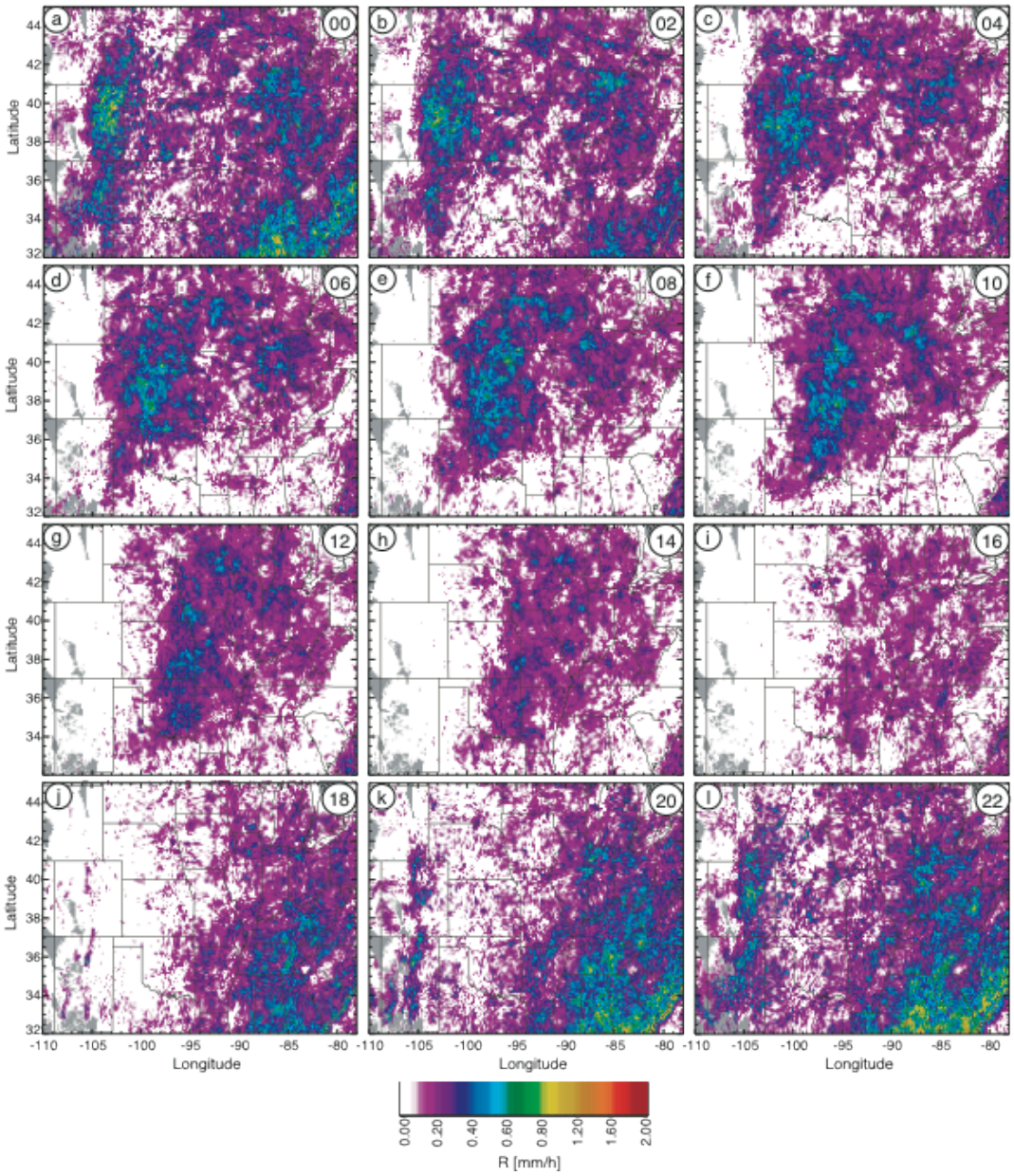

Figure 3.4: Idem figure 3.2 but for the month of July.

Taking into account the full diurnal cycle, August and summer precipitation patterns resemble each other the most (Fig. 3.2 to 3.5). However, August has the smallest rainfall rates over most of the domain analyzed. An exception occurs at 02Z over the eastern lee of the Rocky Mountains between 38N and 40N, where August precipitation intensity is at least 0.2 mm h^{-1} higher than for the summer season (Fig. 3.2b and 3.5b).

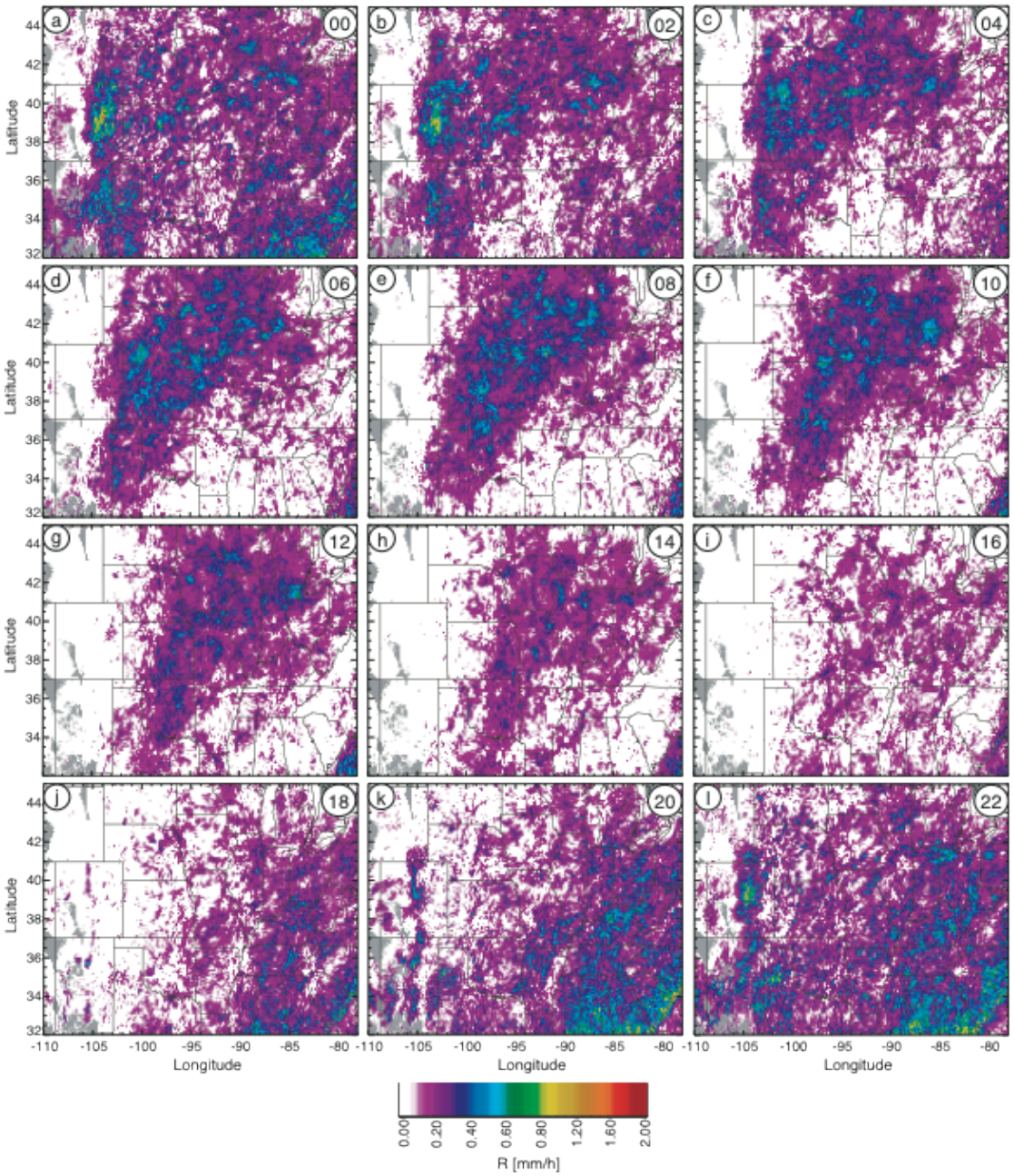

Figure 3.5: Idem figure 3.2 but for the month of August.

3.2 Precipitation characteristics over different sub-domains

From the previous discussion, it is clear that the precipitation field over the domain analyzed has different patterns in different sub-regions. In order to analyze them separately, fields of precipitation coverage, the first (P) and second moment of precipitation (PP), as defined by Eqs. 2.4 and 2.5 respectably, are spatially averaged over the 9 sectors shown in Fig. 3.1.

3.2.1 Summer season

Over the western sectors, the average for the first and second moment of summer precipitation (P and PP respectably) has a well-defined distribution; its maximum occurs during the afternoon (at 00Z) and its minimum (values close to zero) during the morning (around 17Z, Fig. 3.6a to 3.6c and 3.7a to 3.7c). An important feature in this region is the timing asymmetry of the maximum summer value. Over these sectors, summer precipitation is more likely to undergo rapid initiation, with a more gradual decrease in both, P and PP after the maximum value is reached (Fig. 3.6a to 3.6c and 3.7a to 3.7c).

A clear example of this asymmetry can be seen over the South-Western (SW) sector, where the average maximum P of 0.4 (mm h^{-1}) occurs at 00Z and the minimum of 0.2 (mm h^{-1}) at 17Z (Fig. 3.6c). This indicates that, from the time of maximum rainfall activity, it takes 17 hours for the summer P to reach its average minimum but only 7 hours to grow to its highest value.

Over the Central-Western (CW) sector, the average summer precipitation is characterized by a similar behavior to the SW sector but with a less abrupt decay with time (Figs. 3.6b to 3.6c).

Over the North-Western (NW) sector, the maximum P of the summer average of approximately 0.15 (mm h^{-1}) is the smallest maximum of the western longitudes (Figs. 3.6a to 3.6c). Therefore, the average summer rainfall activity affords a slower decay with time over this sector.

The minimum and maximum values of P and PP of the summer average tend to occur at the same time over the western region, indicating that the precipitation systems, on average, seem to have the same lifetime over this area. This suggests that the same forcing could be involved in the initiation and decay of summer rainfall activity. However, the maximum value depends on latitude; similar values characterized the central and southern sectors but decreases to almost half over the northern sector. Therefore, the maximum P and PP of the summer average could be a response to local conditions.

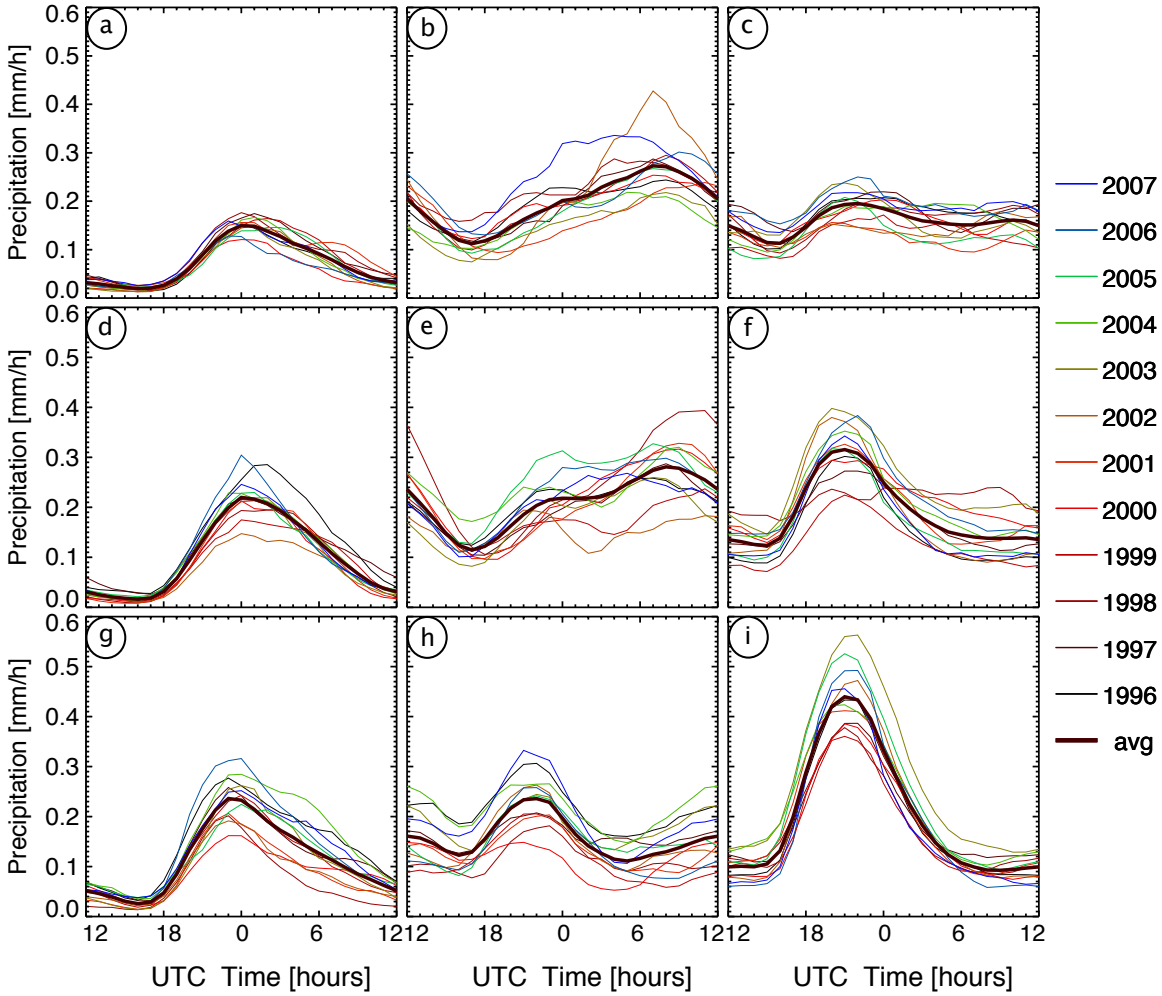

Figure 3.6: The first moment of summer precipitation averaged over the 9 the sub-domains depicted on Fig. 3.1 for each year in the 1996-2007 period (thin color lines) and the 12-year average (thick black line). Note that these curves represent space averages over 512 km^2.

Summer P and PP over the eastern longitudes is also likely to have a uniform distribution with one maximum and one minimum value during the 24-hour period. The time of the maximum value over this region (22Z) tend to be around the same local time as over the western longitudes (Figs. 3.6g to 3.6i and 3.7g to 3.7i). However, the highest value over this region occurs in the southern sector. In particular, the maximum summer P of 0.43 (mm h^{-1}) occurs over the South-East (SE) sector and consistently decreases northward, reaching 0.32 (mm h^{-1}) over the Central-East (CE) sector and 0.19 (mm h^{-1}) over the North-East (NE) sector (Figs. 3.6g to 3.6i). Also, summer rainfall activity over this longitudinal band is likely to be more symmetric with respect to the maximum value than over the western region, especially over the southern sectors (Figs. 3.6c to 3.6i).

Over the Central longitudes the main characteristics of the summer P distribution depend strongly on latitude. Furthermore, the first and second moments of precipitation clearly differ between each other. For the South-Central (SC) sector, the maximum P in the summer season, around 0.23 (mm h^{-1}), occurs at 22Z, and a secondary maximum, of 0.16 (mm h^{-1}) is seen at 12Z over the region (Fig. 3.6f).

Over the Central-Central (CC) and North-Central (NC) sectors, late afternoon and nighttime rainfall activity have a significant large influence on the summer diurnal cycle of precipitation. In particular, summer PP over the CC sector has a maximum value of 0.28 (mm h^{-1}) at night (at 00Z); however, a plateau with values around 0.22 (mm h^{-1}) dominates the late afternoon hours (from 23Z to 03Z) over this sector (Fig. 3.6e). On the other hand, summer PP over the NC sector has a clear nighttime maximum with values close to 0.29 (mm h^{-1}) from 07Z to 08Z (Fig. 3.6d). These results suggest that the influence of nighttime precipitation increases northward over the Great Plains.

With respect to PP, late afternoon and nighttime precipitation has a smaller influence in its summer diurnal cycle than for summer P over the CC

and NC sectors. In particular, summer PP over the CC sector is likely to often reaches its maximum value during the afternoon (at 00Z), and with comparable high PP values during night hours (from 01Z to 08Z, Fig. 3.7e). On the other hand, summer PP over the NC sector does not have a preferred time for its maximum, but instead a plateau with high values occurs during the late afternoon and night (from 23Z to 08Z, Fig. 3.7d). However, relative to the afternoon, the influence of nighttime PP is likely to increase northward over the central longitudes.

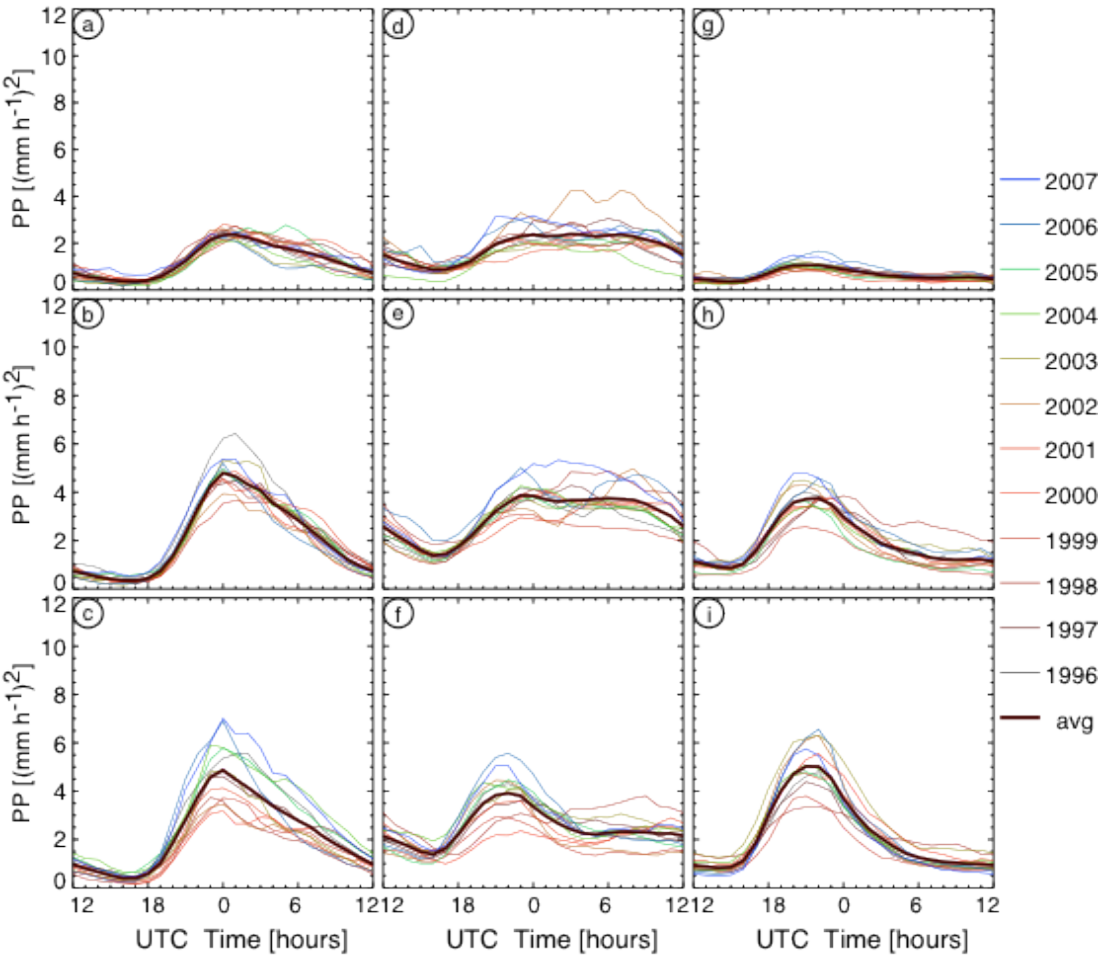

Figure 3.7: Idem Fig. 3.6 but for the second moment of summer precipitation.

One explanation for this difference between the behavior of summer P and PP in the afternoon and night hours could relate to the different intensities

and coverage of the precipitation systems. Summer precipitation is likely to have greater intensity in the afternoon but with a more localized distribution, whereas during nighttime precipitation systems tend to have lower rainfall rates but also a more homogeneous distribution over the Great Plains (Fig. 3.2). This might explain the greater nighttime values of the average precipitation field (P), in comparison to the average of the squared of precipitation field (PP), over the Northern Great Plains.

Finally, it is interesting to note that over the three western and three eastern sectors as well as over the SC sector the size of the area covered by reflectivity values higher than 15 dBZ (0.22 mm h^{-1}) has a diurnal cycle that is very similar to the one described by the first and second moments of precipitation (Figs. 3.6 to 3.8). This is likely to indicate, that over these regions, the time of day with small (large) amounts of precipitation is likely to be well correlated with small (large) variability and small (large) area covered by rainfall activity (Figs. 3.6 to 3.8). On the other hand, the diurnal relationship between the different moments of precipitation over the Great Plains (NC and CC sectors) is more complicated. Over these areas, precipitation coverage has a diurnal cycle comparable to that of precipitation intensity, however its maximum value occurs at least an hour later than the maximum of precipitation intensity (Figs. 3.6d, 3.6e, 3.8d and 3.8e). That is, the average rainfall activity over the Great Plains has a more complex structure than over the rest of Continental United States.

It is important to note that emphasis in this study is placed on the contribution of each spatial scale (given by the wavelet spectrum) to the second moment of precipitation (Eq. 2.7). Therefore, the focus of this work, from this point onward, is mainly in the characteristics of second moment of precipitation.

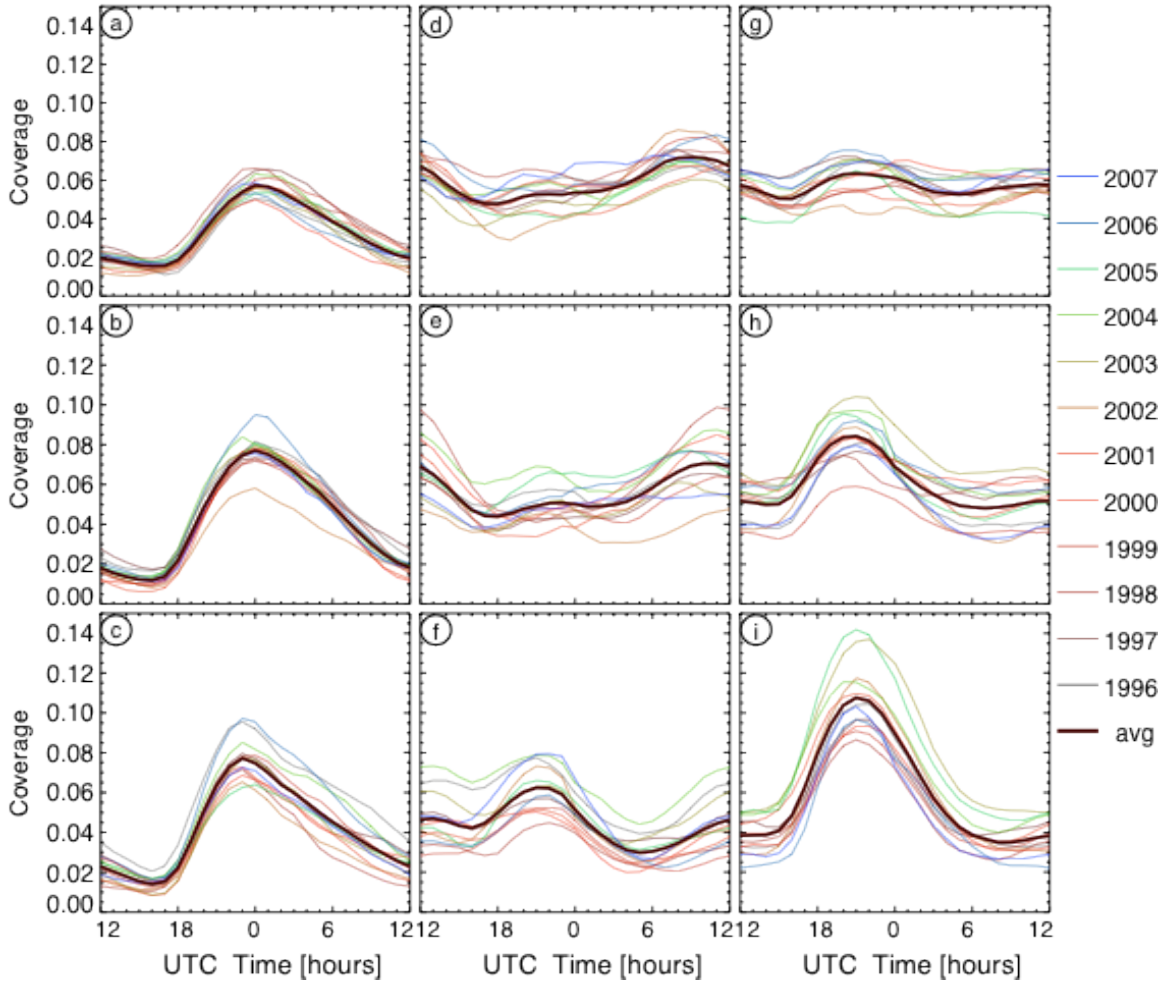

Figure 3.8: Idem Fig. 3.6 but for summer precipitation coverage. Coverage units are number of grid points with precipitation larger than 0.22 mm h^{-1}.

3.2.2 Month-to-month variability

Over the western and central longitudes, June PP is likely to be more intense than summer PP. A clear example can be found over the SW sector, where the average maximum of June PP is higher than the summer average by at least 1.5 (mm h^{-1})^2. Also, in contrast to the summer average, June PP is likely to have a distinct maximum of 3 (mm h^{-1})^2 at 03Z over the NC sector (Fig. 3.9d).

It is clear from Fig. 3.10 that nighttime precipitation is important during the month of July. Over the western longitudes, the decrease in the average nighttime PP does not seem to be as marked for July as for the summer average (Figs. 3.7a to 3.7c and 3.10a to 3.10c). Instead, July PP is likely to have a secondary maximum within night hours (after 03Z) that is most clearly shown in the CW sector (Fig. 3.10b).

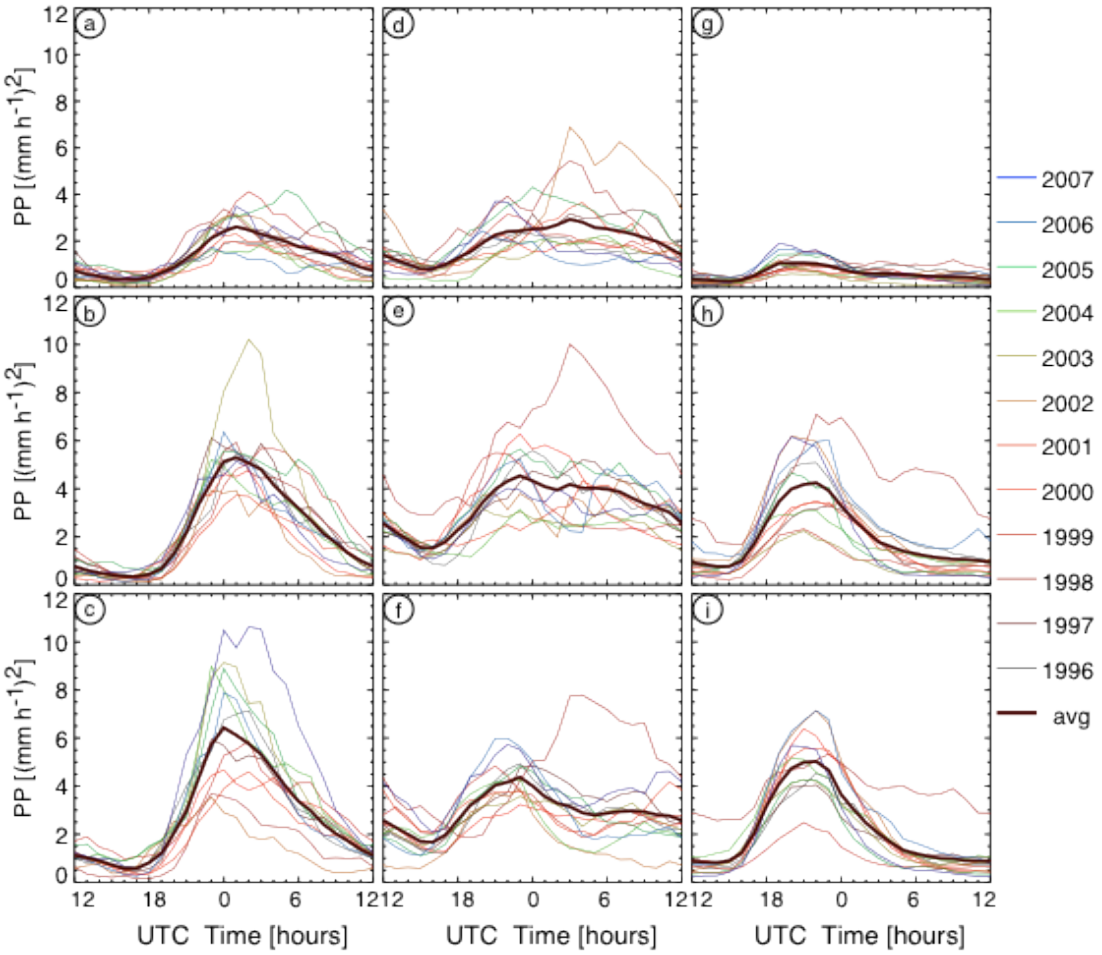

Figure 3.9: Idem figure 3.7 but for the month of June.

Additionally, in the CC sector the maximum PP of the July average occurs after midnight (08Z), slightly exceeding the afternoon secondary maximum reached at 23Z (Fig. 3.10e).

Over most of the domain, the average PP during the month of August presents smaller values than during the summer season (Figs. 3.7 and 3.11). However, the biggest difference between the two periods occurs at night. Over the NC and CC sectors, the average August PP reaches its highest value at 08Z, by contrast to the afternoon maximum present for the summer season (Figs. 3.7d, 3.7e, 3.11d and 3.11e).

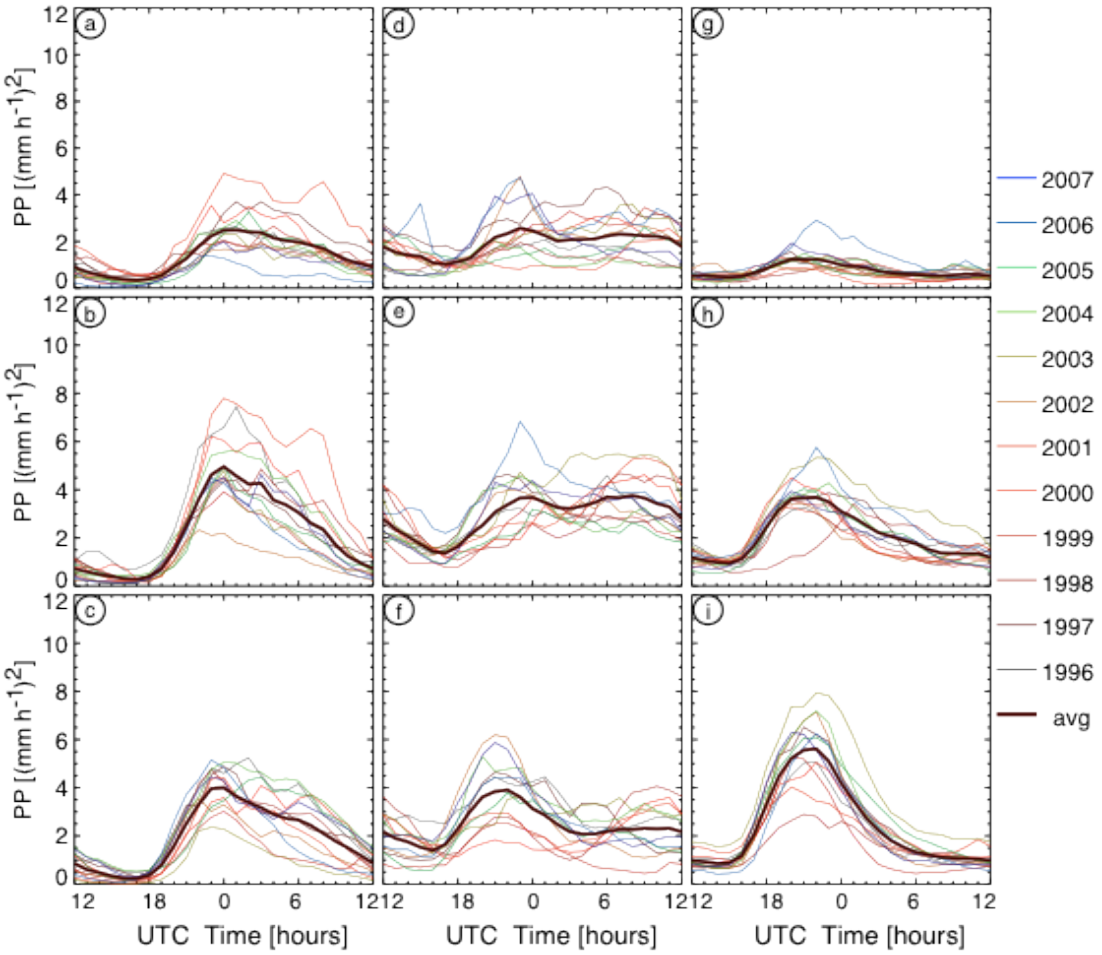

Figure 3.10: Idem fig. 3.7 but for the month of July.

Therefore, nighttime precipitation over the western and central longitudes is likely to play a larger role in the diurnal cycle of precipitation during the months of July and August than during June.

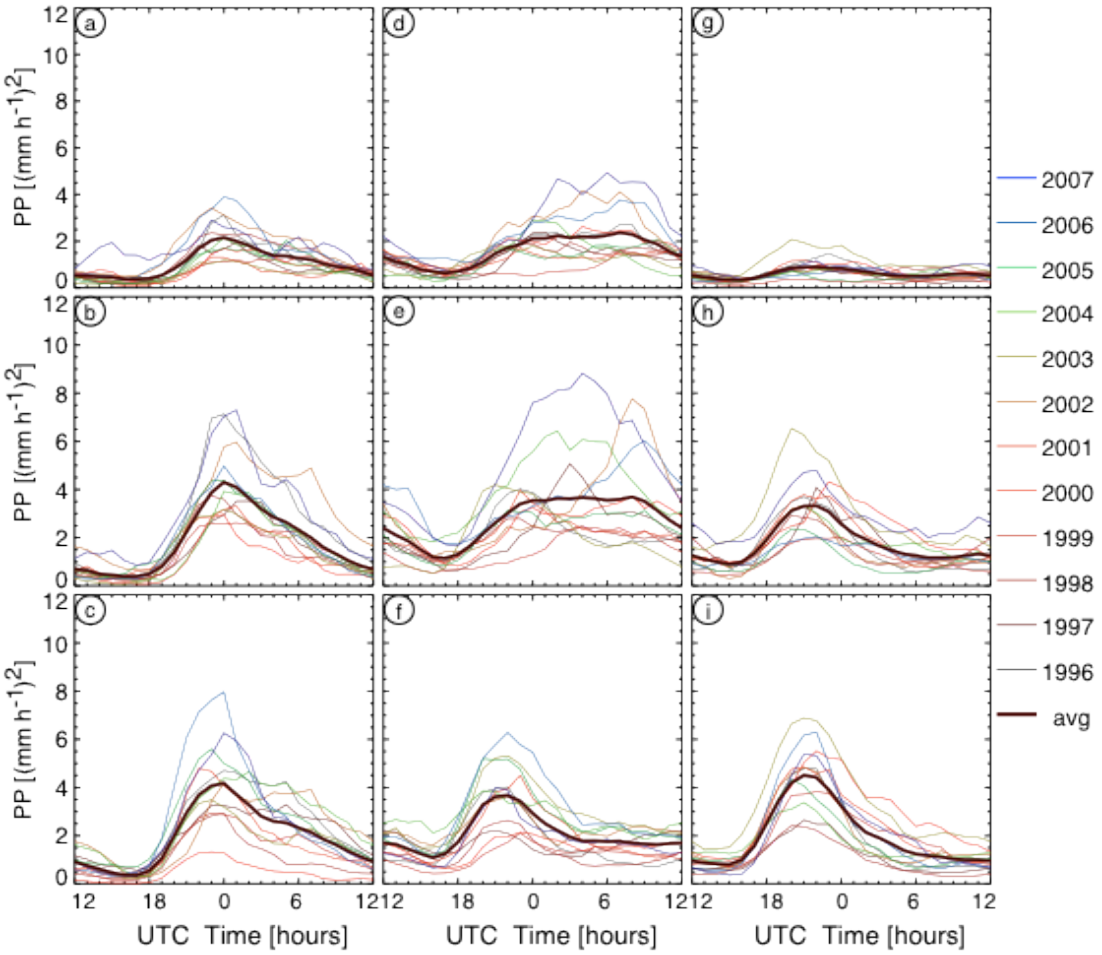

Figure 3.11: Idem fig. 3.7 but for the month of August.

3.3 Interannual variability of PP over the different sub-domains

The yearly distribution of the diurnal cycle of PP in the 1996 – 2007 period and its interannual variance are analyzed in this section. The interannual variance of PP is a useful quantity to evaluate, especially since it provides a measure of the variability of the annual PP around its climatological value. It is calculated as

$$\frac{1}{n}\sum_{i=0}^{n-1}\left(PP_i(x,y,t_d)-\left\langle PP(x,y,t_d)\right\rangle\right)^2 \qquad (3.1)$$

where x is longitude, y is latitude, t_d is the hour of the day, n is equal to 12, representing the 1996 – 2007 period, and $\langle PP \rangle$ is the average of PP in this time period.

3.3.1 Summer season analysis

The maximum of the yearly average summer PP over the NE, CW, and southern sectors occurs at 00Z for every year analyzed. However, its magnitude varies significantly and, therefore, large variance values are found at this time over these sectors (Figs. 3.7 and 3.12).

Another interesting feature of these regions is the little to no yearly-variation in the time and magnitude of the minimum summer PP though the period (Fig. 3.7). Thus, from 15Z to 17Z the variance values over these sectors are extremely close to zero (Fig. 3.12).

Summer PP variance over the NW sector has a different behavior when compared to most sectors, with the variance maximum of 0.25 $(\text{mm h}^{-1})^2$ occurring at 05Z. This difference appears to be related to the varying yearly decay times of the summer PP over the region (Figs. 3.7a and 3.12a).

With respect to the eastern sectors, it is interesting to note the fast decrease of the summer PP variance after 22Z over the SE sector, indicating that the decay of the summer average PP over this region does seem to present a strong variation within the climatology (Fig. 3.12i). On the other hand, three different variance maxima are present during the summer season over the CE sector. The most prominent one occurs at 20Z in association with the different magnitudes of summer PP during each year. However, the other two maxima, (at 01Z and 06Z) mainly associated with the behavior of summer PP in 1998, when almost two times greater-than-average values of PP are present (Figs. 3.7h and 3.12h).

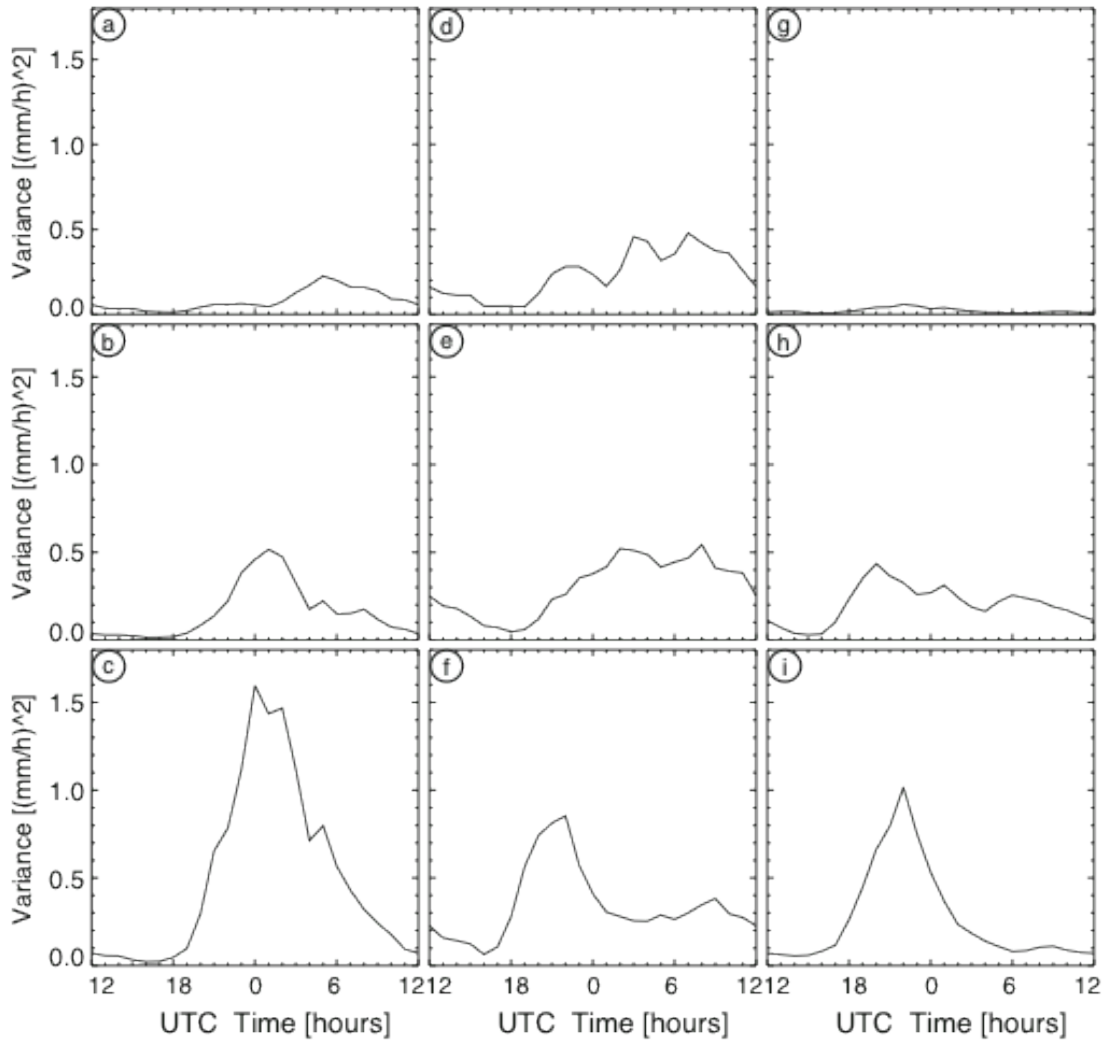

Figure 3.12: Diurnal cycle of summer variance of PP for the 9 sub-domains depicted on fig. 3.1.

Over the central longitudes the diurnal distribution of the summer PP variance is more complex. In particular, over the SC sector, the summer PP variance has a clear maximum at 22Z, in connection with the different magnitudes of the maximum PP during the different years (Figs. 3.7f and 3.12f). A secondary variance maximum occurs at 09Z, not only associated with the large spread around the mean PP but also with the particular high value of the summer PP reached in 1998 (Figs. 3.7f and 3.12f).

Over the CC and NC sectors, summer PP can have an afternoon or nighttime maximum, a broader region with high values throughout the day or two separate maxima depending on the year (Figs. 3.7d and 3.7e). For example, over the CC sector, summer PP in 2007 yields its maximum value at 01Z, in 2002 at 08Z; in 2006 there are two maxima of equal importance (one at 23Z and another one around 08Z), and in 2005 high values of summer PP are produced from 21Z to 09Z (Fig. 3.13a). Comparable patterns of summer PP also occur over the NC sector (Fig. 3.13b). Therefore, it is interesting to note that the variance of summer PP over these regions mainly corresponds to different behaviors of the summer rainfall field for different years (Figs. 3.7d, 3.7e, 3.12d and 3.12e).

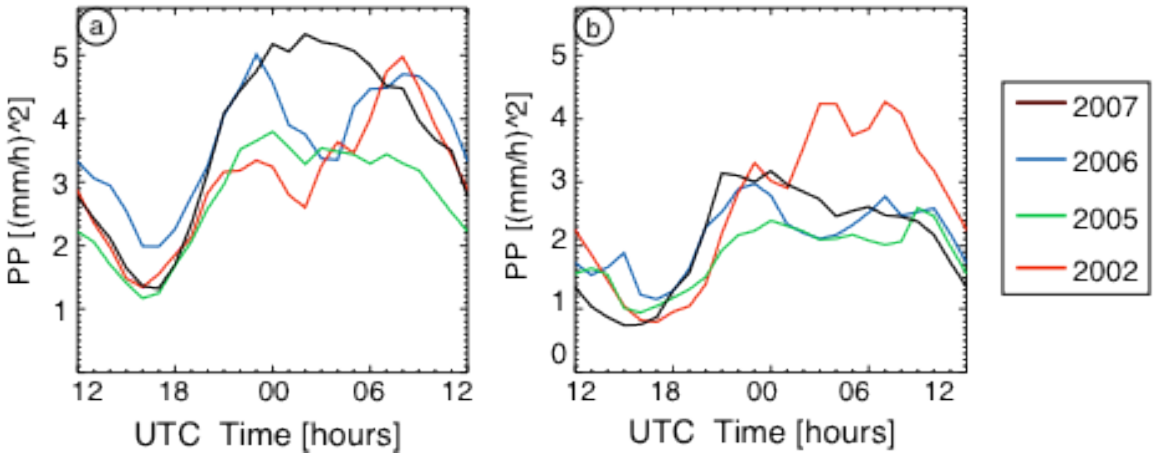

Figure 3.13: Summer average PP for the year 2002 (red line), 2005 (green line), 2006 (blue line) and 2007 (black line) average over the CC (left panel) and NC (right panel) sectors.

In summary, over most sectors the summer average PP pattern remains very similar for the 12-year period, with interannual variability tending to occur in clear association with the different magnitudes of the maximum PP during the summer season for each year. However, over the central longitudes the

maximum variability is mainly related to the behavior of the summer PP, which clearly depends on the year.

3.3.2 Analysis for the summer months

The monthly average of PP variance is always larger than for the summer average (Figs. 3.12 and 3.14). This is related to the greater variability of the monthly average PP, which is eliminated by smoothing the field to produce the summer average (Figs. 3.7 and 3.9 to 3.11).

The monthly average PP over the SE sector is extremely similar for each summer month; furthermore, the monthly and summer variance patterns are in very close agreement with each other for the entire 24-hour period (Figs. 3.12i and 3.14i). In this sector, the maximum variance is associated with the different magnitudes of the average maximum PP for each year (Figs. 3.9i to 3.11i and 3.14i).

By contrast, over the SW sector, the highest values of June and August PP variance are present during afternoon hours, at 00Z (Fig. 3.14c). However, the maximum of July variance (1.3 $(\text{mm h}^{-1})^2$) occurs at night, at 06Z, due to the large spread of the average PP during the decay of the precipitation systems (Figs. 3.10c and 3.14c).

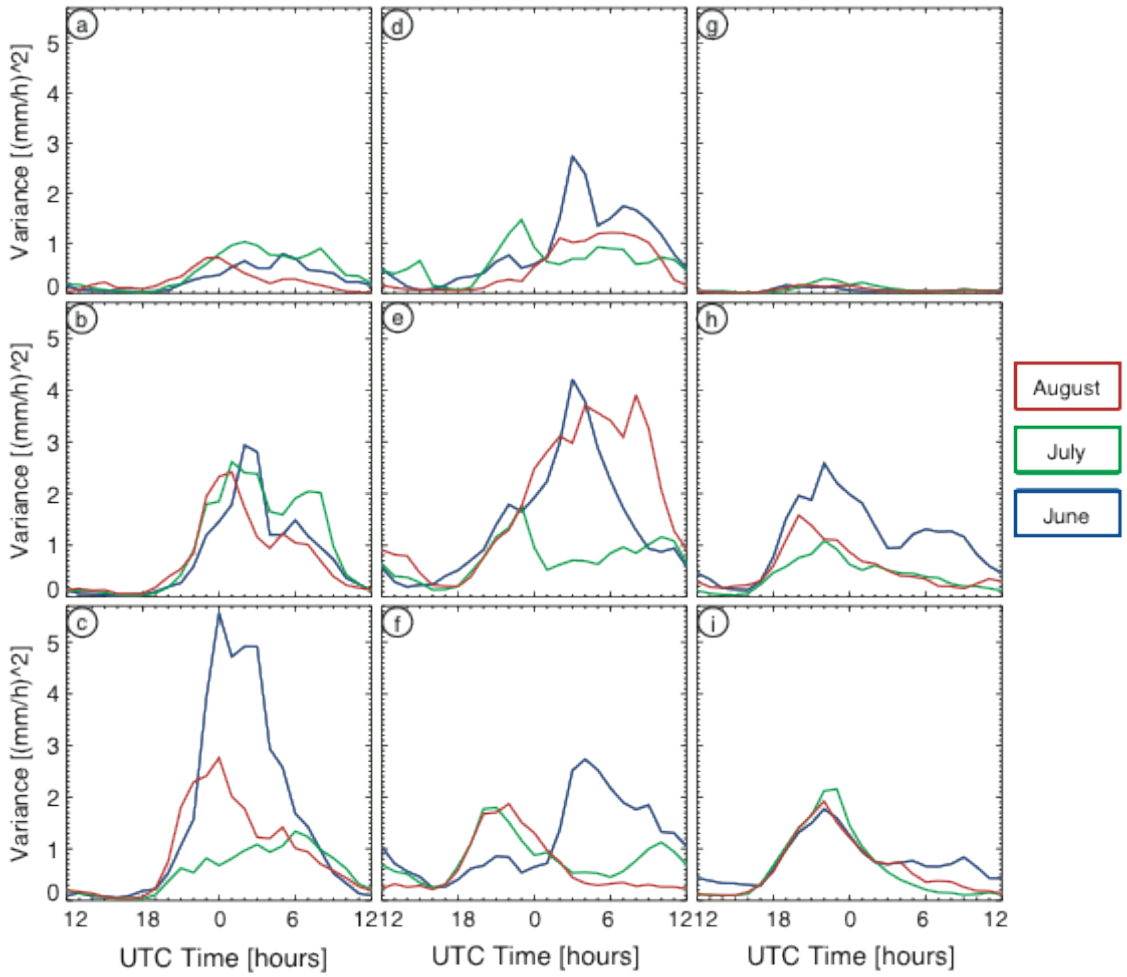

Figure 3.14: Idem Figure 3.12 but for the month of June (blue line), July (green line) and August (red line).

Over the CC sector, the variance of the June PP presents its maximum value, higher than 4.2 $(\text{mm h}^{-1})^2$, at 03Z (Fig. 3.14e). This maximum is mainly related to rainfall activity in 1998, when PP during night hours almost doubles its 12-years average (Fig. 3.9e). From 00Z to 09Z, August variance also presents high values over this sector, greater than 3 $(\text{mm h}^{-1})^2$, but with three local peaks embedded in it (Fig. 3.14e). An explanation for these maxima can be found in the behavior of rainfall activity during specific years. The maximum at 02Z is primarily associated with the precipitation pattern in 2005 and 2007; the maximum at 04Z is closely related to the years 1997, 2005 and 2007; and the maximum at 08Z, to the years 2002, 2006 and 2007 (Fig. 3.11e).

Similarly, the variability of July PP is mainly related to different patterns of the precipitation field over this region; however, its maximum variance occurs during the afternoon, at 23Z (Figs. 3.10e and 3.14e).

Over the SC sector, July and August PP has a maximum variance during the afternoon, August PP variance is related to the large spread around the mean value, whereas July variance is mostly related to the different patterns of the monthly average PP (Figs. 3.11f and 3.14f). By contrast, the average June PP yields a maximum variance during the night, essentially as a response to the behavior of PP in 1998 but also to its large spread around the climatological PP (Figs. 3.11f and 3.14f).

Therefore, the variance of summer PP over the SC sector corresponds to a combination of different monthly characteristics of the precipitation field. The nighttime summer variance is mainly related to June variability, whereas the afternoon summer variance is associated with July and August variability (Figs. 3.12f and 3.14f).

In a similar manner, the high variance values of summer PP over the NC sector also correspond to a combination of monthly characteristics of the precipitation field. The high summer variability at night is mainly associated with the behavior of June PP, whereas the summer variability during afternoon hours is connected to July PP (Figs. 3.12d and 3.14d).

Therefore, the variability of the climatologically-averaged PP derives from at least two very distinct sources, the different magnitudes of the maximum yearly PP and the different monthly and yearly characteristics of the diurnal cycle of PP. The former factor is important over most of continental U.S., whereas the later factor is mostly associated with the behavior of rainfall activity over the Central Plains. Hence, the analysis provided here for the Central U.S. should be considered as the climatological-average situation over

the region and not as a representative of the common behavior of PP during the summer season.

Finally, it is important to note that the average rainfall activity for some specific years, such as in 1998, behaves differently than for most other years, especially during June. However, the aim of this work is to present a complete climatology of precipitation for the 1996-2007 period. This includes the year 1998, which was an extreme outlier in the June average and probably greatly influencing the summer average.

3.4 Hovmöller analysis of the second moment of precipitation

The diurnal cycle of precipitation is a multivariable phenomenon. Therefore, it is necessary to reduce the number of dependant variables associated with the precipitation field in order to analyze its behavior in a comprehensive manner. In sections 3.2 and 3.3, the average in latitude and longitude over 9 sectors eliminated the dependence on these two variables. However, in this section, meridional and zonal hovmöller are computed, which entails, averaging only in 1 spatial dimension and analyzing the behavior of the precipitation field as a function of time and space is analyzed (Hovmöller, 1949). Hovmöller diagrams are commonly used for plotting data to highlight the propagation of a certain feature in time. [For further information in the hovmöller calculations, see Appendix A].

3.4.1 Summer season analysis

Figure 3.16 shows the latitudinally-averaged summer PP as a function of longitude and time of the day for the 3 domains shown in Fig.3.15a.

During the summer season the beginning of light precipitation [PP bellow 2 $(\text{mm h}^{-1})^2$] is in phase with the solar time over the 3 domains analyzed (Fig.

3.16). This indicates the relevance of the solar forcing in the initiation of summer precipitation systems. Its importance can also be seen in the maximum of rainfall activity, since the summer maximum PP occurs at almost the same solar time at every longitude (Fig. 3.16).

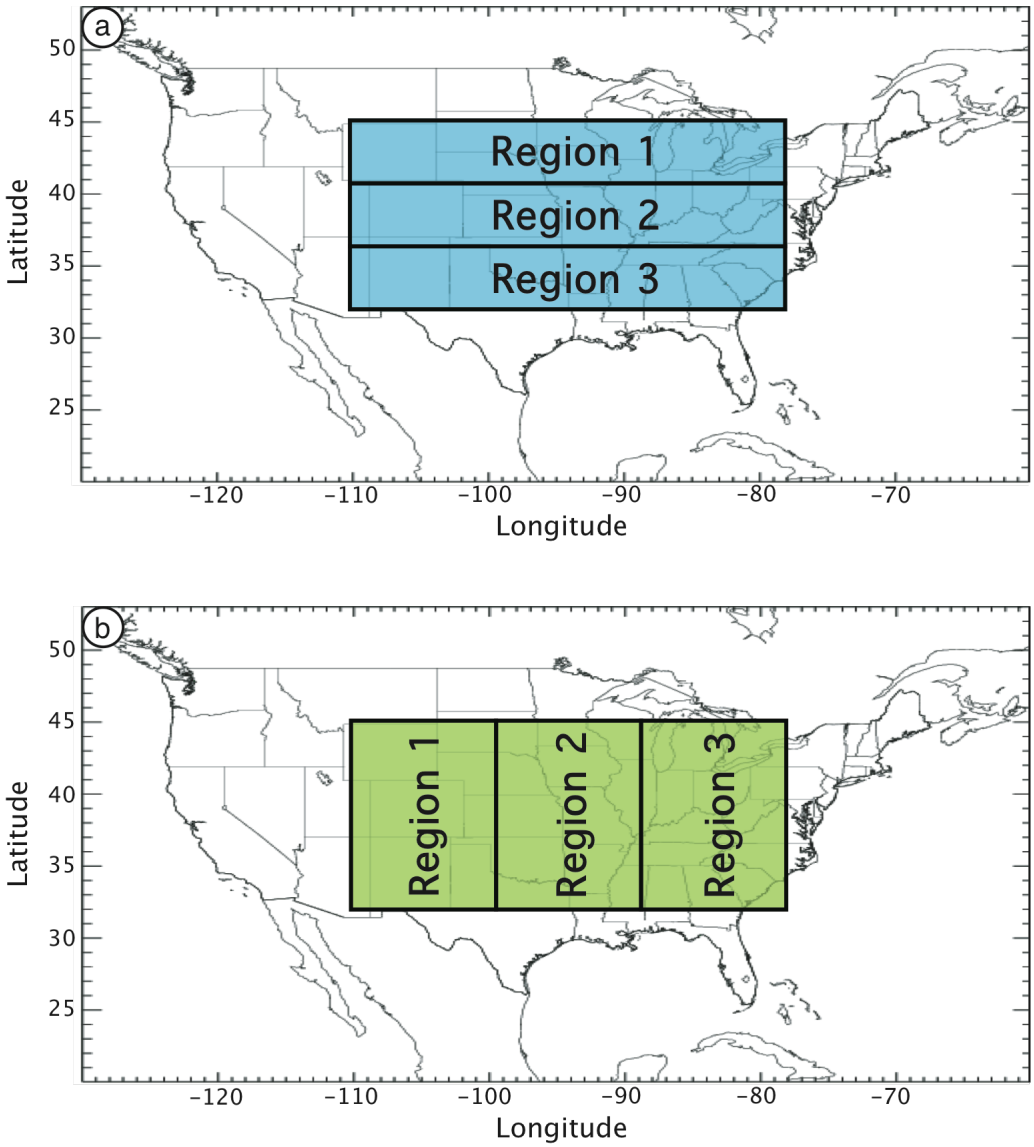

Figure 3.15: Regions where the average for the longitudinal (shaded blue areas in the upper panel) and latitudinal (shaded green areas in the lower panel) Hovmöller diagrams were performed.

Immediately east of the Continental Divide (105W), the maximum of summer PP tilts eastward with time from the western boundary of the domain at 20Z to 96W at 14Z (Fig. 3.16). This positive tilt in the Hovmöller diagram is indicative of an eastward propagation in time of the precipitation pattern over the region.

The phase velocity at which the rainfall systems propagate varies with latitude. Greater propagation speed is found over the central band 66.2 km h^{-1} and decreases both south 62.5 km h^{-1} and north 42.5 km h^{-1} from it (Fig. 3.16). One interesting observation concerning the summer PP over the northern region is that, in comparison to the area covered over the central and southern domains, the propagation of the rainfall pattern occurs over a smaller longitudinal area (Fig. 3.16).

In agreement with what was described in Section 3.2, summer rainfall activity over the western region presents its maximum intensity during afternoon hours. Over the central and southern regions, the maximum PP reaches values higher than 7 $(mm\ h^{-1})^2$ at 00Z around 105W (Figs. 3.16b and 3.16c). On the other hand, over the northern region the maximum PP, smaller than 3 $(mm\ h^{-1})^2$, occurs further east, around 103W (Fig. 3.16a). Afterwards, these maxima tend to propagate eastward, leading to high values of PP over central longitudes at night. This pattern is in agreement with what was found for the region by Wallace 1975, Carbone et al. 2002 and Lee et al. 2007, among others.

As also mentioned in Section 3.2, the initiation of summer rainfall activity over the three latitudinal bands is quite fast. However, once the maximum precipitation value is reached, the following decrease in intensity is much slower (Fig. 3.16).

Between 94W and 82W, the summer PP presents some clear differences at each latitude. Over the southern region, the maximum PP, smaller than

5(mm h^{-1})^2, occurs around 21Z and remains stationary over the region (Fig. 3.16c). On the other hand, the maximum PP over the central latitudes, smaller than 4(mm h^{-1})^2, presents a westward propagation in time from 84W at 16Z to 92W at 02Z (Fig. 3.16b). Finally, in the northern latitudes, the summer PP has values smaller than 2(mm h^{-1})^2 over most of the region with no preferred time for a maximum (Fig. 3.16a).

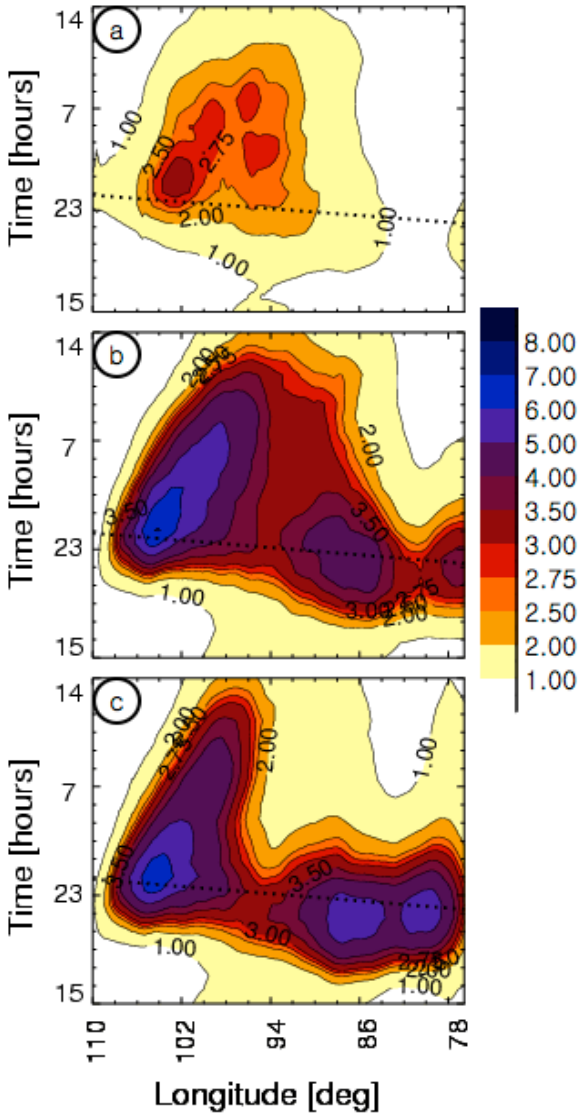

Figure 3.16: Hovmöller diagrams of summer season PP latitudinally-averaged over the northern region (Region 1 in Fig 3.15a) in the upper panel, over the central region (Region 2 in Fig 3.15a) in the middle panel and over the southern region (Region 3 Fig. 3.15a) in the bottom panel. The 1800 solar time is also indicated by the dotted black line.

The pattern of summer PP over the northern latitudes is more homogeneous than over the central and southern regions. Between 98W and 94W, two isolated PP maxima are present after 02Z (Fig. 3.16a). Both maxima are found around 94W with no obvious propagation in time (Fig. 3.16a).

It is interesting to note that the high values of summer PP at night over the NC and CC sectors (Figs. 3.7b and 3.7e) seem to have two different origins. Over the NC sector it appears to be related to local rainfall activity over the region (Fig. 3.16a), whereas over the CC sector it seems to be associated with rainfall systems propagating from the east (Fig. 3.16b).

It is also important to note that the asymmetry of the summer average PP around the time of the maximum (mainly found over the western longitudes) seems to be related to the eastward propagation of summer precipitation systems. The area where the average for the western sectors was done includes a part of the region where the systems propagate. Therefore, the eastward propagation of these systems leads to the slow decay of the average PP after its maximum value is reached (Figs. 3.7a to 3.7c and 3.16). The much slower decay of the summer average PP over the CW sector is related to the higher values of summer PP that propagate eastward over the central latitudes (Figs. 3.7d and 3.16b).

Figure 3.17 shows the longitudinally-averaged summer PP as a function of latitude and time of day for the 3 domains shown in Fig. 3.15b. The timing of the maximum and minimum summer PP over the eastern longitudes does not seem to depend on latitude, the moment of maximum rainfall activity occurs around 22Z and of minimum around 15Z (Fig. 3.17a). However, the amplitude of the diurnal cycle of summer PP greatly depends on latitude. Summer PP over this region gives a maximum value, higher than 5 $(\text{mm h}^{-1})^2$, over the

southern boundary of the domain and decreases northward with time, with values smaller than 1 (mm h^{-1})^2 north of 42N (Fig. 3.17a).

Almost the entire central longitudinal band is covered with summer PP values higher than 1 mm h^{-1} for the entire 24-hour period (Fig. 3.17b). An important distinction for this region is that there are two maxima of PP, the first over the southern edge of the domain (around 22Z) and the second one over the central part of the domain (around 37N) at 00Z (Fig. 3.17b). However, the most important characteristic of the central longitudes is the difference in the behavior of the summer PP pattern during the afternoon and night hours. Summer PP presents a northward propagation with time until 03Z over almost the entire domain. Afterwards, summer PP remains stationary in the area with values above 3.5 (mm h^{-1})^2 between 43.5N and 37.5N from 22Z to 10Z of the following day (Fig. 3.17b). The northward propagation in time of the precipitation systems occurs in connection with their eastward propagation and, therefore, the rainfall pattern over the central part of the domain is likely to undergo a northeastward propagation during its diurnal cycle (Figs. 3.16b and 18b).

The diurnal cycle of summer PP over the western longitudes has a smaller dependence on latitude than over the central longitudes. Over this region, the maximum summer PP, slightly higher than 6 (mm h^{-1})^2, occurs at 01Z around 37N and decreases to the south and more sharply to the north of this latitude (Fig. 3.17c). However, it is also important to note that the summer average PP over this region is also likely to propagate in time towards higher latitudes. Therefore, the northward and eastward propagation of the summer precipitation pattern and the high value of summer PP at night over the central region of continental U.S. agrees with what was described by several authors: even though solar forcing plays a major role in the diurnal cycle of summer precipitation it is not the only factor involved (Wallace 1975, Riley et al. 1987, Carbone et al. 2002 and Lee et al. 2007, among others).

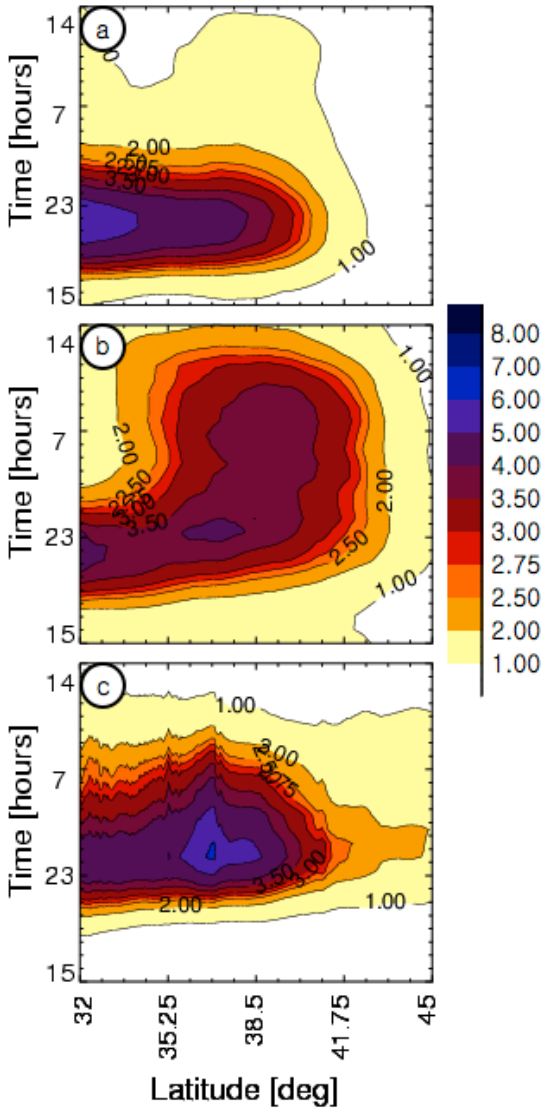

Figure 3.17: Hovmöller diagrams of summer season PP longitudinally-averaged over the eastern region (Region 1 in Fig 3.15b) in the upper panel, over the central region (Region 2 in Fig 3.15b) in the middle panel and over the western region (Region 3 Fig. 3.15b) in the bottom panel. The 1800 solar time is also indicated by the dotted black line.

3.4.2 Analysis for the summer months

The PP pattern over the northern latitudes presents some features that are common to every summer month. Among them are the behavior of light

precipitation and the position of the maximum rainfall activity near 102W in the afternoon (Figs. 3.18a to 3.20c). However this maximum PP presents different monthly characteristics. June PP presents the highest value, higher than 4.0 (mm h^{-1})^2, and clearly propagates eastward with time from 104W at 01Z to 99W at 06Z (Fig. 3.18a), the July PP maximum presents a comparable configuration but values smaller than 3.0 (mm h^{-1})^2 and propagates over a smaller region (Fig. 3.18b), and the August PP maximum occurs earlier (around 23Z) without a clear propagation in time (Fig. 3.18c).

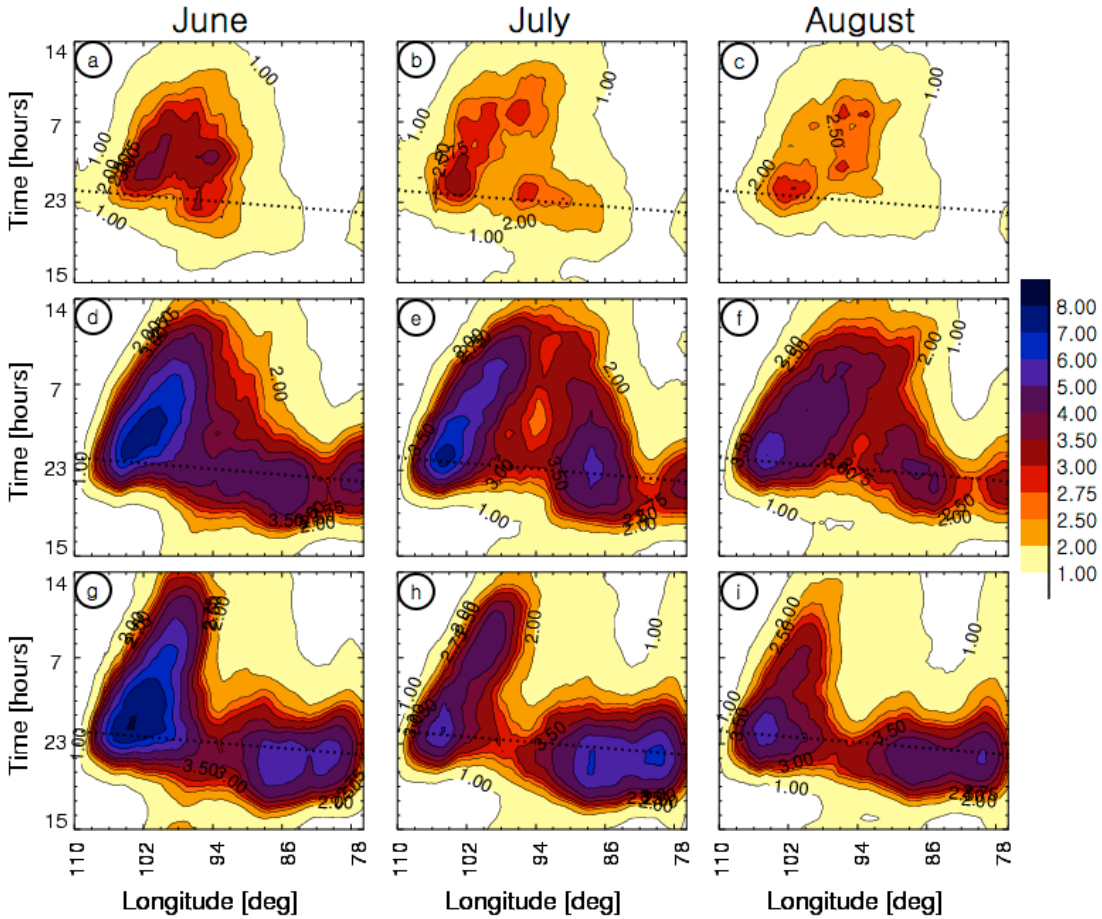

Figure 3.18: Idem Figure 3.16 but for the months of June (left column), July (central column) and August (right column).

A final remark of interest concerning this region is related to the influence of the solar forcing in the precipitation initiation and in the maximum

value achieved by PP. For every summer month, precipitation begins in association with the diurnal cycle of temperature, which occurs in phase with the solar time during afternoon hours (Fig. 3.18). However, July is the month where the solar forcing seems to have the biggest influence on the maximum PP over this region. The local July PP maximum near 95W and the high values of PP between 92W and 83W occur at a similar solar time as the maximum around 102W, and therefore, showing the importance of the solar forcing during this month (Fig. 3.18b).

The greatest differences occur over the central latitudes. In this region, June PP east of 92W does not show a clear propagation with time at night as it does for the summer season (Figs. 3.18d and 3.18g) whereas, July PP presents a well-defined maximum at 88W with a stronger westward propagation in time (Fig. 3.18e).

Regarding the changes in latitude, the largest difference between monthly and summer PP occur over the central longitudes. Around 39N, July PP presents a secondary maximum at night (Fig. 3.19e). Also around this location, August PP presents its maximum value during night hours (Fig. 3.19f). Both behaviors show the importance of nighttime rainfall activity during these months and contrast to the afternoon maximum found for the month of June and the summer season (Figs. 3.17e and 3.19e).

The western longitudinal band is another region with differences in the monthly average PP. June PP presents its maximum value of 7 $(\text{mm h}^{-1})^2$ over the southern boundary of the domain and decreases northward (Fig. 3.19f). On the other hand, July PP presents its maximum value of 6 $(\text{mm h}^{-1})^2$ at 37N and decreases north and south from this position at similar rates. These characteristics further differ from the June and summer PP, for which the maximum value occurs around 37N with a more rapid decrease to the north (Fig. 3.19h).

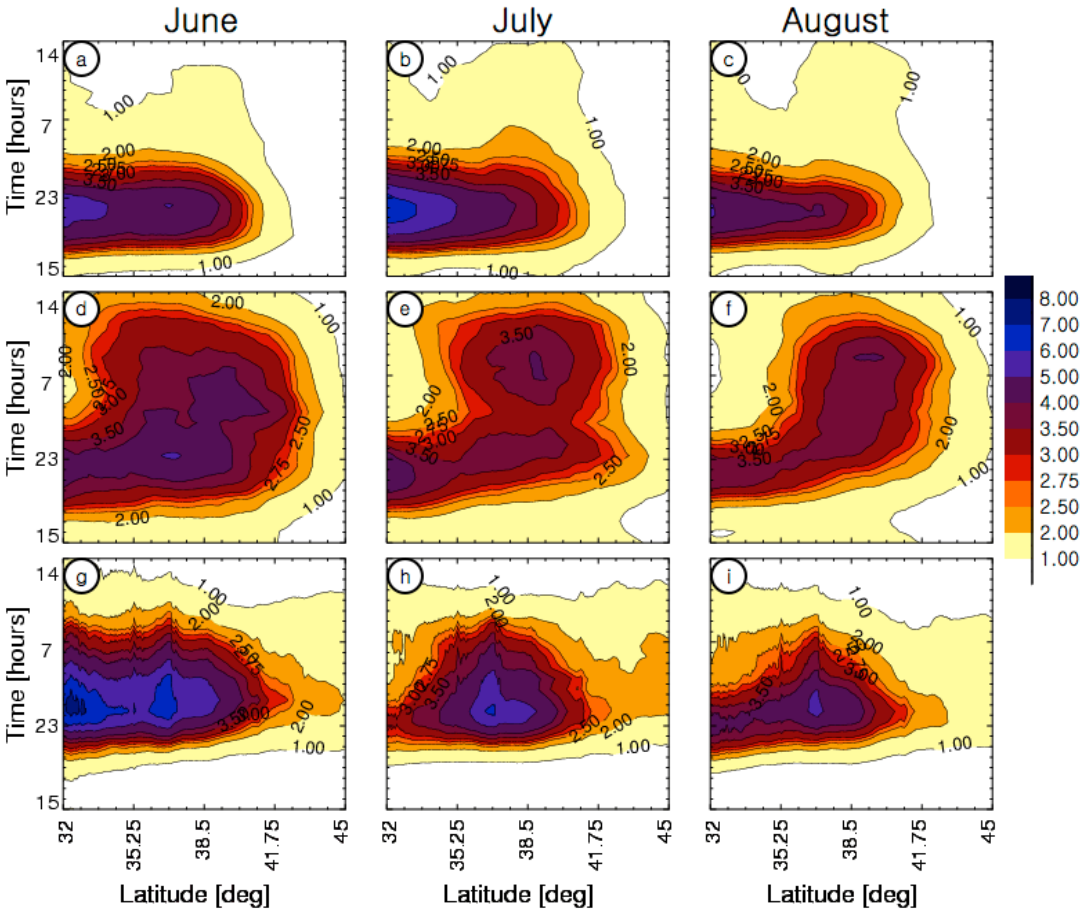

Figure 3.19: Idem Figure 3.17 but for the months of June (left column), July (central column) and August (right column).

Chapter 4

Description of precipitation field at different spatial scales

The goal of this chapter is to analyze the influence of different spatial scales in the behavior of precipitation patterns over the Continental U.S. Wavelet functions are applied to the rainfall field in order to separately analyze the influence of spatial scales ranging from 8 to 512 km in the diurnal cycle of precipitation.

4.1 Influence of spatial scales in the second moment of precipitation over different sub-domains.

4.1.1 Summer season

Figure 4.1 shows the summer average of the relative contribution of different spatial scales, ranging from 8 to 512 km, to the second moment of precipitation (RPP as defined by Eq.5).

The summer RPP at 8 km presents a well-defined distribution, with its maximum contribution occurring during the afternoon (between 18Z and 19Z) over every sector (Fig. 4.1 and Table 4.1). However, the time of its minimum influence varies depending on the sector analyzed, ranging from 06Z over the SW, CW and CC sectors to 12Z over the SE and CE sectors (Fig. 4.1 and Table 4.1). The greatest influence of RPP at 8 km occurs over the western sectors, presenting values higher than 21.1 % for the entire diurnal cycle (Figs. 4.1a to 4.1c and Table 4.1). However, the magnitude of this contribution depends on latitude; the greatest value (22.5 %) occurs over the SW sector and decreases northward, reaching 20.5 % over the CW sector and 19.3 % over the NW sector

(Table 4.1). Over the eastern region, summer RPP at 8 km presents a similar configuration compared to the western sectors. However, the greatest influence on this scale occurs over the NE sector, where summer RPP reaches values higher than 18.1 % (Fig. 4.1g Table 4.1). On the other hand, summer RPP at this scale has the smallest values during the 24-hour period over the central longitudes, with its maximum contribution ranging from 16.1% over the SC sector to 13.7% over the CC sector (Figs. 4.1d to 4.1f and Table 4.1).

Summer RPP at 16 km closely resembles the distribution at the smallest scale; nevertheless, there are two clear differences: the magnitude of RPP and the timing of its maximum value. Over almost every sector the maximum values of summer RPP at 16 km are likely to occur around one hour later than at 8 km (Fig. 4.1 and Table 4.1). This is probably related to the growth of the precipitation systems in time and therefore, to rainfall at larger scales contributing more to the total precipitation later than at smaller scales. An exception occurs over the NE sector, where the maximum summer RPP at both scales occurs at the same time (19Z, Fig. 4.1g and Table 4.1). An explanation of the dynamics of this behavior is desirable but it is beyond the scope of this study. In addition, the RPP at 16 km tends to be greater than at 8 km over the entire domain (Fig. 4.1). It is interesting to note that this spatial scale (16 km) generally has the highest values compared to any scale over the NE and SE sectors and also over the western region (Fig. 4.1).

An important observation about the summer average of the RPP at 8 and 16 km is that its maximum value tends to occur around the same time as the initiation of summer PP (Fig. 4.1). This suggests that summer rainfall activity at these scales is most likely to be related to the development of precipitation systems. This is particularly apparent over the western region, where such systems are often initiated (Fig. 4.1).

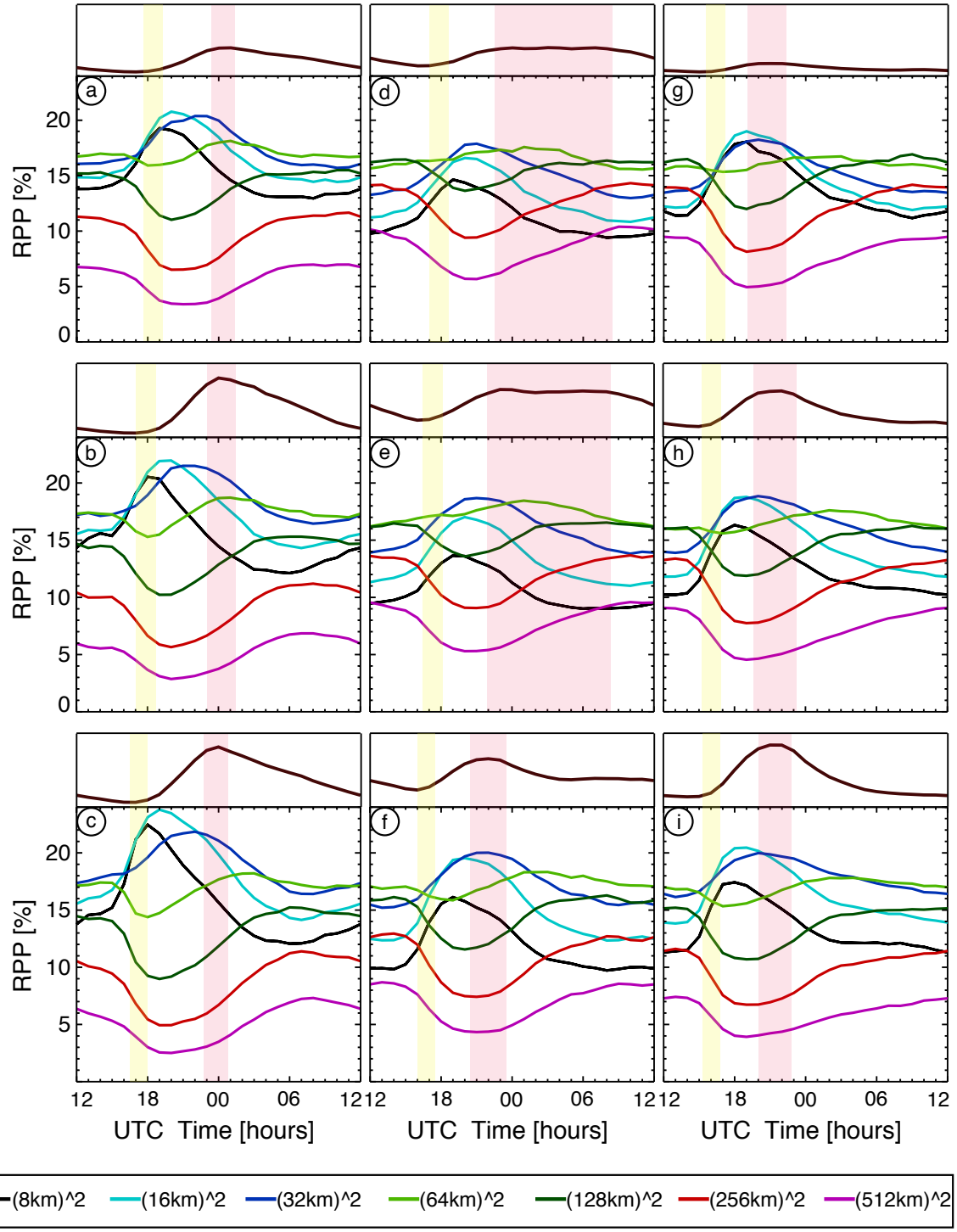

Figure 4.1: Relative precipitation power of each scale for the 12-year average over the 9 sub-domains depicted on Fig. 3.1 for the summer season. The average summer PP over each sector is shown in the upper section of each panel. The time around the initiation and maximum PP over each sector are indicated in yellow and read shaded area respectably.

	Sector / Scale	SW	SC	SE	CW	CC	CE	NW	NC	NE
Maximum RPP (%)	8 km	22.5	16.1	17.4	20.5	13.7	16.3	19.3	14.7	18.1
	16 km	23.8	19.5	20.5	22.0	17.0	18.8	20.8	16.6	19.0
	32 km	21.8	20.0	20.0	21.5	18.7	18.9	20.4	17.9	18.3
	64 km	18.2	18.3	17.8	18.7	18.5	17.6	18.2	17.6	16.8
	128 km	15.2	16.3	15.2	15.3	16.6	16.3	15.5	16.5	16.9
	256 km	11.4	12.9	11.6	11.2	13.7	13.4	11.7	14.3	14.2
	512 km	7.3	8.7	7.4	6.9	9.6	9.1	7.0	10.4	9.5
Time of the maximum RPP (UTC)	8 km	18	19	18	18	19	18	19	19	19
	16 km	19	20	19	20	20	19	20	20	19
	32 km	22	22	20	21	21	20	22	21	20
	64 km	3	3	4	1	1	2	1	1	3
	128 km	6	8	13	7	8	9	10	15	9
	256 km	7	14	13	8	10	13	11	10	9
	512 km	8	13	13	7	10	12	11	9	12
Minimum RPP (%)	8 km	12.1	9.7	11.3	12.1	9.0	10.2	13.0	9.4	11.2
	16 km	14.1	12.3	13.8	14.3	11.0	11.8	14.5	10.9	11.9
	32 km	16.4	15.2	16.1	16.5	13.8	13.9	15.7	13.0	13.5
	64 km	14.4	15.9	15.3	15.3	16.2	15.6	15.9	15.6	15.4
	128 km	9.0	11.6	10.7	10.2	13.6	11.9	11.0	13.7	12.0
	256 km	4.9	7.4	6.7	5.7	9.1	7.8	6.5	9.4	8.2
	512 km	2.5	4.3	3.9	2.9	5.3	4.6	3.4	5.7	5.0
Time of the minimum RPP (UTC)	8 km	6	8	12	6	6	13	8	8	9
	16 km	7	8	13	7	10	12	10	10	9
	32 km	8	13	13	8	10	13	10	10	12
	64 km	18	19	17	18	12	17	18	11	17
	128 km	19	20	19	19	20	19	20	20	19
	256 km	19	21	19	20	21	19	20	20	19
	512 km	20	21	19	20	20	19	21	21	19

Table 4.1: Maximum and minimum RPP and their time of occurrence at the different scales' over the 24-hour period for the 9 sub-domains shown in Fig. 3.1.

The RPP at 32 km tends to provide a very similar distribution to the one given at 8 and 16 km. However, over the entire domain, the maximum RPP at 32 km is reached between one to three hours after the maximum at 16 km (Fig. 4.1 and Table 4.1). In particular, for the southern and eastern sectors, this characteristic implies that the maximum RPP at 32 km is likely to occur around the same time as the maximum PP. This suggests the important role of this scale in the maximum intensity of summer rainfall rates in the area (Fig. 4.1). Finally, it is interesting to note that 32 km is the most influential scale over the central longitudes during afternoon hours (Figs. 4.1d to 4.1f and Table 4.1).

By contrast to the smaller scale, summer RPP at 64 km has a completely different behavior, with the maximum values occurring at night (from 01Z to 04Z) over every sector (Fig. 4.1). Additionally, the minimum RPP at this scale occurs around the time of the maximum RPP at the smaller scales (approximately at 18 Z, Fig. 4.1 and Table 4.1). Over the Midwest and Great Lakes region (NC, NE, CC and CE sectors), summer precipitation at this scale provides a more uniform distribution during its diurnal cycle, without a clear dependence on time of day (Fig. 4.1). This can clearly be seen over the NE sector, where the difference between the minimum and maximum values of summer RPP at this scale (approximately 1.4 %) is the smallest value of all scales analyzed (Fig. 4.1g and Table 4.1).

A further observation can be made about the NC and CC sectors, where the influence of the 64 km scale to PP is greater than at the two smallest scales for the entire diurnal cycle (Figs. 4.1e and 4.1g). In addition, the maximum values of summer RPP at this scale, slightly smaller than the greatest contribution made by any other scale, occurs at 01Z, in association with the highest values of summer PP over this region (Fig. 4.1e). It is further important to note that over the NW and CW sectors, RPP at 64 km also tends to have its maximum influence around the same time as the maximum PP during the summer season (Figs. 4.1a and 4.1b). This suggests that the major role of the

64 km scale occurs in connection to the maximum intensity of rainfall activity over the NW, NC, CW and CC sectors.

The distribution of the summer RPP at 128 km is similar to the one at 64 km (Fig. 4.1 and Table 4.1). However, the timing of the maximum influence of RPP at this 128 km has a stronger dependence on location, from 06Z over the SW sector to 13Z over the SE sector (Table 4.1). Also, the greatest contribution of summer rainfall activity at this scale occurs over the eastern sectors, with its magnitude decreasing to the south, from 16.9 % over the NE sector to 16.3 % over the CE sector and finally to 15.2 % over the SE sector (Figs. 4.1g to 4.1i and Table 4.1). It is also important to note that during the night and early morning hours (from 06Z to 15Z), RPP at this scale provides the predominant contribution to PP over the Midwest and Great Lakes region (Figs. 4.1d, 4.1e, 4.1g and 4.1h).

Similarly, the 256 km scale tends to be most influential over the Midwest and Great Lakes at night, with summer RPP at this scale higher than 13.4 % over the CC and CE sectors and higher than 14.2 % over the NC and NE sectors (Fig. 4.1d, 4.1e, 4.1g to 4.1h and Table 4.1). By contrast, the smallest values of RPP at this scale (smaller than 11.7%) are likely to occur over the western longitudes (Figs. 4.1a to 4.1c). It is interesting to note that during the entire diurnal cycle, the distribution of RPP at 256 km has smaller magnitudes (by approximately 3%) than RPP at 128 km (Fig. 4.1).

With respect to the largest scale analyzed in this work, the greatest values of summer RPP at 512 km (around 9%) are also likely to occur at night over the Midwest and Great Lakes region, from 09Z over the NC sector to 12Z over the eastern sectors (Figs. 4.1d, 4.1e, 4.1g, 4.1h and Table 4.1). The most significant feature of the 512 km scale occurs over the NC and CC sectors, where summer RPP at this scale is larger than at 8 km during the night and

early morning (from 07Z to 13Z, Fig. 4.1d). Furthermore, its influence is even greater over the NC sector, where it has similar values as the 16 km scale from 08Z to 10Z (Fig. 4.1d).

An important feature is that the maximum values of summer RPP at scales larger than 128 km tend to occur after the maximum values of summer PP in every sector (Fig. 4.1). This suggests that rainfall activity at these scales is more likely to be linked to the longevity of the precipitation systems.

To summarize, the moment at which summer rainfall activity at different scales contributes most to PP clearly depends on time of day and the region under analysis. It is also clear that there is no unique scale at which summer rainfall activity represents the majority of the PP for the whole domain. For every sector analyzed, the scale at which summer RPP shows the greater value does not remain as the most influential scale for the entire 24-hour period. In the SC sector, as well as in the western and eastern longitudes, the time of the maximum values of RPP is likely to occur during early afternoon hours, in connection with precipitation at the smaller scales (8, 16 and 32 km). However, over the NC and CC sectors, summer rainfall activity at 64 km provides the highest contribution to PP during the late afternoon hours. Furthermore, over the Midwest and Great Lakes region, summer rainfall activity at the two largest scales shows a greater influence to PP during evening and early morning. This indicates the importance of larger scales in the nocturnal precipitation regime over central U.S. for the summer season.

In general, the time at which the maximum contribution is achieved shifts towards later times as the scale increases, with RPP at 64 km acting as a transition regime between the behaviors of summer rainfall activity at small and larger scales. Summer rainfall activity at the smaller scales (8, 16 and 32 km) mostly contributes to PP during afternoon hours, whereas the major contribution of the larger scales (128, 256 and 512 km) to PP tends to occur during the night and early morning hours. This can be related with the

different stages of the precipitation life cycle. In particular, with the smaller scales greatly influence the onset and the maximum rainfall activity, which will organize later into larger rainfall patterns, mostly represented by the larger scales.

4.1.2 Month-to-month variability

Figures 4.2 to 4.8 show the monthly average of RPP at different scales. It is interesting to note that the behavior of RPP at 8 and 16 km is in good agreement with each summer month in most sectors (Figs. 4.2 and 4.3). The greatest month-to-month difference occurs between June RPP (with considerably smaller values) and July and August RPP (both with larger values) over the western longitudes. In particular, the 8 km scale shows the greatest discrepancies over the SW sector, with July and August RPP greater than June RPP by more than 3%, from 18Z to 01Z (Figs. 4.2a to 4.2c and 4.3a to 4.3c). On the other hand, over the central and eastern sectors, RPP at 8 and 16 km demonstrates comparable distributions for every summer month, with the monthly difference between RPPs smaller than 2 % for the entire diurnal cycle (Figs. 4.2c to 4.2i and 4.3c to 4.3i).

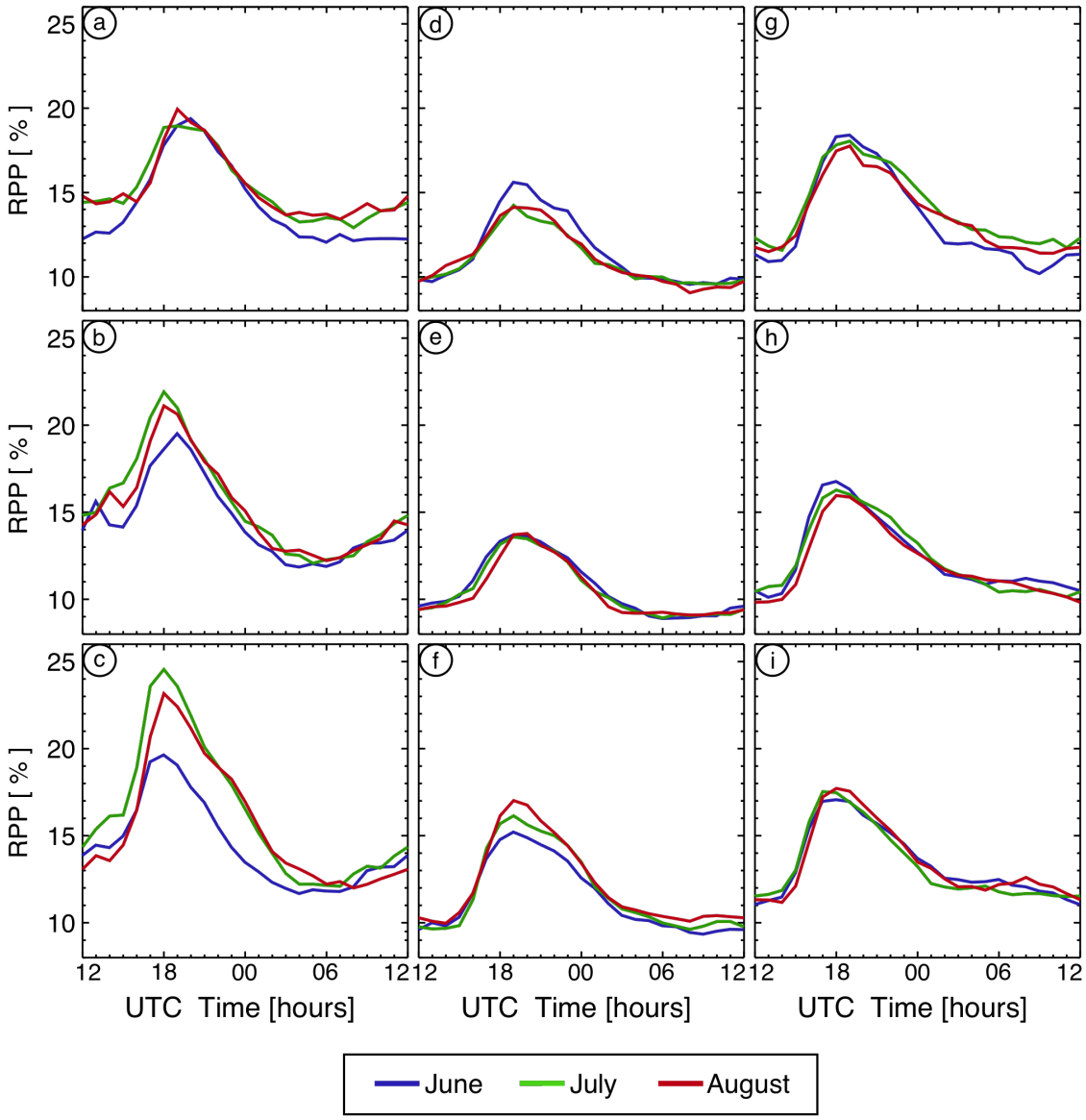

Figure 4.2: RPP at 8 km as a function of hour of day (UTC) for the summer period (black line), June (blue line), July (green line) and August (red line) for the 9 sectors depicted in Fig. 3.1.

It is further important to relate the behavior of July and August RPP at these scales with the monthly averaged PP discussed in Section 3.2.2. This indicates that the expected high values of July and August PP over the eastern

lee of the Rocky Mountains is associated with the greater contribution of rainfall activity at 8 and 16 km during these months.

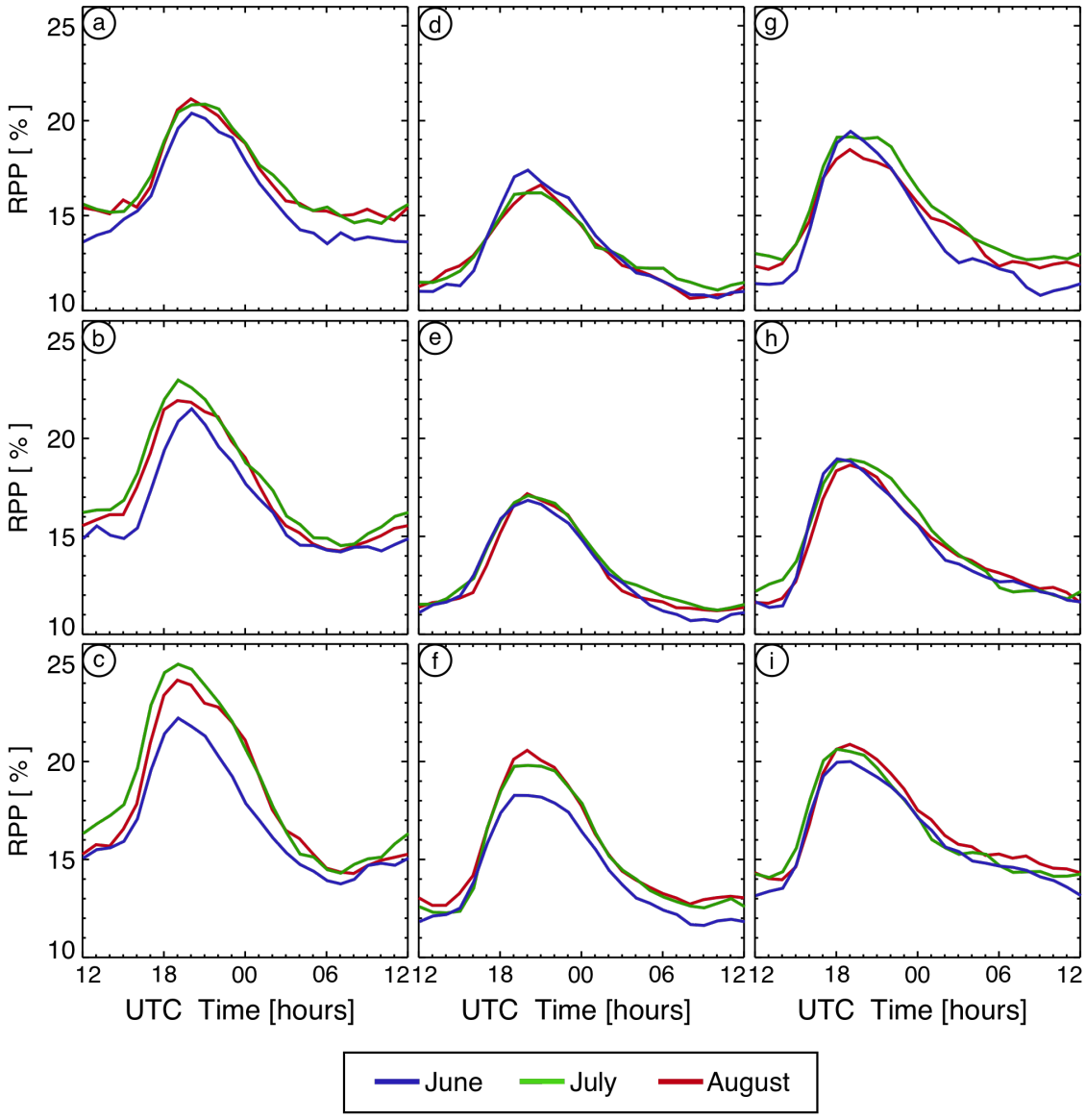

Figure 4.3: Idem Fig. 4.2 but at 16 km.

By contrast to the behavior of the smallest scales, the RPP at 32 km has similar magnitudes for each summer month over the western sectors (Figs. 4.4a to 4.4c). This is particularly clear over the SW sector, where the RPP at 32 km

is in close agreement for each month, especially around the time of the maximum value (Fig. 4.4c). The largest month-to-month difference of RPP at 32 km occurs over the NW, CC and SC sectors and over the eastern region where, July and August RPP have similar higher values in comparison to June RPP for most of the diurnal cycle (Figs. 4.4a, 4.4e and 4.4f). Furthermore, the greatest differences are found over the SC sector, where July and August RPP is greater than June RPP by at least 2 % (Fig. 4.4f). From 02Z to 13Z, July and August RPP at this scale produces considerably higher values than June RPP over the NC and CC sectors (Figs. 4.4d and 4.4e).

For most of the 24-hour period, the monthly RPP at 64 km yields the smallest values over the central and eastern sectors for the month of June. By contrast, over the SW sector June RPP has greater values (close to 2%) compared to July and August RPP from 17Z to 04Z (Figs. 4.5c to 4.5i). It is important to note that, over the NC and CC sectors, July and August RPP at 32 km and at 64 km have greater values than in June at night and in the early morning (Figs. 4.5d, 4.5e and 4.5g). This suggests that rainfall activity at these scales is mainly responsible for the nighttime maximum of July and August PP over the NC and CC sectors (Figs. 3.9d, 3.9e. 3.10d and 3.10e). In addition, the June RPP at scales smaller or equal to 64 km is likely to have smaller values than for the other summer months (with the exception of the 64 km scale over the SW sector) for most of the diurnal cycle.

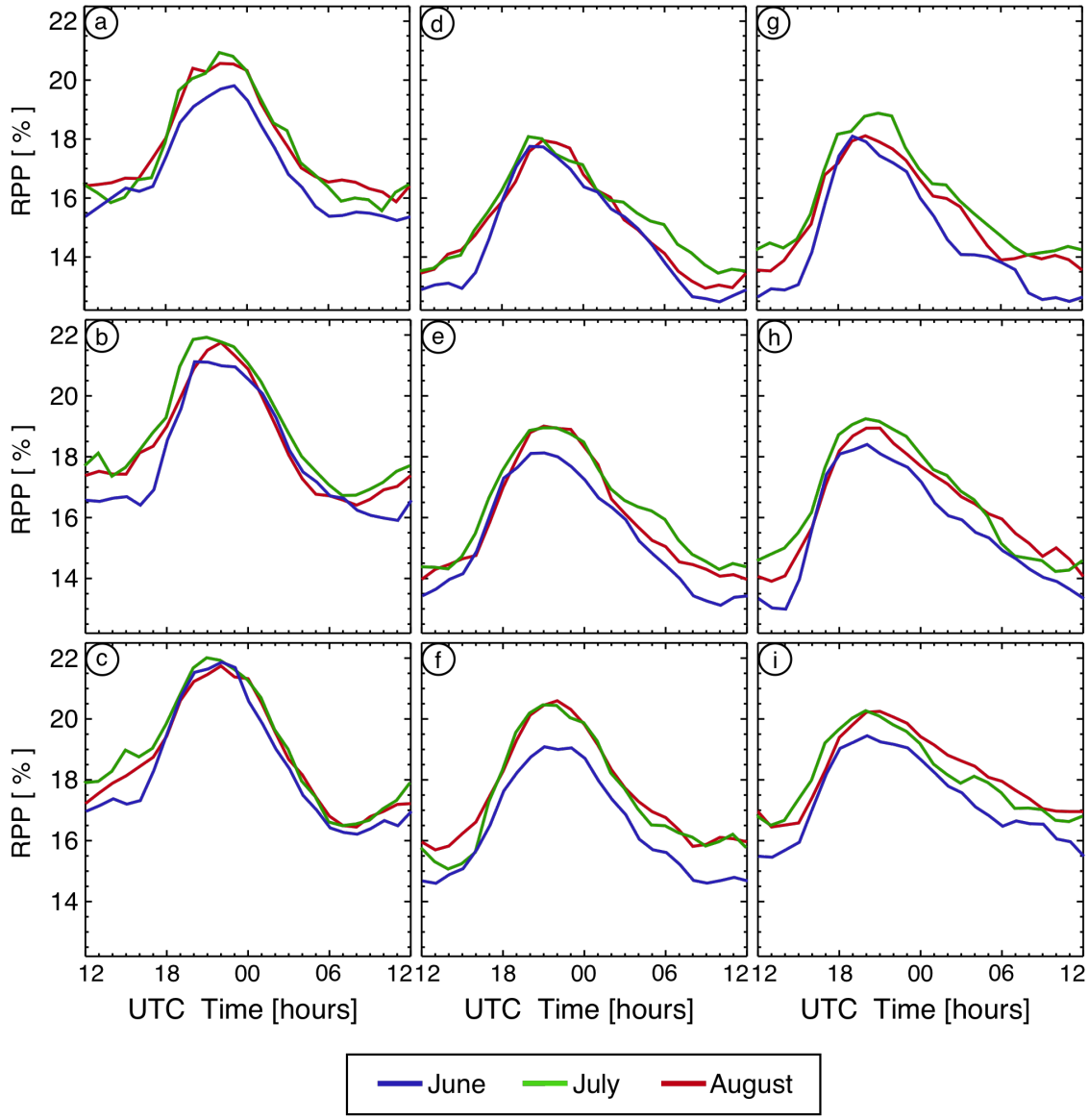

Figure 4.4: Idem Fig. 4.2 but at 32 km.

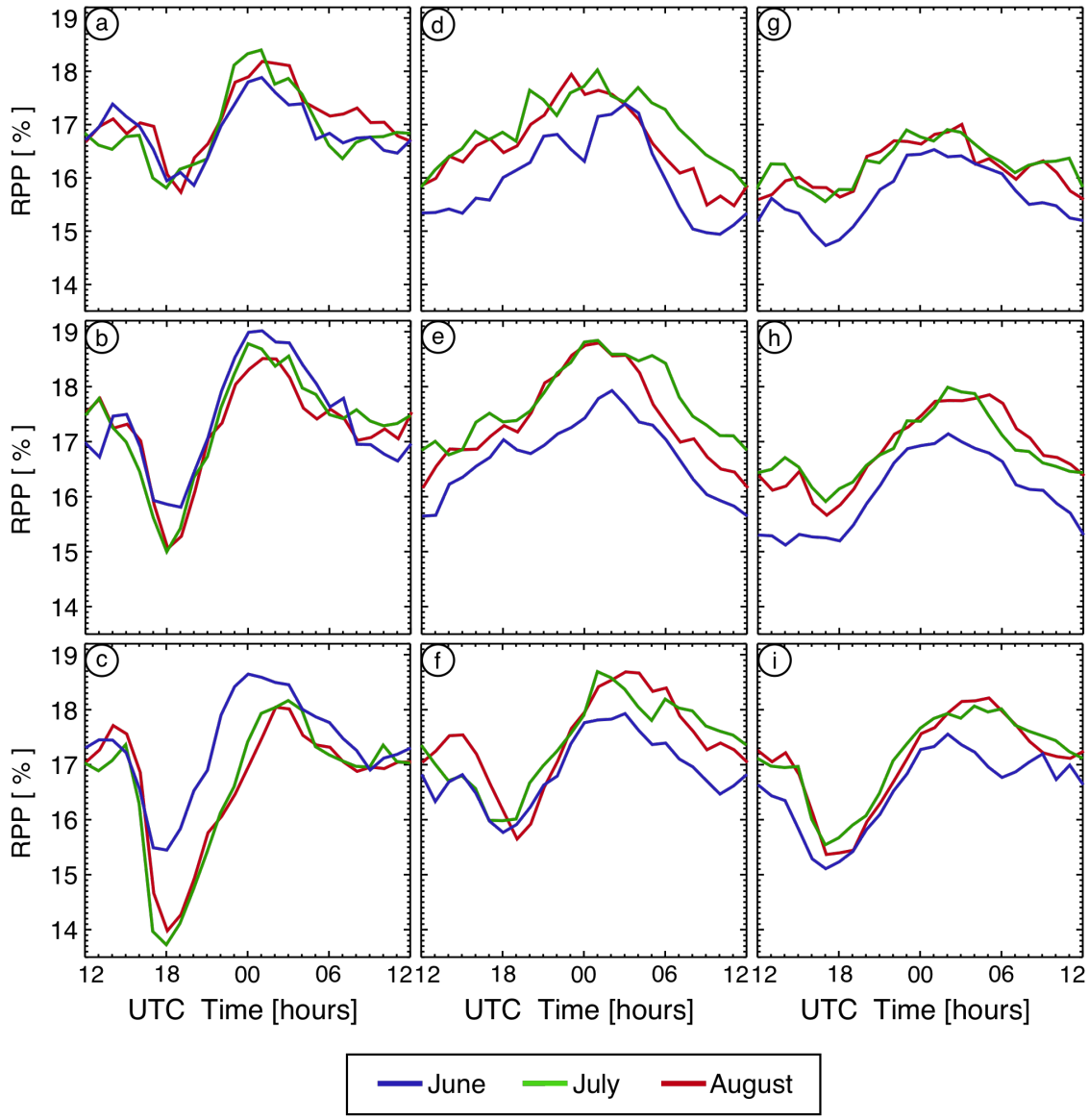

Figure 4.5: Idem Fig. 4.2 but at 64 km.

Over most sectors, the RPP at 128 km and 256 km are more similar to each other for each summer month than the small-scales pattern (Fig. 4.6). However, over the SW and SC sectors, the magnitude of the minimum RPP at these scales clearly depends on the summer month, with June RPP at both scales having greater values (close to 2 %) than July and August RPP from 18Z to 02Z (Figs. 4.6c and 4.6f).

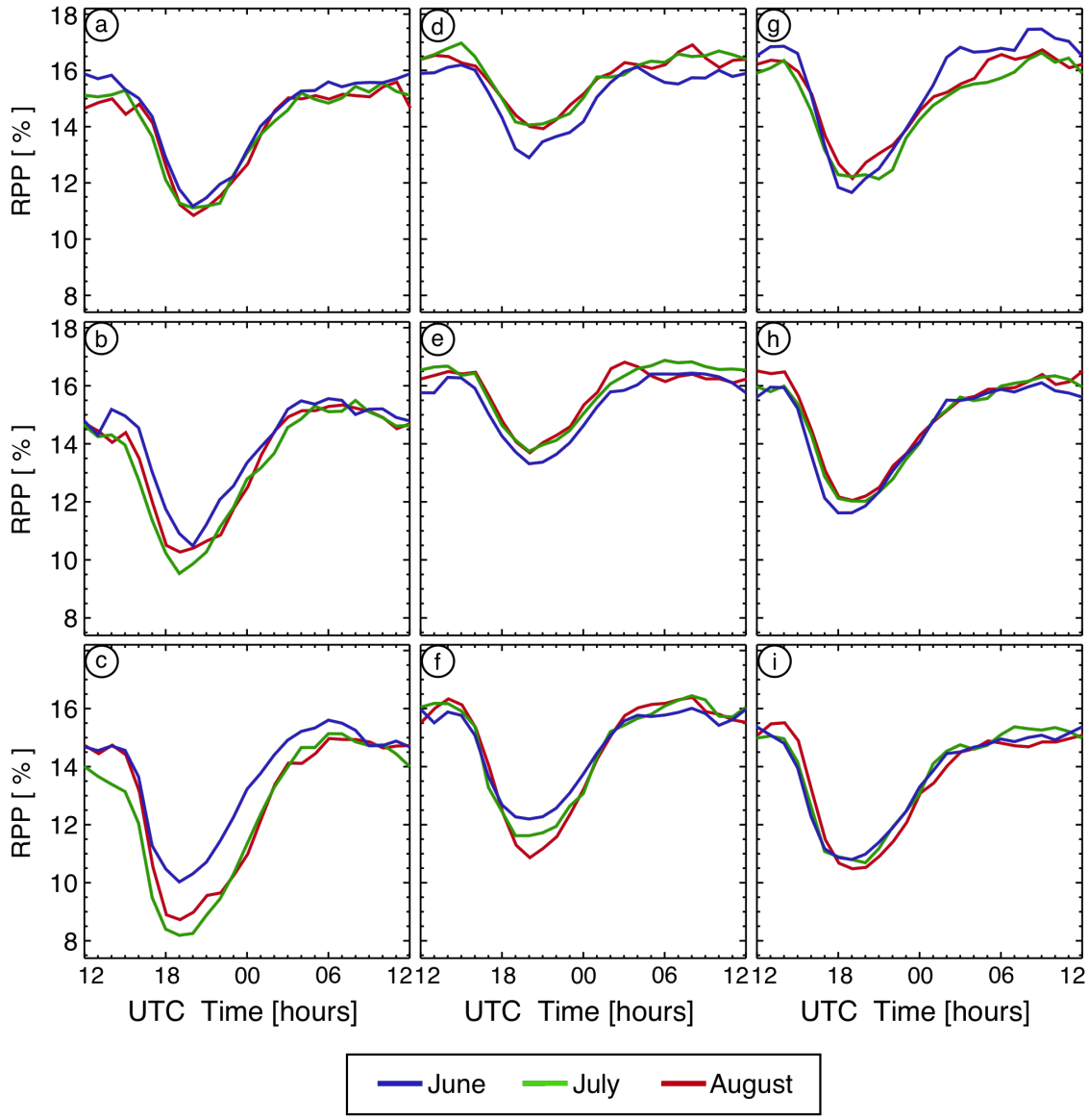

Figure 4.6: Idem Fig. 4.2 but at 128 km.

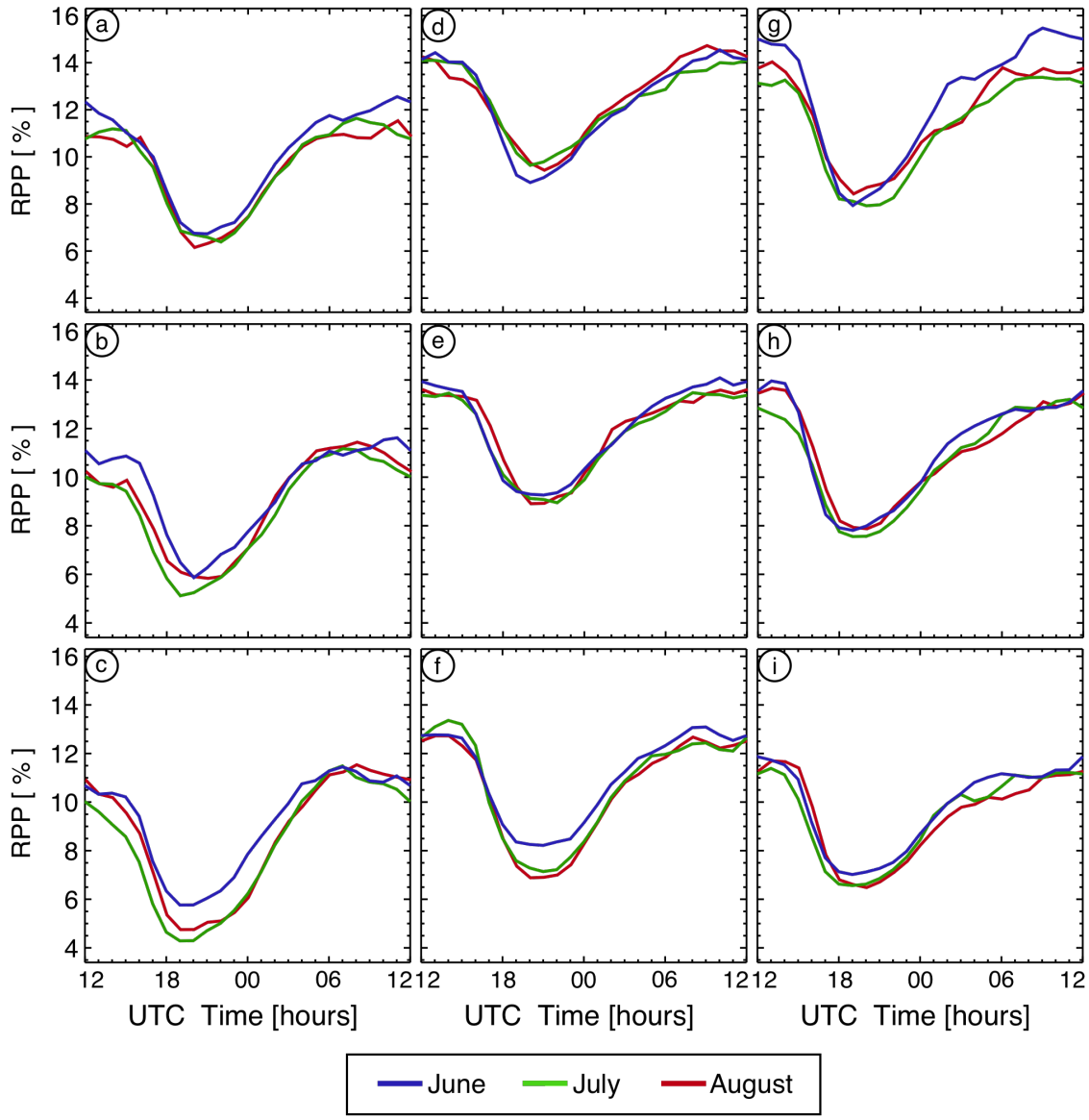

Figure 4.7: Idem Fig. 4.2 but at 256 km.

Compared to these scales, the RPP at 512 km is associated with a greater variability for each summer month (Figs. 4.8). The most significant feature of this scale is that the large month-to-month difference that occurs over the SW sector and the central longitudes, where the June RPP has higher values during most of the day (Figs. 4.8d to 4.8f).

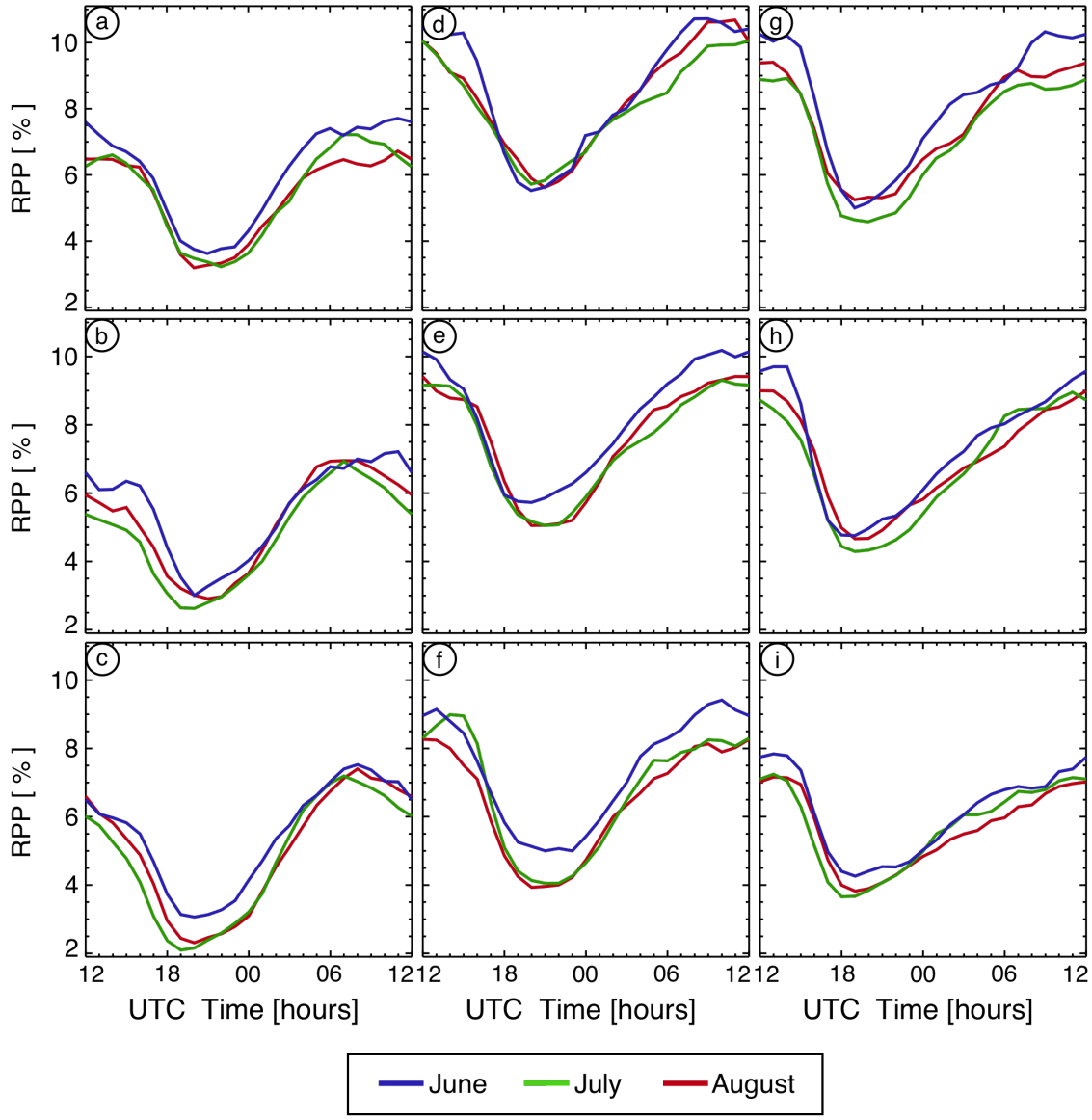

Figure 4.8: Idem Fig. 4.2 but at 512 km.

It is important to note that over the western and eastern sectors, the June RPP at scales larger or equal to 128 km is expected to have higher values in comparison to the July and August RPP. This suggests that the higher intensity of June rainfall activity, described in Section 3.2.2, is likely to be related to the influence of the large scales (128, 256 and 512 km), which are

expected to counteract the relative smaller effect that the small scales (8, 16 and 32 km) have on June's precipitation(Figs.10, 4.6, 4.7 and 4.8).

4.2 Interannual variability of RPP over the different sub-domains

Figures 4.9 to 4.12 show the annual variance of summer RPP at 16, 64 and 256 km. For clarity, the 8, 32, 128 and 512 km scales are not shown in this figure. However, the information from the omitted scales is similar to that given by the scales depicted in the figures. The variability of RPP at 16 km is comparable to the variability at the 8 and 32 km scales and therefore, representative of the variability of the contribution of the smaller scales. Similarly, the variability of RPP at 256 km is characteristic of the large-scale variability, and the RPP at 64 km represents the transition scale.

4.2.1 Summer season variability

Over most of the domain, the maximum variance of summer RPP is likely to occur in association with the small and large scales (Fig. 4.9). However, the variance of summer RPP at every scale behaves in a similar manner over the western region, with the maximum value occurring at night and in the morning (from 06 to 18Z) and its minimum during the late afternoon (from 22Z to 03Z, Figs. 4.1, 4.9a to 4.9c).

Further to the east, the variability of summer RPP strongly depends on latitude and scale. In particular, over the SE sector, RPP at large and small scales show a variance pattern for the 24-hour period, with three moments of high values present at 03Z, 09Z and at 17Z (Fig. 4.9i). The greatest variability of the RPP at small scales occurs around the 17Z maximum, whereas for the large scales it happens around the 09Z peak. On the other hand, the RPP at 64 km indicates a period (06Z to 15Z) of high variability over the region (Fig. 4.9i). Over the NW and CE sectors, the summer RPP at every scale tends be evenly-distributed in time for the 24-hour period, but with slightly higher variability

during night and morning hours (from 07Z to 13Z) in the NE sector (Fig. 4.9g, 4.9h).

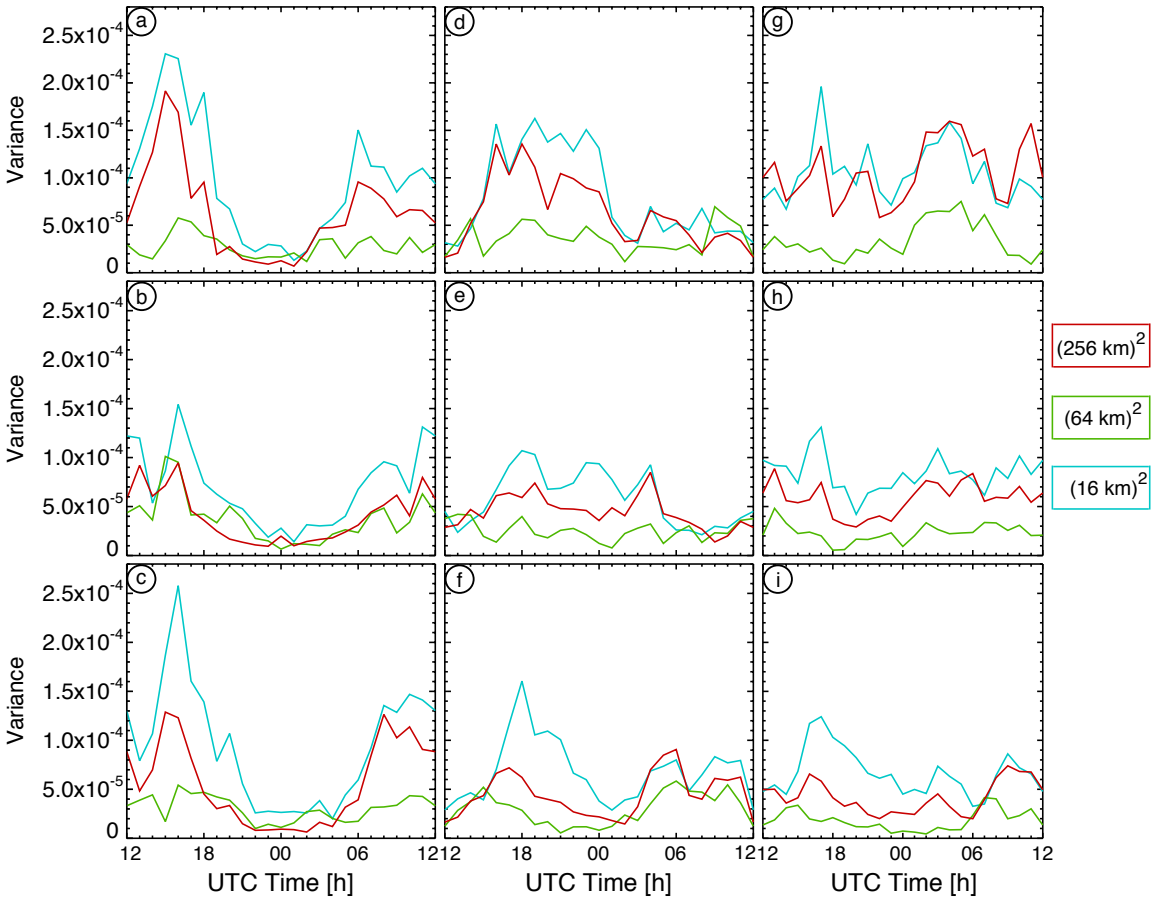

Figure 4.9: 12-years variance of summer RPP at different scales average over the 9 sub-domains depicted on Fig. 3.1.

Over the central longitudes, the main characteristics of the variability of RPP also depend on the latitude. Over the SC sector, summer RPP has two periods of high variability, one around noon (from 16Z to 18Z), with the highest variance corresponding to the 16 km scale, and another, present for every scale, from 02Z to 11Z (Fig. 4.9f). Just to the north, the RPP at most scales (except at 64 km) shows a period with high variability over the CC sector from 15Z to 05Z (Fig. 4.9e). Similarly, in the NC sector, the summer RPP at small

and large scales is associated with high variability during late morning and afternoon hours (Fig. 4.9d).

In summary, summer RPP at the transition scale (64 km) does not have a notable period of maximum or minimum variability over the course of the diurnal cycle over most sectors. By contrast, the summer RPP at small and large scales is likely to experience a similar variance pattern over the Continental U.S., with the variability maximum depending on the region. Over the eastern lee of the Rocky Mountains, the greatest variance occurs during night and morning hours, in association with the decay of summer PP. However, the greater variability of RPP over the central longitudes is likely to occur in the afternoon, in agreement with the period of precipitation intensification in this region.

4.2.2 Monthly variability

The monthly RPP at each scale has higher variance values than the summer average (Figs. 3.18 to 4.12). As mentioned in Section 3.2.3, this is probably due to the smoothing effect when performing the summer average.

The variability of monthly RPP presents some clear differences with the summer. In particular, the variance of June RPP has the greatest differences with the summer average over the NC sector. Over this region, June RPP at most scales presents two variance maxima, one during the late morning and afternoon hours and another one (not seen in for the summer average) at nighttime (Figs. 4.9d and 4.10d). Also, over the CE sector, June RPP at 16 and 64 km is likely to have high variability around 12Z, unlike the summer variance, which is evenly-distributed during the 24-hour period (Figs. 4.9h and 4.10h).

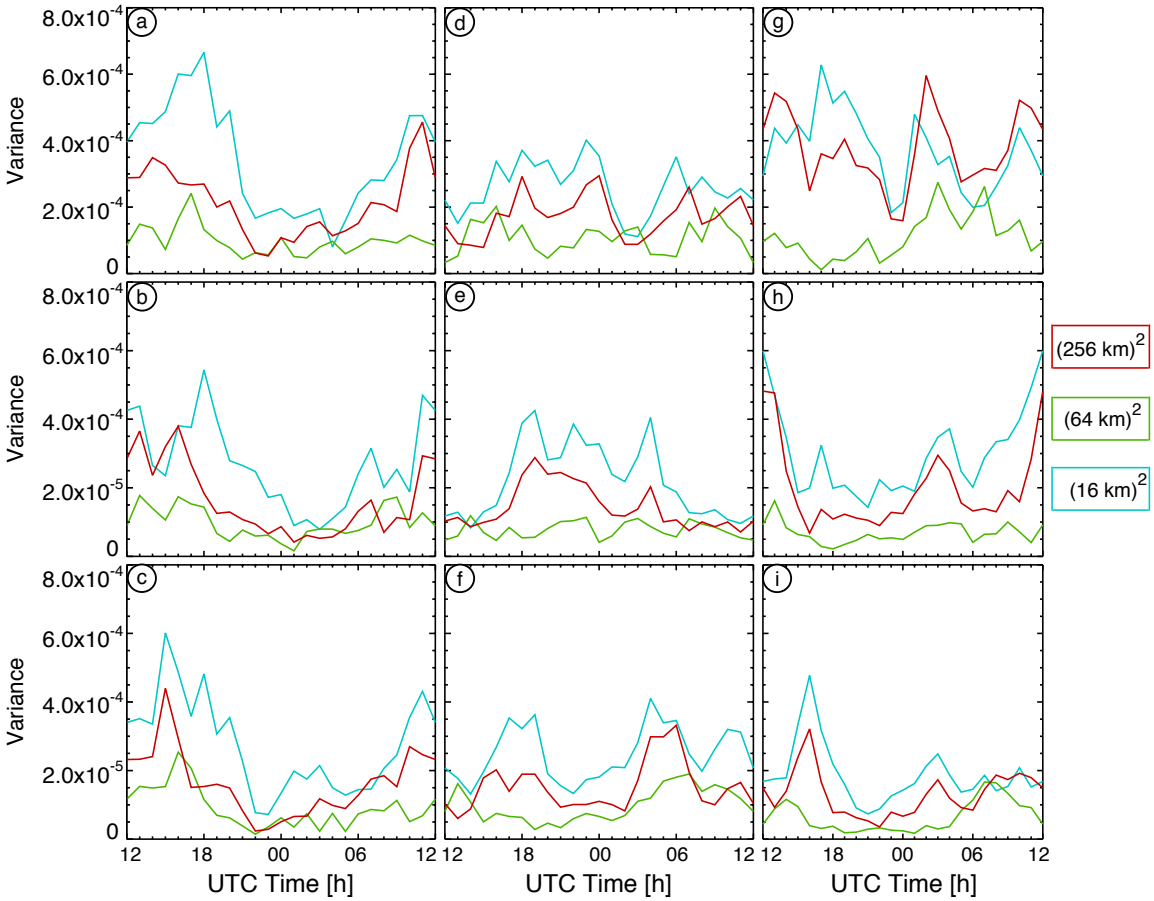

Figure 4.10: Idem Fig. 4.9 but for the month of June.

With respect to the variability of July RPP, the most notable differences between the monthly and summer averages occur over the central longitudes. Particularly over the NC sector, the July RPP at the each scale does not seem to have a preferred time for higher variability during the afternoon, as seen for the summer average (Figs. 4.11d and 4.11e). On the other hand, July RPP over the SC sector has minimum variability from 02Z to 07Z (a period when summer RPP has its highest variability for most scales, Figs. 4.9g and 4.11g).

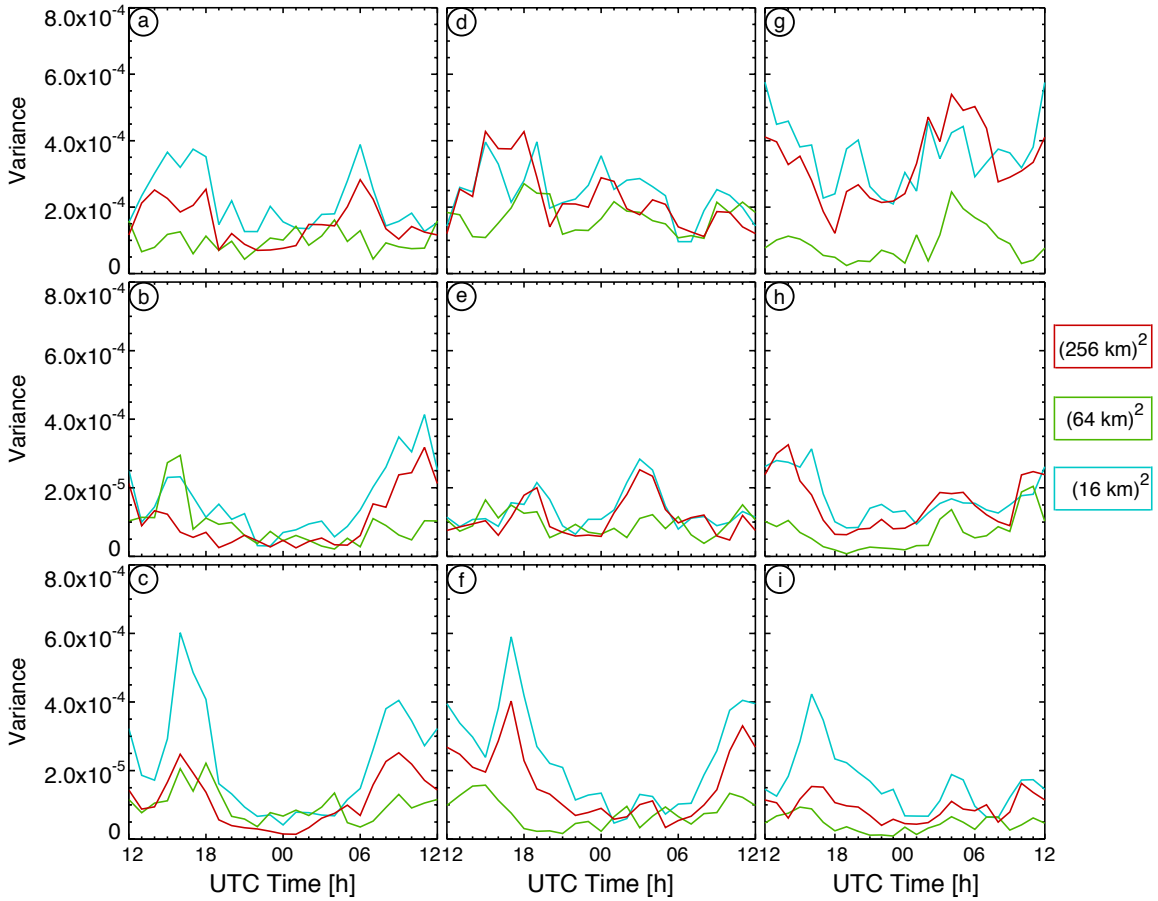

Figure 4.11: Idem Fig. 4.9 but for the month of July.

It is interesting to note that August RPP at every scale is not likely to have higher variance at night and morning hours over the SW sector. This is a clear departure from the summer average, as well as for the months of June and July, when the greatest RPP variability occurs over the entire western region (Figs. 4.9c, 4.10c, 4.11c and 4.12c). Also, August RPP further shows some clear differences with respect to the summer average over the central longitudes. In particular, the August RPP has a nighttime variability maximum over the CC sector, in contrast to the minimum summer variance present.

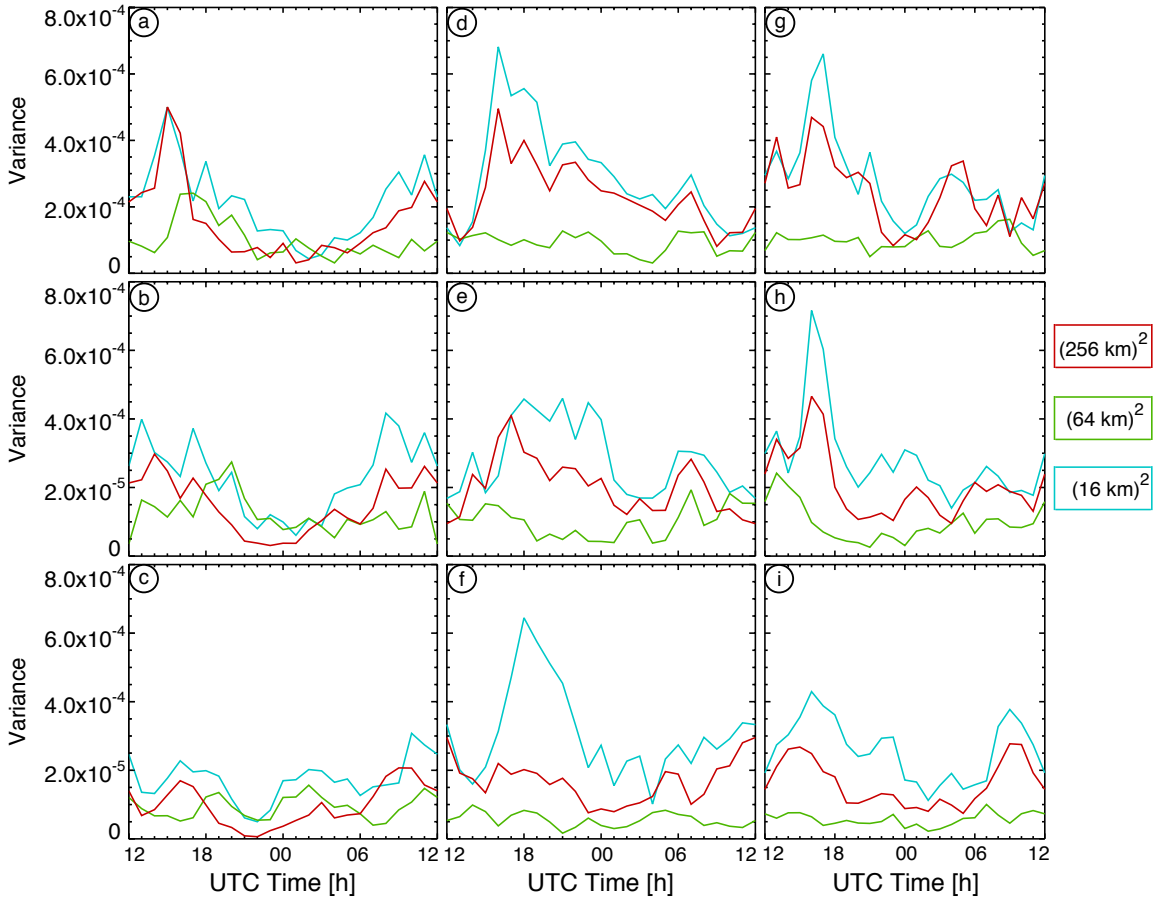

Figure 4.12: Idem Fig. 4.9 but for the month of August.

Overall, the variance pattern of RPP at most scales is very similar for each summer month over the eastern lee of the Rocky Mountains (with the exception of August RPP over the SW sector). By contrast, monthly RPP at most scales is likely to present a greater month-to-month variation over the central longitudes. Finally, it is interesting to note that the variance pattern of RPP at the transition scale is likely to be evenly-distributed in time over most regions of the Continental U.S., without showing a clear dependence on the summer month.

4.3 Hovmöller analysis of the precipitation power.

Figure 4.13 shows the Hovmöller diagram of RPP at 16, 64 and 256 km. RPP at 8, 32, 128 and 512 km is excluded from analysis here because these scales are not expected to provide further information than what can be inferred from the scales depicted in the figures. Due to the continuous behavior of RPP with scale described in the previous sections, the 16 km scale is analyzed as representative of the small scales (8 to 32 km), the 64 km of the transition scale, and the 256 km of the large scales (128 to 512 km).

4.3.1 Summer season.

The RPP at different spatial scales strongly depends on the time of day and location. As discussed in Section 4.1, RPP at small scales is likely to present largest values during late morning hours (Figs. 4.13a to 4.13c). However, in the region west of 108W, the influence of precipitation at these scales tends to persist for a longer period of time over the central and southern latitudes. In particular, for the 16 km scale, the RPP is greater than 20% over the southern and central regions from 16Z to 05Z, whereas over the northern region it is greatest from 17Z to 00Z (Figs. 4.13a and 4.13c). Therefore, over the eastern lee of the Rocky Mountains, the small scales are likely to have a strong impact in the initiation of rainfall activity over the northern region, whereas they extend their influence in time over the southern and central regions.

East of 105W, the summer RPP at small scales has its maximum influence in phase with the solar time. This provides a clear indication of the importance of the solar forcing in the behavior of rainfall activity at small scales over the region east of the Continental Divide. Afterwards, RPP diminishes in magnitude, showing the smallest value of the 24-hour period from 01Z to 15Z in the region between 100W and 89W (Figs. 4.13a to 4.13c). As a result, the high values of summer PP found during this period over the Great Plains (especially over the central latitudes) are not expected to be associated with precipitation

at 8 to 32 km (Figs. 3.15b and 4.13b). Another interesting feature of the small scales is that their influence east of 86W is more localized and with a slightly larger dependence on longitude than west of this position. Furthermore, rainfall activity at 16 km presents a region of maximum influence around 83W in the morning (from 17Z to 22Z) and slowly decreases in intensity with longitude and time (Figs. 4.13a to 4.13c).

The RPP at 64 km is also likely to show a clear dependence on longitude and time of day. The minimum values of summer RPP at this scale are likely occur during late morning and afternoon hours (from 15Z to 00Z), whereas there is no clear moment for its maximum influence over the western boundary of the domain (Figs. 4.13d to 4.13f). It is interesting to note that RPP at the transition scale shows the largest differences for each latitudinal band east of 102W. Over the northern latitudes, the summer RPP at this scale has almost constant values (between 15% and 17.5%) eastward of 102W, for most of the diurnal cycle (Fig. 4.13d). Over the central latitudes, summer RPP provides a maximum value (higher than 20%) over the region between 102W and 100W around 00Z (Figs. 3.15b and 4.13e). The RPP at this scale also has great importance over this latitudinal band (RPP higher than 17.5 %) from 23Z to 07Z bounded longitudinally from 102W to 84W. On the other hand, the maximum values of RPP at 64 km tend to shift eastward with time over the southern latitudes, influencing the region around 102W in the afternoon (around 22Z) and close to 88W in the morning (11Z, Fig. 4.13f). Hence, rainfall activity is likely to provide a different configuration over the southern latitudinal band, with a clear eastward propagation in time of high values in the transition scale over the Great Plains (Figs. 3.15c and 4.13f).

As described in Section 4.1.1, the dependence of the RPP at large scales with longitude and time has several clear differences with respect to the smaller scales. In particular, it is interesting to note that the influence of large scales in rainfall activity during morning and afternoon hours shows a similar

dependence with longitude and time as the smaller scales. However, it is the reduced influence of RPP at large scales that is expected to be in phase with the solar forcing, in contrast to the behavior of the highest RPP at the small scales (Figs. 4.13g to 4.13i).

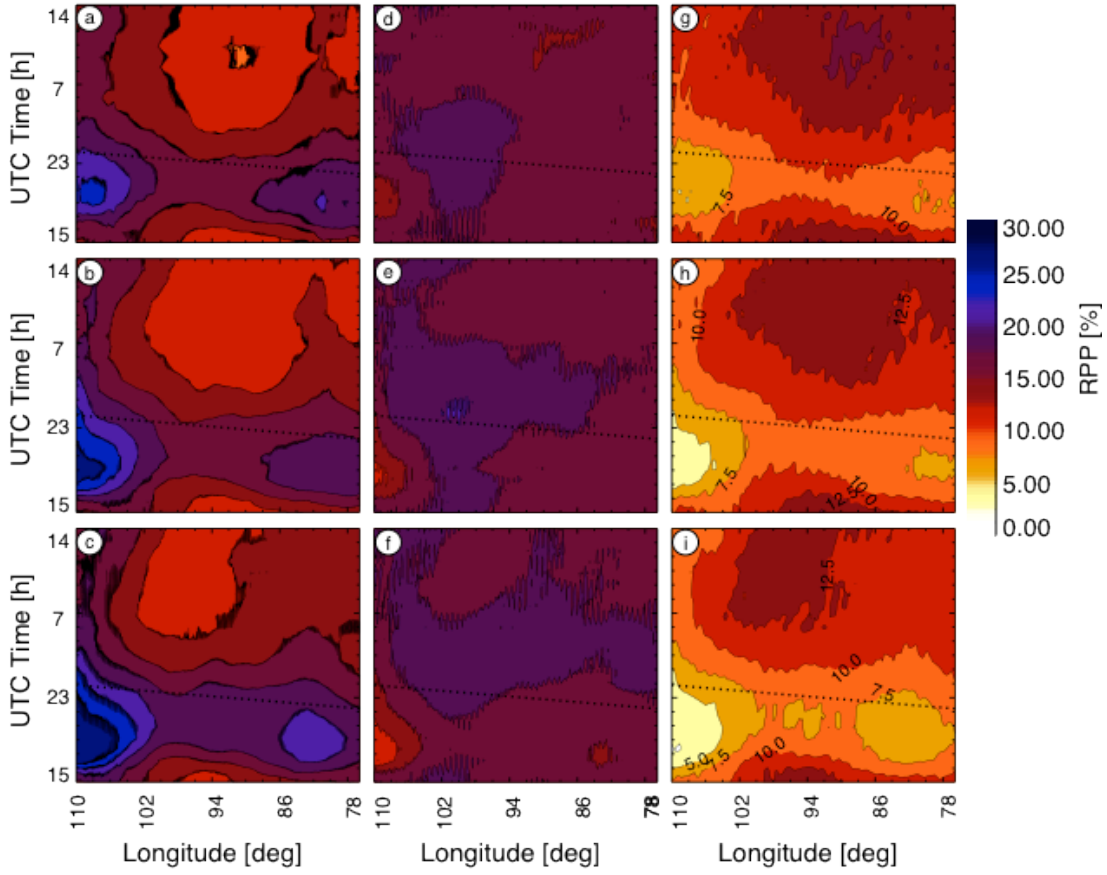

Figure 4.13: Idem Fig. 3.15 but for RPP at 16 km (left column), 64 km (central-left column), 128 km (central-right column) and 256 km (right column) for the summer

It is further important to note that rainfall activity at large scales and its importance relative to the smaller scales depends on latitude, longitude and time of day. In particular, the RPP at 256 km is larger than at 16 km over the southern region between 102W and 91W from 06Z to 16Z (Fig. 4.13i). Similarly, in most of the region east of 99W, rainfall activity over the central latitudes at 256 km is more important than at 16 km from 06Z at 15Z. Furthermore, the

largest difference between the influences of these two scales occurs over the northern latitudes, where the RPP at 256 km is greater (by more than 5%) than at 16 km between 92W to 88W from 09Z to 11Z (Figs. 4.13a and 3j). This feature shows the critical importance of the large scales in nighttime precipitation over the Continental U.S., especially in Midwest and Southern Great Lakes region.

Analyzing the dependence of RPP with latitude and time, it can be seen that the maximum values of RPP at the small scales are likely to occur close to the southern boundary of the domain. The effect of RPP at these scales tends to decrease with latitude (Figs. 4.14a to 4.14c). In particular, this feature is present during the entire diurnal cycle for the 16 km scale over the central and eastern longitudinal band, whereas over the western longitudes, the RPP at this scale tends to yield comparable values north of 37N (Figs. 4.14a to 4.14c).

The RPP at the transition scale presents a more homogeneous pattern for the 24-hour period over the entire latitudinal range analyzed; however, its dependence with time and latitude clearly varies for each longitudinal band. Over the eastern region, the maximum values of RPP (greater than 17.5%) occur during a brief time frame (from 00Z to 06Z) between the southern boundary of the domain and 38N (Fig. 4.14d). However, north of 39N in the eastern region, the RPP at this scale is not likely to depend on latitude or time of day (Fig. 4.14d). On the other hand, the summer RPP over the central longitudes has a clear dependence on time and latitude (Fig. 4.14e). Over this region, RPP greater than 17.5% is likely to show its maximum values over central latitudes during the afternoon (from 21Z to 04Z) and then shift southward with time, influencing the southern boundary of the domain during late afternoon and night hours (from 00Z to 10Z, Fig. 4.14e). Over the western region, the summer RPP at 64 km shows a different configuration than over the previous regions, with its minimum value (smaller than 12.5%) over the southern

latitudes around 18Z (Figs. 4.14c and 4.14f). This behavior of RPP at the transition scale seems to confirm the relationship between the transition scale and the high rainfall rates present at night over the Great Plains.

The RPP at large scales shows greater values over the northern region and steadily decreases in magnitude southward (Figs. 4.14g to 4.14i). In particular, for the 256 km scale, rainfall activity provides the smallest influence (RPP less than 5%) in the afternoon over the western longitudinal band and between 32.5N and 35N (Fig. 4.14g).

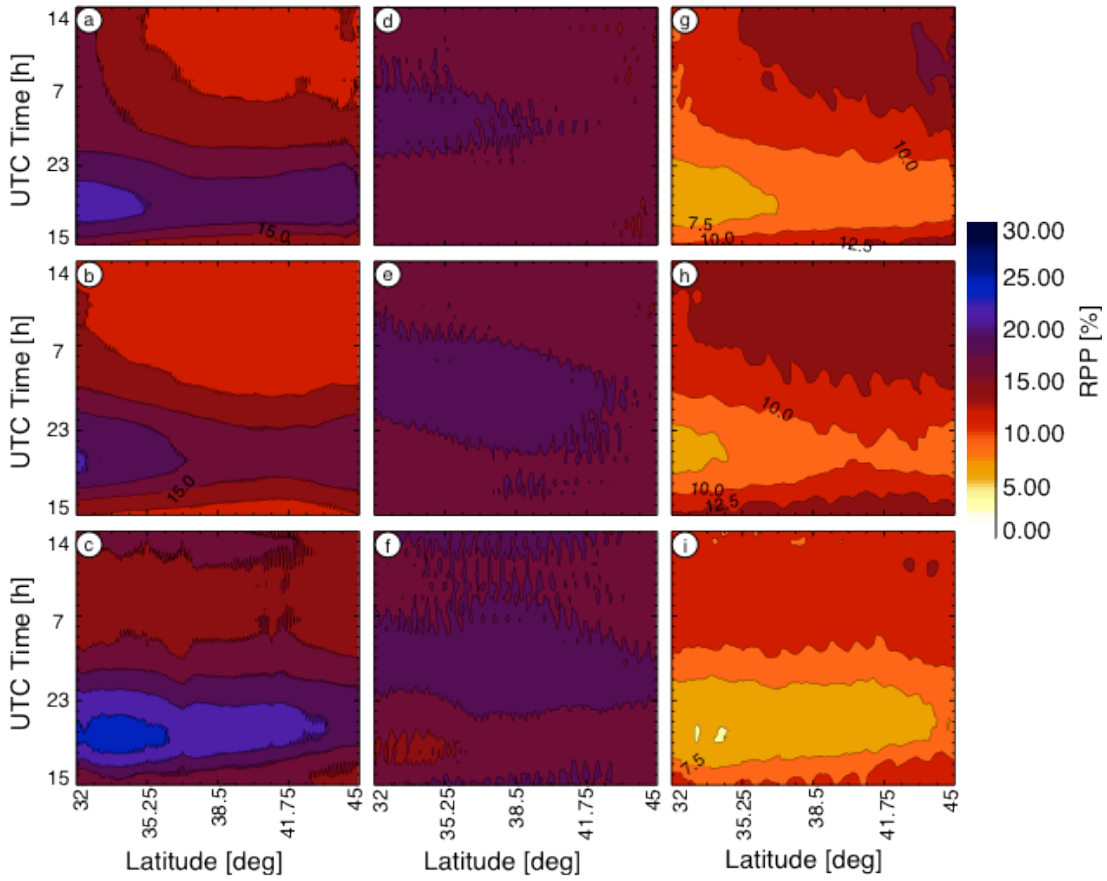

Figure 4.14: Idem Fig. 3.16 but for RPP at 16km (left column), 64 km (central-left column), 128 km (central-right column) and 256 km (right column) for the summer

It is important to note that over the western longitudinal band, RPP at the transition and large scales provides its minimum contribution, which is in agreement with the location and time of the small scale greater influence (during the afternoon over southern latitudes). However, this is not the case over the central latitudes, where high values of RPP at most scales are present. This suggests that the lower influence of the transition and large scales in PP could counteract the high influence of the small scales over the southern latitudes. Therefore, this could be the cause for the maximum values of summer PP over the western longitudinal band to occur over the central latitudes (around 37N) and not over the southern boundary of the domain, in agreement with the greater influence of the small scales (Figs. 3.16c, 4.14c, 4.14f and 4.14i).

Finally, the RPP at large scales increases in importance northward during the 24-hour period over the central longitudes (Fig. 4.14j). A similar behavior, but with a faster increase in magnitude at night, also occurs over the eastern longitudes. In particular, for the 256 km scale, the summer RPP presents values higher than 12.5% south of 35N from 05Z to 16Z in association with the decay period of PP (Figs. 3.16a and 4.14g). This provides further support to the link between the large spatial scales and the longevity of precipitation systems during night and morning hours over the Midwest and Southern Great Lakes region (Figs. 3.16c and 4.14g).

4.3.2 Analysis for the summer months.

The patterns of monthly and summer RPP resemble each other at most scales. Over the entire domain, the month-to-month difference is mostly related to the behavior of RPP at the transition and large scales. Over the central latitudinal band, the maximum influence of June RPP at 64 km tends to be restricted to the area west of 94W from 20Z to 07Z (Fig. 4.15e). However, during July and August, the RPP is likely to extend its coverage eastward to

86W (Figs. 4.16e and 4.17e). Furthermore, the July RPP at this scale is expected to influence the central region (from 98W to 86W) for a longer period of time (from 19Z to 09Z, Fig. 4.16e). The large scales also have a generally greater effect over this region for the months of July and August. In particular, for the 256 km, July and August RRP greater than 12.5% occurs earlier (around 05Z) in comparison to June RPP between 96W and 84W (Figs. 4.15e, 4.16e and 4.17e). This provides further support to the influence of the transition scale in the late afternoon maximum of July and August PP east of 92W as well as the large scales in the persistent high values of PP at night hours during these months

Further analysis and the monthly meridional Hovmöller diagrams can be seen in Appendix B.

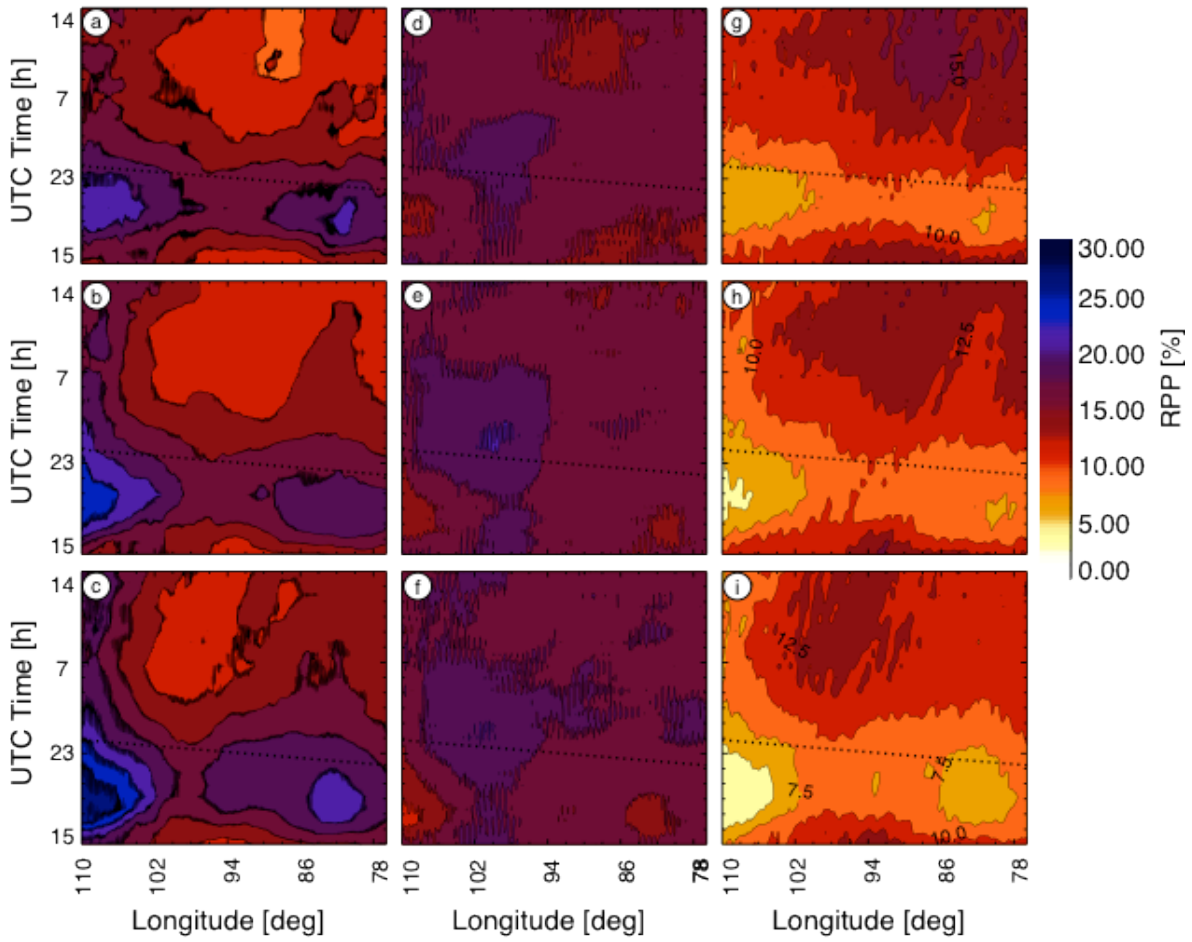

Figure 4.15: Idem Fig. 4.13 for the month of June

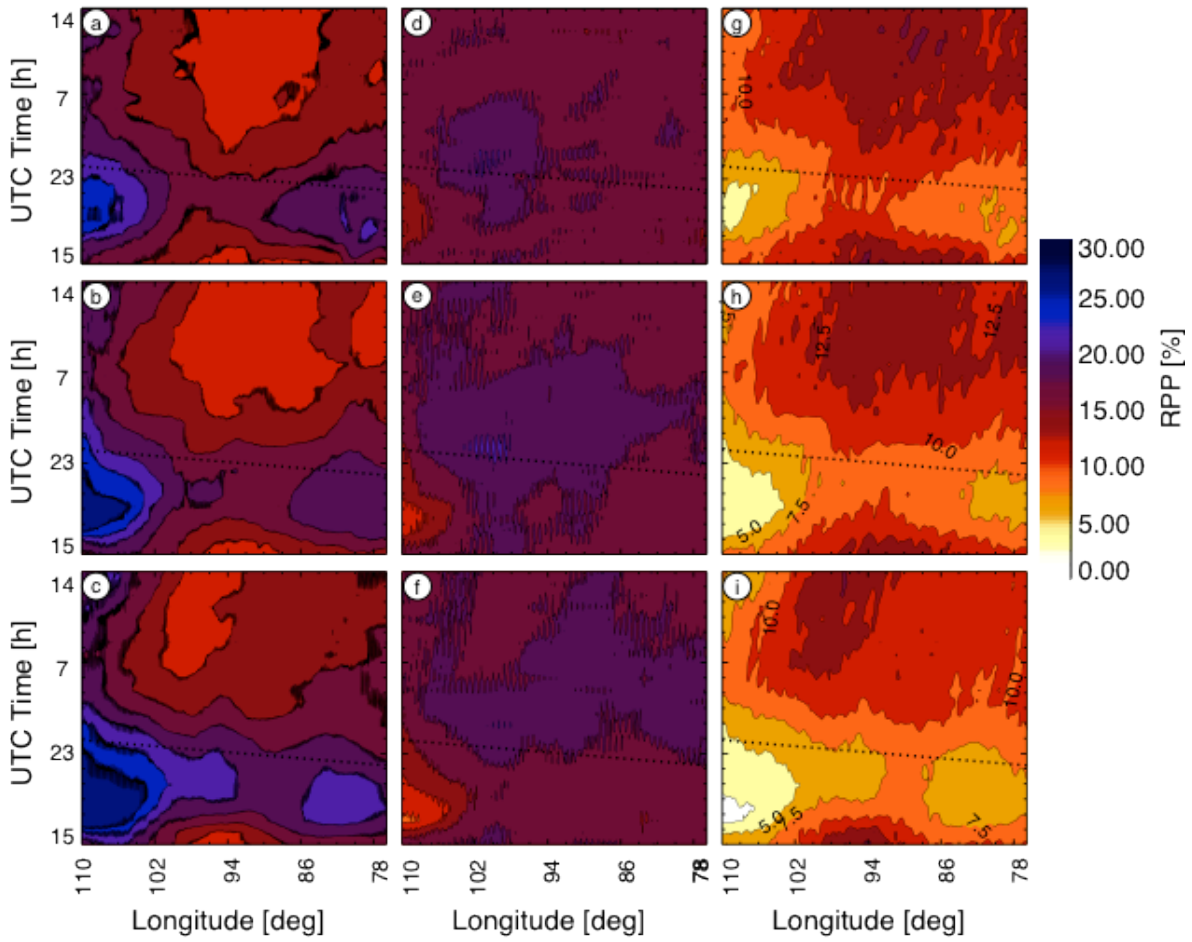

Figure 4.16: Idem Fig. 4.13 for the month of July.

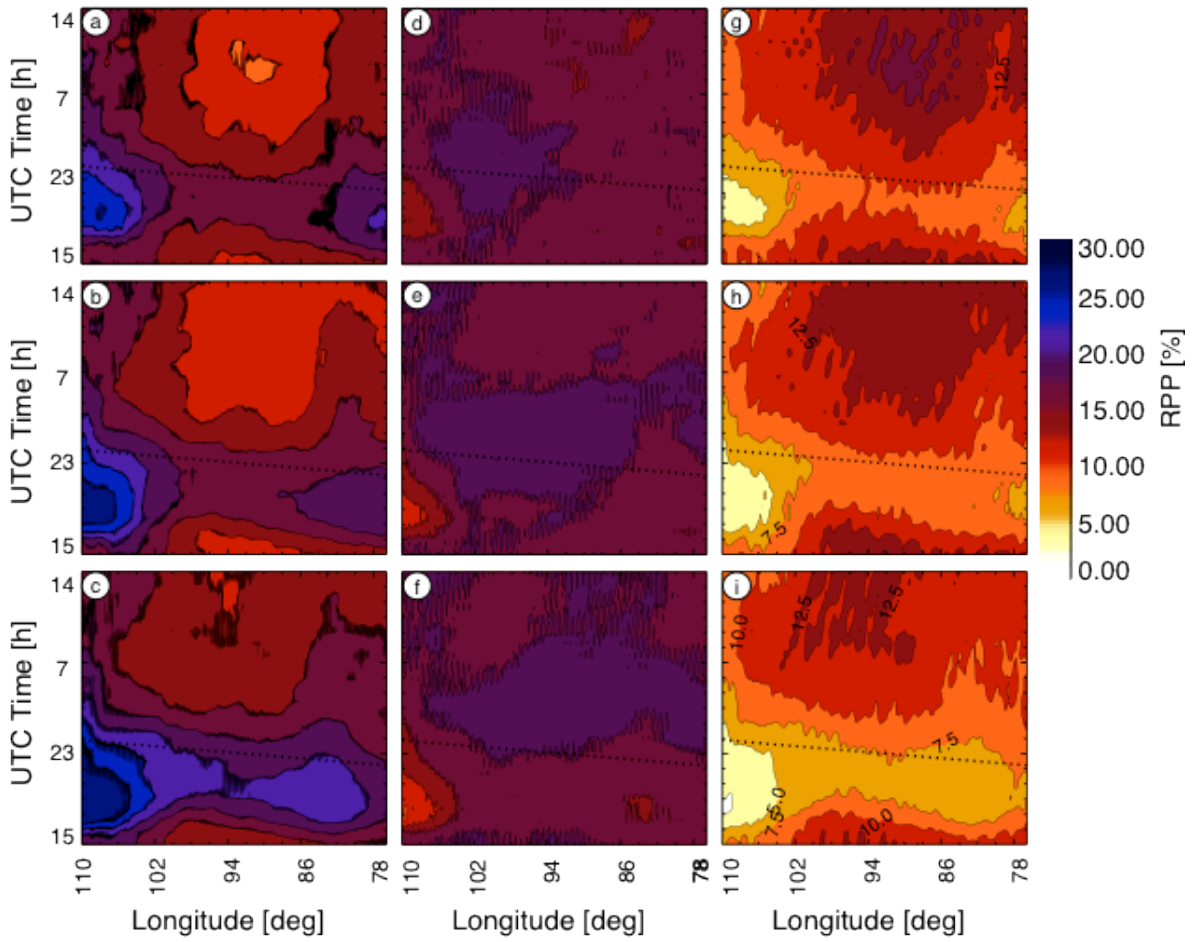

Figure 4.17: Idem Fig. 4.13 for the month of August.

Chapter 5

Summary and Conclusions

The main objective of this thesis is to investigate the geographical and scale variability of the diurnal cycle of precipitation over the Continental United States. The results of this study suggest that the eastern lee of the Rocky Mountains is a clear region for the initiation of precipitation during late morning and afternoon hours. Over this region, summer rainfall activity gives a well-defined diurnal cycle, with a maximum value in the afternoon and a minimum during the morning. The maximum value of the summer average of the RPP at 8 and 16 km tends to occur around the same time of the initiation of summer precipitation. This suggests that summer rainfall activity at these scales is likely to have a stronger impact on the development of precipitation systems in the Lee of the Rockies.

After the maximum value is achieved, rainfall activity tends to propagate eastward, leading to high values of precipitation over the Great Plains during the late afternoon and night hours. These maximum values occur in association with the greatest contribution of the RPP at 64 km at late afternoon, suggesting that there is a connection between RPP at this scale and the maximum intensity of rainfall activity in the region. On the other hand, the RPP at scales larger than 128 km tends to have a greater influence in the Great Plains after the highest values of summer PP occurs, indicating that rainfall activity at these scales is more likely to be linked to the prolonged presence of the precipitation systems in the region.

The propagation of the summer precipitation pattern and the high values of summer PP during night hours over the Great Plains, suggests that solar forcing plays a major role in the diurnal cycle of summer precipitation but is

also not the only factor involved (Wallace 1975, Riley et al. 1987, Carbone et al. 2002 and Lee et al. 2007, among others).

Summer PP over the eastern longitudes is also likely to produce a uniform distribution in time, with an afternoon maximum (associated with the small scales) and a morning minimum (associated with the large scales). However, rainfall activity over this area is more localized, with a maximum value present in the afternoon over the southern boundary of the domain and decreasing northward in space and time. This behavior reflects the fact that precipitation over the region is likely to be a response to land-sea breeze circulation, with the maximum intensity occurring closer to the thermal forcing (in the afternoon over the southern latitudes) and decreasing away from it (in the evening and night over the northern latitudes).

It is clear that there is no unique scale at which summer rainfall activity represents the majority of PP for the entire domain. In the lower Mississippi Valley, as well as in the eastern lee of the Rocky Mountains, the time of the maximum values of RPP is likely to occur in connection with precipitation at small scales (8, 16 and 32 km) in the afternoon. However, over the Midwest and Great Lakes region, summer rainfall activity at 64 km provides the highest contribution to PP during late afternoon hours.

In general, RPP at different spatial scales strongly depends on the time of day and the location over the Continental U.S., with the timing of the maximum contribution shifting towards later times as the scale increases. This is probably related to the growth of the precipitation systems in time and therefore, to rainfall at larger scales contributing more to the total precipitation later than at smaller scales. Summer rainfall activity at the smaller scales mostly contributes to PP during afternoon hours, whereas the primary contribution of the large scales tends to occur during night and early morning hours, with the RPP at 64 km acting as a transition regime between the patterns of summer precipitation at small and large scales. This observation

can be related to the different stages of the precipitation life cycle. In particular, the smaller scales greatly influence the onset and the maximum rainfall activity; then systems often organize later into larger rainfall patterns, mostly represented by the larger scales.

The beginning of light precipitation and its maximum value east of the Continental Divide is likely to occur in phase with the solar forcing during the summer season. Furthermore, this behavior occurs in clear association with the maximum values of rainfall activity at small scales. This provides a clear indication of the importance of the solar forcing in the diurnal cycle of precipitation and its relationship to small scales over most of the Continental U.S.

Rainfall activity at large scales and its importance relative to the smaller scales depends on latitude, longitude and time of day. The largest difference between the influences of these two scales is likely to occur between the 256 km and 8 km scales, over the Midwest and Southern Great Lakes region, showing the critical importance of the large scales in the nocturnal precipitation regime precipitation over Central U.S. during the summer season.

It is noteworthy to observe that the summer PP over the eastern lee of the Southern Rocky Mountain mostly presents smaller values than its 12-years average prior to the year 2002, and it is almost always greater than the climatology from 2003 onward. It is further interesting to note that the variability of the climatologically-averaged summer PP derives from at least two distinct sources: the different magnitudes of the maximum yearly rainfall activity and the different monthly and yearly characteristics of the diurnal cycle of precipitation. The former feature is important over most of continental U.S., whereas the later feature is mostly associated with the behavior of rainfall activity over the Central Plains.

It is also important to note that summer precipitation for each individual month has very similar characteristics in comparison to the average summer season. However, over the Great Plains some distinctive differences between the two averages occur. In particular, July and August PP is more likely to have larger values during late afternoon hours, whereas June systems tend to have less influence in the diurnal cycle, most notably at night. This pattern further agrees with a stronger nighttime influence of the transition and large scales over the Great Plains during the months of July and August. Therefore, this provides further support to the association between the scales larger or equal than 64 km with the occurrence of nighttime rainfall activity over the Central U.S.

It was shown in this work that the diurnal cycle of precipitation over continental United States has distinctive characteristics for each spatial scale. Even though further work is required before there can be a complete understanding of the behavior of rainfall activity at different spatial scales, it is of interest that this thesis can provide some guidance in the improvement of the simulation of the diurnal cycle of precipitation in regional and operational models. Surcel et al. (2010) showed that data assimilation plays an important role in very-short term forecasting. Therefore, advancing in the representation of rainfall activity at the scales that have the highest impact in the diurnal cycle of precipitation can potentially improve the deficiencies of the short-term forecasts.

Appendix A

Computation of Hovmöller diagrams

Hovmöller diagrams are a commonly used method for plotting data to highlight its behavior with time and distance (Hovmöller, 1949, Rossby 1949, Carbone et al. 2002, Lang et al. 2007, Trier et al. 2010, among others). In general, a Hovmöller diagram maps a variable in a time-distance diagram. In order to do this, the variable is average over the spatial dimension orthogonal to the dimension plotted in the Hovmöller diagram. For a zonal Hovmöller diagram of a field F, first the fields has to be averaged in latitude over the region of interest as,

$$F(x,t)\big|_{\ell a} = \frac{1}{\Delta \ell a} \int_{\ell a} F(x,y,t) d\ell a \qquad \text{(A1)}$$

where, $F(x,t)\big|_{\ell a}$ is the latitudinally-averaged F, x is longitude, y is latitude and ℓa is the latitudinal band where the average is performed.

It is important to note that meridional information is lost in the averaging process and, therefore, zonal Hovmöller diagrams do not provide any information on the variations of the variable displayed with latitude. To account for this, meridional Hovmöller diagram of F can also be computed as,

$$F(x,t)\big|_{\ell o} = \frac{1}{\Delta \ell o} \int_{\ell o} F(x,y,t) d\ell o \qquad \text{(A2)}$$

where, $F(x,t)|_{\ell_o}$ is the longitudinally-averaged F and ℓ_o is the longitudinal band where the average is performed. In this case the zonal information is lost in the calculations.

It is important to note that a horizontal line in the zonal (meridional) Hovmöller diagram represents a stationary feature with a marked dependency with time but without a preferred longitude (latitude). On the other hand, a vertical line in the zonal (meridional) Hovmöller diagram implies a preferred longitude (latitude) where no changes of the variable displayed occur in time. Finally, a diagonal line represents a connection between the spatial dimension and time and, therefore, a propagation of the signal in time. A positive tilt in the zonal (meridional) Hovmöller diagram implies an eastward (northward) propagation of the variable displayed, whereas a negative tilt implies a westward (southward) propagation in time.

In this work, the characteristics of the PP with longitude and time as well as with latitude and time are analyzed over three different regions. Therefore, three different zonal and meridional Hovmöller diagrams are constructed. The regions of interest for the zonal Hovmöller diagrams are three latitudinal areas placed equidistant between 32N and 45N covering the region from 110W to 75W (shaded areas delimitated by solid, bold rectangles shown in Fig. 16a). Over each of these regions, PP was latitudinally-averaged according to Eq. A1, and afterwards $PP(x,t)|_{\ell_a}$ is plotted in a longitude-time space to finally construct the zonal Hovmöller diagram.

In a similar manner, the regions of interest for the meridional Hovmöller diagrams are three longitudinal areas placed equidistant between 110W and 75W covering the region from 32N to 45N (shaded areas delimitated by solid, bold rectangles shown in Fig. 16b). Over these regions the longitudinal average of PP is performed according to Eq. A2 and then, $PP(x,t)|_{\ell_o}$ is plotted in a

latitude-time space to finally construct the zonal meridional Hovmöller diagram.

Appendix B

Meridional Hovmöllers

The influence of the transition scale in nighttime PP over the central latitudes of the Great Plains is also visible in the behavior of monthly RPP with latitude and time (Figs. B.1 to B.3). Over the central latitudinal band, June RPP is likely to present its maximum values (greater than 17.5%) south of 42N for a narrow period of time (from 23Z to 05Z, Fig. B.3e). However, the maximum values of July and August RPP at this scale are expected to occur earlier, influencing the region between 35N and 42N from 20Z to 07Z (Figs. B.3e and B.3e). Therefore, the July and August secondary PP maximum present around 39N over the central longitudes (absent for the month of June) is likely to be related to the high intensity of rainfall activity at 64 km during these particular months (Figs. B.2e and B.3e).

It is further interesting to note, as also mention in Section 4.1, that the behavior of PP seems to be strongly influenced by rainfall activity at all scales over the western longitudinal band. Over this region and similar to the behavior of summer RPP at the transition and large scales, July and August RPP at these scales, is likely to show its minimum influence around the same

location and time of the maximum RPP at the small scales (Figs. B.3c, B.2f, B.2i, B.3c, B.3f and B.3i). Therefore, the effect of these scales is likely counteract each other, leading to the maximum July and August PP to be displayed further north, where high values of RPP at most scales are located (Figs. B.2c, B.2f, B.2i, B.3c, B.3f and B.3i). In contraposition, June RPP at the transition and large scales is not likely to show any dependence with latitude during most part of the day over the western longitudinal band. However, June RPP at the small scales presents its maximum influence south of 34N (Fig. B.1i). As a result, the maximum value of June PP occurs south of this position in clear association with the behavior of the small scales (Fig. B.1c).

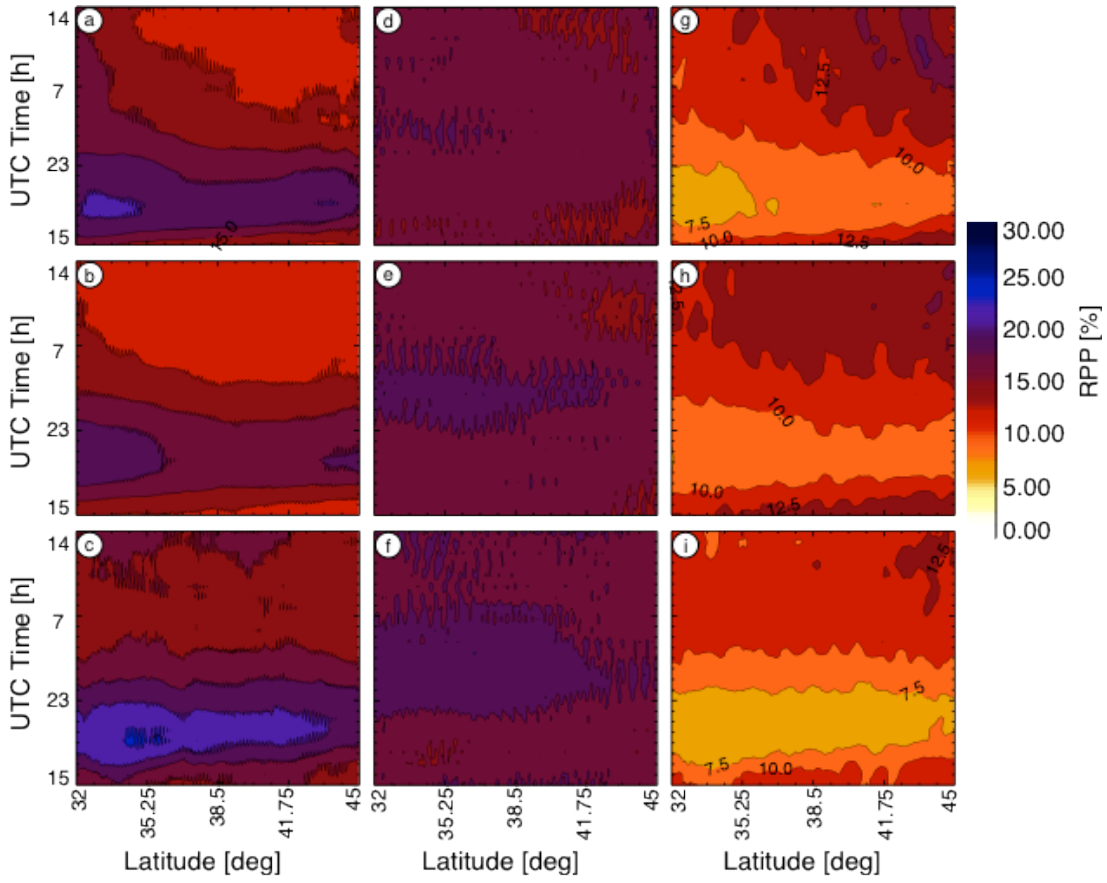

Figure B.1: Idem Fig. 4.14 for the month of June

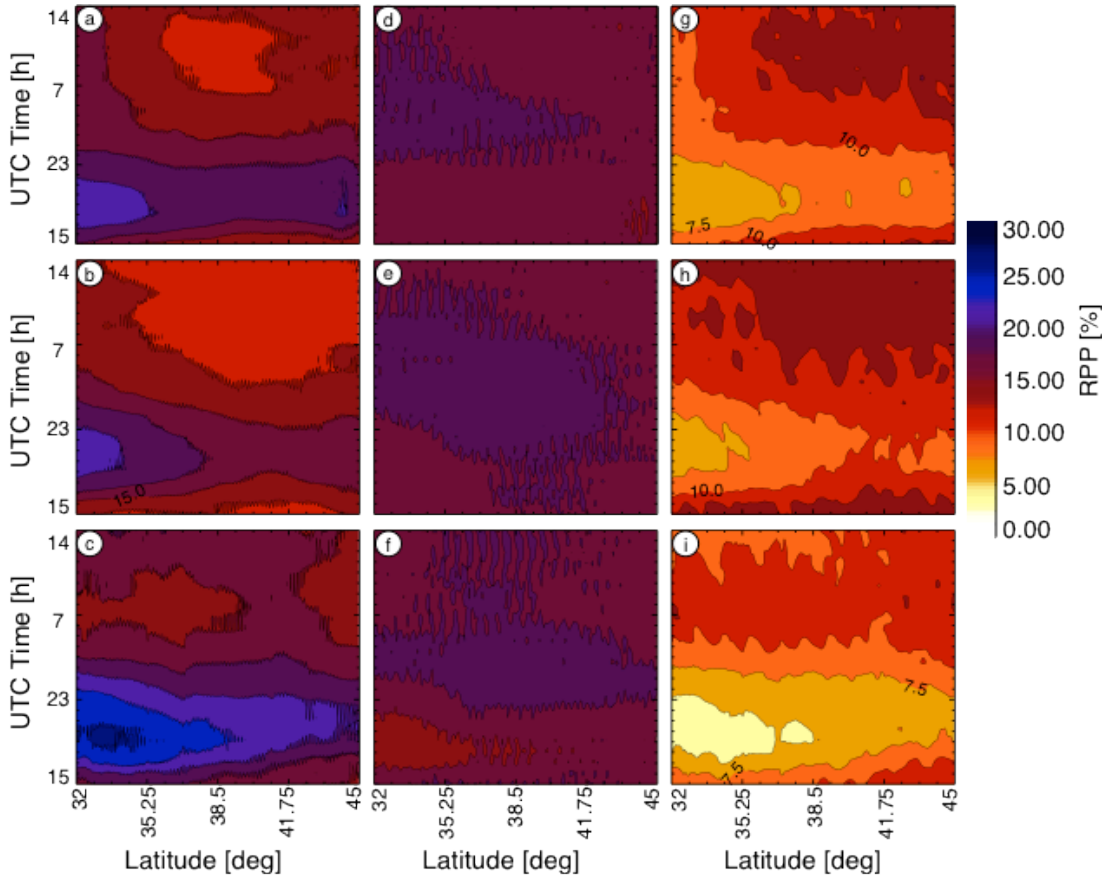

Figure B.2: Idem Fig. 4.14 for the month of July.

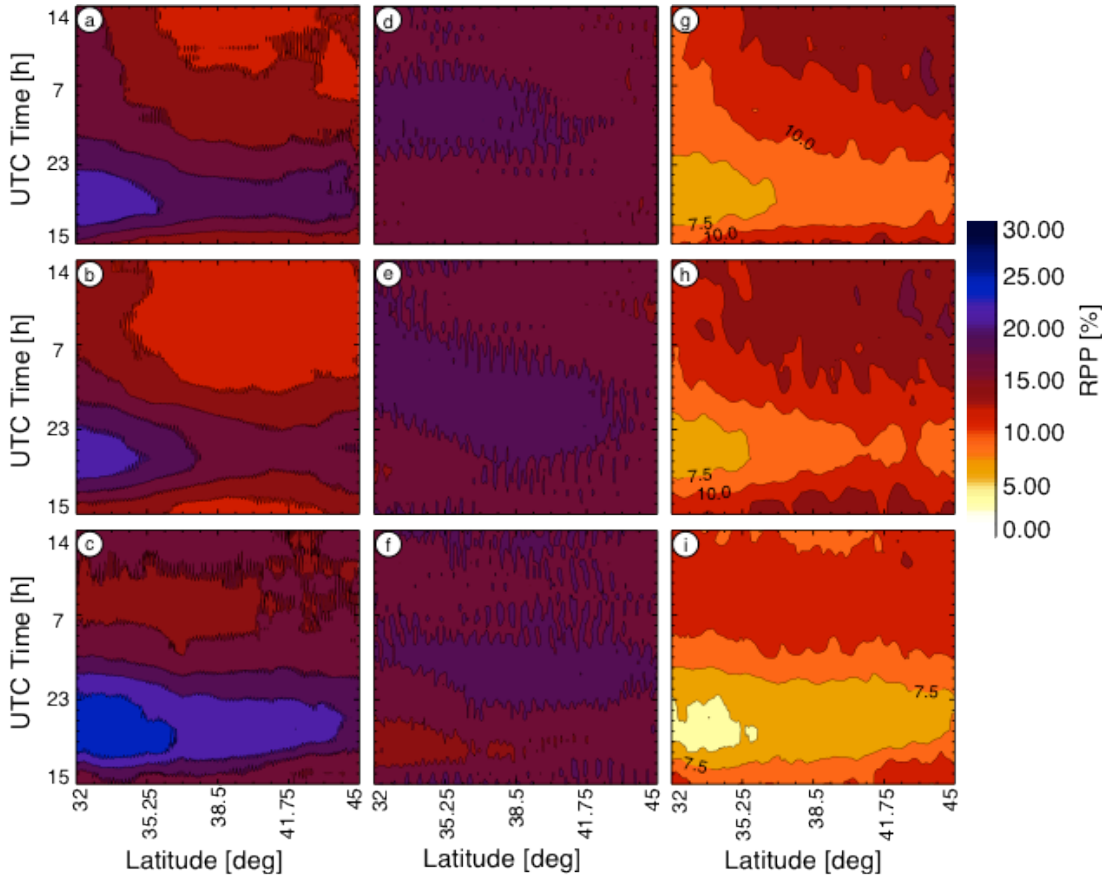

Figure B.3: Idem Fig. 4.14 for the month of August.

Bibliography

Ahijevych, D.A., C.A. Davis, R.E. Carbone, and J.D. Tuttle, 2004: Initiation of Precipitation Episodes Relative to Elevated Terrain. *J. Atmos. Sci.*, **61**, 2763–2769.

Alexander, H.F., 1938: A study of the hourly precipitation at Oklahoma City, Okla. *Mon. Wea. Rev.*, **66**, 126–130.

Balling, R.C., 1985: Warm Season Nocturnal Precipitation in the Great Plains of the United States. *J. Appl. Meteor.*, **24**, 1383–1387.

Bonner, W.D., 1968: Climatology of the Low Level Jet. *Mon. Wea. Rev.*, **96**, 833–850.

Carbone, R.E., and J.D. Tuttle, 2008: Rainfall Occurrence in the U.S. Warm Season: The Diurnal Cycle. *J. Climate*, **21**, 4132–4146.

Carbone, R.E., J.D. Tuttle, D.A. Ahijevych, and S.B. Trier, 2002: Inferences of Predictability Associated with Warm Season Precipitation Episodes. *J. Atmos. Sci.*, **59**, 2033–2056.

Cook, A.W., 1939: The Diurnal variation of summer rainfall at Denver. *Mon. Wea. Rev.*, **67**, 95–98.

Hovmöller, E., 1949: The Trough-and-Ridge diagram, *Tellus* **1**, 62-66.

Kincer, J.B., 1916: Daytime and nighttime precipitation and their economic significance. *Mon. Wea. Rev.*, **44**, 628–33.

Kumar, P., and E. Foufoula-Georgiou, 1997: Wavelet analysis for geophysical applications. *Rev. Geophys.*, **35**, 385-412.

Lang, Timothy J., David A. Ahijevych, Stephen W. Nesbitt, Richard E. Carbone, Steven A. Rutledge, Robert Cifelli, 2007: Radar-Observed Characteristics of Precipitating Systems during NAME 2004. *J. Climate*, **20**, 1713–1733.

Lee, M.I., S.D. Schubert, M.J. Suarez, I.M. Held, N.C. Lau, J.J. Ploshay, A. Kumar, H.K. Kim, and J.K.E. Schemm, 2007: An Analysis of the Warm-Season Diurnal Cycle over the Continental United States and Northern Mexico in General Circulation Models. *J. Hydrometeor.*, **8**, 344–366.

Parker, M.D., and D.A. Ahijevych, 2007: Convective Episodes in the East-Central United States. *Mon. Wea. Rev.*, **135**, 3707–3727.

Pielke, R.A., 1974: A Three-Dimensional Numerical Model of the Sea Breezes Over South Florida. *Mon. Wea. Rev.*, **102**, 115–139.

Riley, G.T., M.G. Landin, and L.F. Bosart, 1987: The Diurnal Variability of Precipitation across the Central Rockies and Adjacent Great Plains. *Mon. Wea. Rev.,* **115**, 1161–1172.

Rossby, C-G., 1949: On A Mechanism for the Release of Potential Energy in the Atmosphere. *J. Meteor.*, **6**, 164–180.

Schwartz, B.E., and L.F. Bosart, 1979: The Diurnal Variability of Florida Rainfall. *Mon. Wea. Rev.*, **107**, 1535–1545.

Surcel, M., M. Berenguer, I. Zawadzki, 2010: The Diurnal Cycle of Precipitation From Continental Radar Images and Numerical Weather Prediction Models. Part I: Methodology and Seasonal Comparison. *Mon. Wea. Rev.*, **In press.** doi: 10.1175/2010MWR3125.1

Tian, B., I. M. Held, N.C. Lau, and B.J. Soden 2005, Diurnal cycle of summertime deep convection over North America: A satellite perspective, *J. Geophys. Res.*, **110**, D08108, doi:10.1029/2004JD005275.

Trier, S. B., C. A. Davis, D. A. Ahijevych, 2010: Environmental Controls on the Simulated Diurnal Cycle of Warm-Season Precipitation in the Continental United States. *J. Atmos. Sci.*, **67**, 1066–1090.

Turner, B., I. Zawadzki, and U. Germann, 2004: Predictability of precipitation from continental radar images. Part III: Operational nowcasting implementation (MAPLE). *J. Appl. Meteor.*, **43**, 231–248

Wallace, J., 1975: Diurnal Variations in Precipitation and Thunderstorm Frequency over the Conterminous United States. *Mon. Wea. Rev.,* **103**, 406–419.

Winkler, J.A., B.R. Skeeter, and P.D. Yamamoto, 1988: Seasonal Variations in the Diurnal Characteristics of Heavy Hourly precipitation across the United States. *Mon. Wea. Rev.*, **116**, 1641–1658